DEVELOPMENT OF A NOVEL FAST-WARM STAMPING (FWS) TECHNOLOGY FOR MANUFACTURING HIGH-STRENGTH STEEL COMPONENTS

By

YUHAO SUN

A thesis submitted to Imperial College London for the degree of
Doctor of Philosophy

Department of Mechanical Engineering
South Kensington Campus
Imperial College London
London SW7 2AZ
U.K.

2020

Declaration of originality

This thesis hereby presented is based on research by the author at the Department of Mechanical Engineering of Imperial College London. I declare that the work contained in this thesis is only author's own work. The work of this thesis has not been submitted elsewhere for any other degree or qualification.

Copyright Declaration

Abstract

Hot and warm stamping are preferable sheet metal forming technologies used in manufacturing high-strength parts with the twofold objectives of reducing fuel consumption and improving automotive crashworthiness. Great efforts have been made to improve the production rate in these processes and it is difficult to further improve productivity. Therefore, the development of new forming technologies may be an alternative solution to form high-strength steels into complex shapes whilst reducing the cycle time.

The present work aims to develop a novel lightweight forming technology, namely fast-warm stamping (FWS) technique, to manufacture high-strength steel components with the desired properties. The concept of this process is to utilise ultra-fast heating of a steel blank to an appropriate temperature, whilst minimising the major negative changes to microstructure which are detrimental to the post-form strength. Mechanical properties such as ductility and post-form strength (PFS) of the MS-W900Y1180T (MS1180) steel were examined via uniaxial tensile tests at various temperatures (25–500°C) and strain rates (0.01–5/s). Special attention has been afforded to the effect of heating rate on thermo-mechanical properties and microstructure of the MS1180 steel with different heating rates. The results suggest that the ductility and post-form hardness of the MS1180 steel were simultaneously improved by 25.7% and 5%, with an increase in heating rate from 1 to 150°C/s. The increased hardness is attributed to the finer precipitated carbides and lower recovery at fast heating rate conditions, which was validated by microstructural observations.

The validation of the FWS technology was conducted by forming U-shaped components through a dedicated pilot production line caller *Uni-form*. The fast-warm stamped components exhibited over 92% mechanical strength of the original as-received material consisting of 1140MPa post-form strength and 370HV hardness. The overall manufacturing cycle time in the FWS process was within 10 seconds. Springback of the formed parts under FWS conditions

was successfully characterized at various temperatures and forming speeds. Close agreements were achieved between the experimental and simulated results for temperature, thickness distribution and springback prediction of the formed parts which validated the accuracy of the developed finite element (FE) model.

FWS technology is a promising solution to manufacture components with desirable mechanical properties and dimensional accuracy. In this work, a feasibility study of the FWS technology was extended from martensitic steels to 60Si2Mn spring steel by producing commercialized disc springs. A separate forming tool set with a replaceable forming surface was developed to reduce manufacturing cost. Experimental results showed that a disc spring was successfully formed using the proposed forming process with the required dimensional precision, post-form strength and surface roughness. This forming technique has shown to enable a tremendous reduction of overall cycle time from 30 minutes to less than 20 seconds and subsequent productivity improvement for a mass-production setting.

Acknowledgements

First and foremost, I would like to express my sincerest gratitude to my supervisor Dr Liliang Wang, for his continuous guidance, unlimited support and tremendous encouragement during my PhD journey. I gratefully appreciate him for introducing me to the sheet metal forming, a field I was initially unfamiliar with. He provided me with great opportunities over the last four year, which have enhanced my knowledge of materials and manufacturing processes infinitely. His great patience, enthusiasm for research and thoughtful visions are valuable wealth which will enrich me to become a better person for a lifetime. I would like to express my appreciation to my co-supervisor Dr Jun Jiang for his valuable advice ad great help on my research through my PhD studies.

I am incredibly grateful for the funding that was provided by the China Academy of Launch Vehicle Technology (CALT), which enabled me to undertake this project and collaborate with leading researchers from the UK and China. I would like to thank thyssekrupp Steel for supplying the raw materials for my research.

I was very fortunate to be a part of my research group and worked directly with many of its members. I would like to give my sincere thanks to the technical staff, Amit Choda, Mark Holloway and Suresh Viswanathan Chettiar, Alex Toth and Dr Ruth Brooker, for their friendly help and assistance on my experimental work. A special thanks to Dr Kehuan Wang for his constant supporting, valuable discussion on my research work. I would like to thank Dr Denis Politis for the supporting on the scientific papers and thesis. I would also like to thank my colleagues, past and present, Dr Jun Liu, Dr Omer El Fakir, Dr Minh-Son Pham, Dr Haoxiang Gao, Dr Kang Ji, Dr Yiran Hu, Xi Luan, Zhaoheng Cai, Mateusz Kopec, Yang Xiao, Shaksam Dhawan, Yu Zhu, Qinmeng Luan, Jun Liu and Xiaochen Lu. Huge thanks to all who supported me in any way during the completion of the project. I would also like to extend my thanks to

Dr Ailing Wang, Dr Xiaochuan Liu, Dr Qunli Zhang and Yang Zheng, in particular, my PhD time wouldn't have been the same without you.

I would like to thank many undergraduate and graduate students: Tingfung Pang, Nickolas Atherton, Zonghao Guo and Richard Brooks, who supported me at different stages of my research. I would like to thank Laochen for making my life more colourful and delightful by sharing your unique performances which I couldn’t have learnt from a textbook.

Last but not the least, I would like to express heartfelt gratitude to my family. I would like to thank my beloved parents for their constant supporting throughout my PhD studies and my life. I owe my deepest thanks to Xiaocan Wang for her unconditional love and inclusiveness. Your understanding and selfless accompanying are truly what enables me to conquer the difficulties and keep constant progress. This thesis is dedicated to you.

Contents

List of Figures

List of Tables

List of Publications

Sun, Y., Wang, K., Politis, D. J., Chen, G., Jiang, J., Wang, L., 2019. An experimental investigation on the ductility and post-form strength of a martensitic steel in a novel warm stamping process. J. Mater. Process. Technol. Doi: 10.1016/j.jmatprotec.2019.116387

Sun, Y., Wang, K., Politis, D. J., Cai, Z., Wan, L., Wang, Y., Wang, L., 2018 A novel stamping process of 60Si2Mn steel disc springs. Advanced high strength steel and press hardening. 295-300. Doi: 10.1142/9789813277984_0046

Sun, Y., Wang, K., Politis, D. J., Atherton, N., Pang, T., Knoerr, L. O., Captaine, H., Wang L., 2017. Flow behavior characterization of an ultra-high strength steel under warm stamping conditions. 2nd International Conference on Lightweight Materials and Engineering Structures, 13-14 November 2017, London, United Kingdom.

Sun, Y., Cai, Z., Politis, D. J., Luan, X., Chen, G., Wang, L., 2019. Springback characteristics of UHSS for warm u-shape bending: experiments and FE simulation. 38th International Deep-Drawing Research Group Conference. 3-7 June 2019, Enschede, Netherlands. Doi:10.1088/1757-899X/651/1/012055

Liu, X., **Sun, Y.,** Yang, X., Wang, L., 2019. Characterisation of the thermomechanical boundary conditions of martensitic steel in a FAST forming process. J. Mater. Process. Technol. (Under review)

Cai, Z., **Sun, Y.,** Fakir, O. EL., Liu, J., Zhang, Q., Wang, L., 2019. Study of springback behaviours of AA7075 under hot/warm stamping. 3rd International Conference on Light Materials – Science and Technology. 5-7 November 2019, Manchester, United Kingdom.

Cai, Z., Batthyangy, P., Dhawan, S., Zhang, Q., **Sun, Y.,** Luan, X., Wang, L., 2018. Study of springback for high strength aluminium alloys under hot stamping. Advanced high strength steel and press hardening. 117-121. Doi: 10.1142/9789813277984_0019

Patent:

Sun, Y., Ji, K., Luan, X., Liu, X., Fakir, O. EL., Cai, Z., Wang, L., 2017. Fast warm stamping of ultra-high strength steel sheets, Publication number: WO/2019/038556.

Sun, Y., Cai, Z., Luan, X., Politis, D. J., Fakir, O. EL., Lin, J., Ying, Q., Wang, L., 2019. Method of forming parts from reinforced thermoplastic composites. Patent application number: 201910707800.X

Luan, X., **Sun, Y.,** Zhang, Q., Fakir, O. EL., Cai, Z., Wu, G., Lin, J., Wang, L., 2019. A device for simulating the hot stamping process of a sheet. Patent application number:201910707785.9

Cai, Z., Fakir, O. EL., Dhawan, S., Zhang, Q., **Sun, Y.,** Luan, X., Wu, G., Wang, L., 2019. A data guided approach to manufacturing light-weight components. Patent application number: 201910786108.0

Industrial project report:

Sun, Y., Jiang, J., Lin, J., Wang, L., 2016. Fast warm stamping of 60Si2Mn2 spring steel. Stage I. Report No: CALT-2016-11-29-SUN. *Confidential*

Sun, Y., Jiang, J., Lin, J., Wang, L., 2017. Fast warm stamping of 60Si2Mn2 spring steel. Stage II. Report No: CALT-2017-09-05-SUN. *Confidential*

Chen, G., Liu, J., **Sun, Y.,** Lin, J., Wang, L., 2018. Summary of metal forming technology. Report No: CALT-2018-12-20. *Confidential*

Sun, Y., Jiang, J., Lin, J., Wang, L., 2019. Annual activity report. Report No: CALT-2019-11-17. *Confidential*

Abbreviation

AHSS	Advanced high-strength steel
AUST	Austenitic stainless
BIW	Body-in-white
CP	Complex-phase
DIC	Digital image correlation
DP	Dual phase
FE	Finite element
FWS	Fast-warm stamping
HSLA	High-strength low-alloy
HSS	High strength steel
L-IP	Light-steel with induced plasticity
MS	Martensitic
PFH	Post-form hardness
PFS	Post-form strength
PHS	Press hardened steels
Ra	Surface roughness
SEM	Scanning electron microscope
TEM	Transmission electron microscope

TRIP	Transformation-induced plasticity
UHSS	Ultra high-strength steel
UTS	Ultimate tensile strength
YS	Yield strength

Nomenclature

δ	Engineering stress	Pa
$\boldsymbol{\sigma}$	True tress	Pa
e	Engineering strain	/
$\boldsymbol{\varepsilon}$	True strain	/
L_0	Original length	mm
L	Corresponding length	mm
F	Force	N
A_0	Area	mm^2
ΔT	Temperature difference	°C
θ_1	Sidewall springback angle	◦
θ_2	Flange springback angle	◦

Chapter 1. Introduction

1.1 Background

The automotive industry is facing a huge global challenge to reduce fuel consumption and minimize carbon dioxide (CO_2) emissions. Since the automotive sector accounts for almost 12% of total European Union (EU) CO_2 emissions, the European Commission has set a target for new cars to achieve 130g/km of CO_2 by 2015 (European Commission, 2018a). The average CO_2 emissions from new UK passenger cars has been steadily declining and has achieved a new low of 120.1g/km in 2015, as shown in Figure 1.1. This figure was 32.9% below the 2000 level of 181.0g/km and has reduced significantly from 164.9g/km in 2007 (SMMT, 2017). EU legislation has set an ambitious target for new vehicles to achieve 95g/km of CO_2 emissions by 2021 (European Commission, 2019). In the United States, the Environmental Protection Agency (EPA) has targeted an improvement in average automobile fuel efficiency from 27.5 miles per gallon in 2012 to 54.4 miles per gallon in 2025 (Megan, 2016). Given the increasingly stringent regulations pertaining to automobile emissions, reducing the weight of automobiles has become an important consideration for the automotive industry. Weight reduction is an effective way to improve a vehicle's efficiency that is beneficial to fuel economy and environmental friendliness (Burakova et al., 2018). Reducing an automobile's weight by a 50 kg (110 lbs) reduces CO_2 emissions by up to 5g per kilometre and increases fuel economy by up to 2% with no sacrifice in vehicle safety and performance attributes (DuPont., 2017). One of the most straightforward and effective solutions to achieve weight reduction is using materials with a high strength/weight ratio.

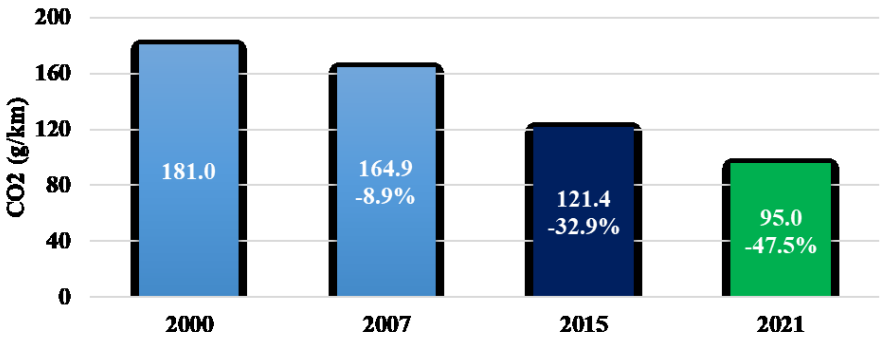

Figure 1.1 Average CO_2 emissions from new UK vehicles and EU 2021 target (SMMT, 2017).

Safety is one of the most important driving factors for the selection of material and design of a vehicle structure in the automotive sector. With the increasing awareness of car safety, governments and regulatory agencies have been passing stricter safety regulations for cars. In 2018, the European Commissions proposed a paradigm shift in standard vehicle safety equipment to improve overall road safety (European Commission, 2018b). The UK government adopted safety and environmental standards applicable to new vehicles to enhance road safety and reduce carbon emissions (Government Response, 2018). The automotive industry started to manufacture a safer car with improved crashworthiness. The term 'crashworthiness', defined as the ability of a vehicle to withstand a collision or crash with minimal bodily injury to its occupants, has been well understood and incorporated into current vehicle design (Singh, 2016). An effective way to improve crashworthiness is increasing the strength and ability to absorb the energy of safety components.

Due to the demand for reduced vehicle weight, improved safety and crashworthiness, lightweight alloys such as aluminium, magnesium, high strength steels (HSS) and advanced high-strength steels (AHSS) have been increasingly utilized and new forming technologies have been developed. Steels are still the dominant material in manufacturing cars today because of their relatively low cost, high strength and good weldability.

1.2 High strength steels for automotive applications

Steel, the material typically used in vehicle structures, has allowed for the economical mass production of millions of vehicles since 1920. In 1975, the average vehicle was manufactured with 55.9% mild steel and 3.6% medium and high strength steels. By 2007, the percentage of medium and high strength steels used in an average car had increased by over 230% (Posco, 2017). By selectively incorporating higher strength materials throughout the design, automotive manufacturers can balance safety and weight concerns and build both safe and efficient vehicles. High strength steels are primarily used in the automotive industry for the fabrication of parts of the body in white (BIW). The BIW components of the second generation Volvo XC90 is illustrated in Figure 1.2. These components are mainly structural components such as front bumper, B-pillar, roof rail and door beam.

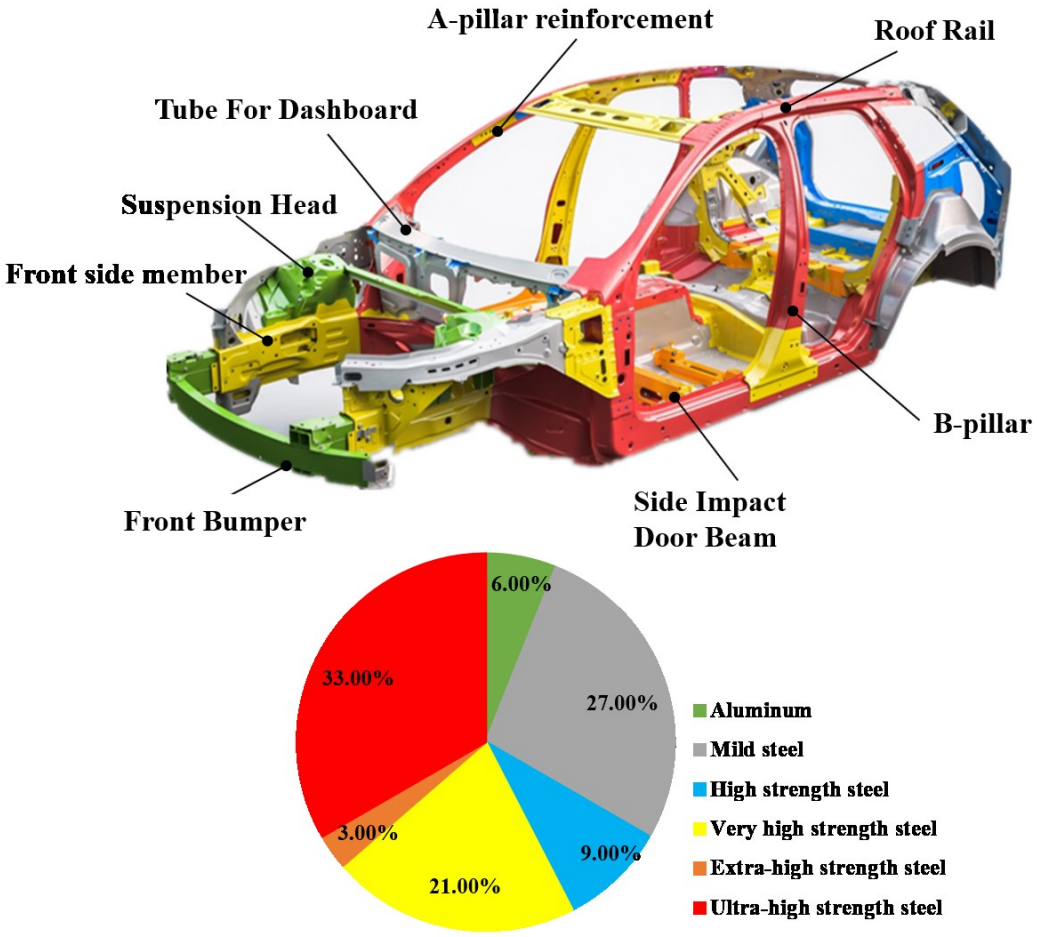

Figure 1.2 Components in the body in white (BIW) of the second generation of the Volvo XC90, utilising different AHSS alloys (Volvo, 2016).

1.3 Manufacturing methods for high strength steel components

AHSS sheets are generally formed into automobile structural components through cold or hot stamping processes. Cold stamping conventionally forms steel sheets with the tensile strength of up to 1000MPa. With the increasing tensile strength of the steels, cold forming of these steel sheets is difficult due to low formability and considerable springback, which limits its wider applications of complex components. To deploy ultra high-strength steel (UHSS) in mass scale automotive manufacturing, an efficient and economical sheet metal forming technique is required. Forming techniques such as hot or warm stamping are preferable for forming high strength parts from steel sheets (Mori et al., 2007). The main advantage of the hot stamping process is to manufacture springback-free (UHSS) components with 1500MPa tensile strength (Mori et al., 2017). Moreover, only about 20–40% forming force of cold stamping is required

to form UHSS in hot stamping processes (Li, 2013). In addition to the hot stamping process, warm stamping technology has been developed to improve the formability of the hot workpiece (Konrad and Feuser, 2015; Wang et al., 2017b). Compared to hot stamping, an intermediate cooling stage was conducted after the blank austenitization, followed by forming and quenching simultaneously in cold dies. Warm stamping technology has been primarily implemented on 22MnB5 boron steel and medium-Mn steel (Chang et al., 2016). The increasing demand for a higher efficiency forming process inevitably results in the requirement for total forming cycle time to be reduced. However, it is still challenging to improve the production rate in these forming technologies. The development of new forming technology may be an alternative solution to form UHSS into complex shapes whilst reducing the cycle time.

1.4 Aim and objectives of research

The aim of this study is to develop a novel forming technology entitled 'fast-warm stamping' (FWS) for manufacturing complex-shaped components from the MS1180 steel with desirable mechanical properties and microstructures in reduced cycle time. The MS1180 steel provides extremely high tensile strength but with poor ductility at room temperature which limits its further applications. The implementation of the proposed FWS technology was also conducted on 60Si2Mn spring steel by manufacturing a commercial disc spring. The following list of objectives was conducted to realise the aim of this work:

- Investigate material characterisation through experiments on the MS1180 steel including uniaxial tensile test, strength degradation test and metallographic test.
- Develop a further understanding of the influence of processing parameters on thermo-mechanical properties and microstructures and investigate the mechanism behind it.
- Validate the FWS process by forming U-shaped components and evaluate the post-form properties of formed components.
- Verify the experimental results via the Finite Element Analysis (FEA).
- Implement the FWS technology on 60Si2Mn steel by manufacturing a commercial disc spring with required dimensional accuracy and post-form properties.

1.5 Major tasks

To achieve the objectives, the following distinct tasks were completed:

1) Review of the state-of-the-art forming technologies for AHSS. Particular attention has been paid to hot and warm stamping processes.
2) Review of the effects of temperature, heating rate and soaking time on microstructure and mechanical properties of martensitic steels.
3) Conducted uniaxial tensile test to understand the flow behaviour and ductility of the MS1180 steel at various temperatures, heating rates and strain rates. Strength degradation tests are used to investigate the post-form hardness (PFH) at different conditions. Metallographic tests were performed to gain a better understanding of the relationship between microstructures and thermo-mechanical properties.
4) Conducted U-shaped forming tests using a dedicated pilot production to validate the feasibility of the FWS technology with the MS1180 steel.
5) Evaluated post-form strength and microstructure of fast-warm stamped components. The effect of forming temperature and forming speed on springback was investigated.
6) Developed a finite element (FE) model of the FWS process in PAM-STAMP and verified the FE model with experimental results.
7) Conducted a feasibility study of the FWS technology for 60Si2Mn steel. The proposed process was validated by forming disc springs. Additionally, the post-form properties of disc springs were evaluated.

1.6 Thesis structure

In this thesis, the novel forming technology ‘fast-warm stamping’ was developed to form complex-shaped parts from a given material in reduced cycle time.

Chapter 2 provides an introduction to AHSS and an overall review on the present forming technologies of AHSS. The effects of temperature, heating rate and soaking time on microstructure and mechanical properties of martensitic steels are reviewed.

Chapter 3 introduces experimental methods that characterise the thermo-mechanical properties and microstructural evolutions of the MS1180 steel under various FWS conditions.

Chapter 4 discusses the analysis of the experimental results. The effects of temperature, heating rate and strain rate on the thermo-mechanical properties are explored. Additionally, a discussion of the relationship between microstructures and mechanical properties is provided.

Chapter 5 presents the forming trials of the FWS process with the MS1180 steel. A study of springback of the formed components at various temperatures and forming speeds are given. Forming parts made of these materials are more affected by springback than parts made from conventional steel. An FE model is developed to predict the springback after forming which can minimize the risk of costly changes to tools. The FE simulation results are experimentally verified.

Chapter 6 presents a case study of the FWS process for manufacturing disc springs with 60Si2Mn steel.

Chapter 7 summarises the conclusions of the research and proposes suggestions for future study.

Chapter 2. Literature review on the forming technologies of advanced high-strength steels (AHSS)

2.1 Introduction to AHSS

Weight reduction and crashworthiness improvement of vehicles can be primarily realized by using materials with a high strength/weight ratio. Therefore, lightweight alloys such as advanced high-strength steels (AHSS) has been increasingly used over the years. AHSS are newer generations of steel grades which can provide superior strength-ductility combinations compared to conventional steels. These materials are uniquely characterised by microstructures and engineering capacities to meet the diverse functional performance demands of various applications (Bouaziz et al., 2013).

2.1.1 Development history of AHSS

High-strength low-alloy steels (HSLA steels) were the first widely used high strength steels (HSS) in automotive applications (Tamarelli, 2011). Compared to conventional carbon steels, HSLA steels can provide improved mechanical properties and greater atmospheric corrosion resistance. In general, the yield strength of HSLA steel grades ranges from 270 to 550MPa (Vasundhara et al., 2016). However, the trade-off between strength and ductility limited the applications and manufacturability of these steel grades. In order to meet the challenges of vehicles for stringent safety regulations and emissions reduction, the development of new generation steel materials with improved strength-ductility combinations was highly desirable.

The global steel industry has met this requirement via the development of new AHSS grades beginning the early 1980s (Bouaziz et al., 2013; Venezuela et al., 2015). AHSS are complex materials with multiphase microstructures resulting from precisely controlled thermo-mechanical processing. The microstructure of AHSS grades consist of a ferrite matrix,

martensite, bainite, and/or retained austenite in quantities and combinations, which can provide extremely high strength while maintaining good formability required for manufacturing. AHSS grades show superior strength with yield strengths greater than 550MPa compared to the HSLA steel grades while maintaining the same ductility. AHSS often has other advantageous mechanical properties, such as high strain-hardening capacity (Tamarelli, 2011). New grades of AHSS enable carmakers to reduce vehicle weight by 25–39% compared to conventional steel.

The first and second generation AHSS grades were developed to meet the functional performance demands of certain components over the last two decades. The first generation AHSS family includes Dual Phase (DP), Complex-Phase (CP), Transformation-Induced Plasticity (TRIP), and Martensitic (MS) grades. Members of the second generation include Twinning-Induced Plasticity (TWIP), Light-Steel with Induced Plasticity (L-IP) and austenitic stainless steel (AUST SS). Figure 2.1 shows the relationship between tensile strength and elongation percent of various steel grades. DP and TRIP steels are developed with excellent formability and high crash-energy absorption which have great performance in the crash zones of the vehicle. For structural components of the passenger compartment, an extremely high strength level steel grade above the HSLA steels is required. Martensitic and boron-based Press Hardened Steels (PHS) can provide UTS of up to 1500MPa which lead to improved safety performance. Austenitic stainless steel has excellent ductility while maintaining high strength compared to the first generation AHSS grades. The increased ductility of this steel allows for greater component complexity, which results in more manufacturing flexibility.

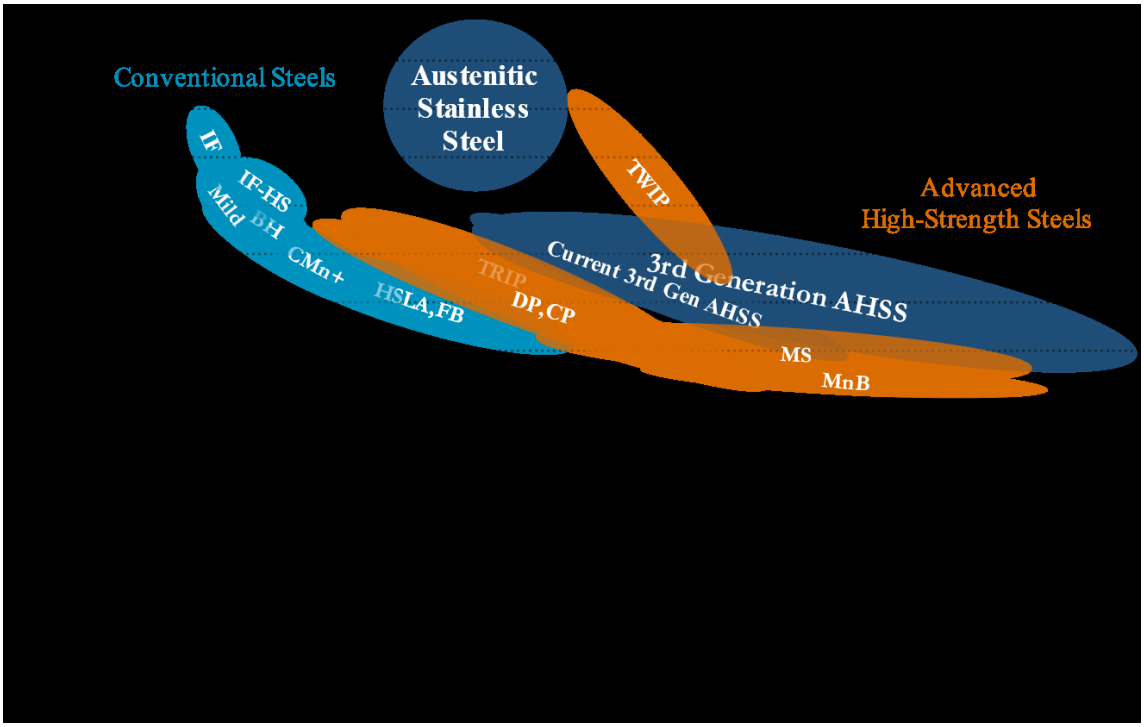

Figure 2.1 Strength-elongation relationships for different categories of steels (Keeler et al., 2017).

Recently, there has been increased interest in developing the third generation AHSS grades. Compared to present grades, 3rd generation AHSS are expected to achieve improved strength-ductility combinations with potential for more efficient joining capabilities at a significantly lower cost. In order to obtain these desired properties, a unique alloy and microstructure combinations are required (Matlock and Speer, 2009). Currently, the 3rd generation of steels is still in the early stages of development.

2.1.2 Introduction to press hardened steels (PHS)

Press hardened steels (PHS) have become a popular used material in car body manufacturing due to its excellent safety and lightweight potential. These steels are also known as hot-formed steels. Boron was added in these steel grades to improve quenchability. PHS undergo the hot stamping process to obtain a formed part with tensile strength up to 1800MPa. More details of the hot stamping process are given in section 2.2.1.

The most widely used PHS steel grade is boron steel 22MnB5, which offer a commercial name as Usibor1500 by ArcelorMittal. Different steel suppliers, such as ArcelorMittal,

ThyssenKrupp and SSAB, have been commercializing this steel under different names. The chemical composition of 22MnB5 born steel is shown in the Table 2.1.

Table 2.1 Chemical composition of 22MnB5 boron steel (ArcelorMittal, 2018b).

Composition	C	Mn	B	Si	P	S
Max. Wt%	0.25	1.4	0.005	0.4	0.03	0.010

Figure 2.2 indicates a schematic of the hot stamping process with changes in microstructure and tensile strength for 22MnB5 boron steel. As-received boron steel has a mixture of ferrite and pearlite microstructure with a UTS of approximately 600MPa and ductility of 15%. Following heat treatment and quenching process, the austenitic microstructure transforms to fully martensite which leads to an increased UTS up to 1800MPa and reduced ductility of 5% (Naderi, 2007).

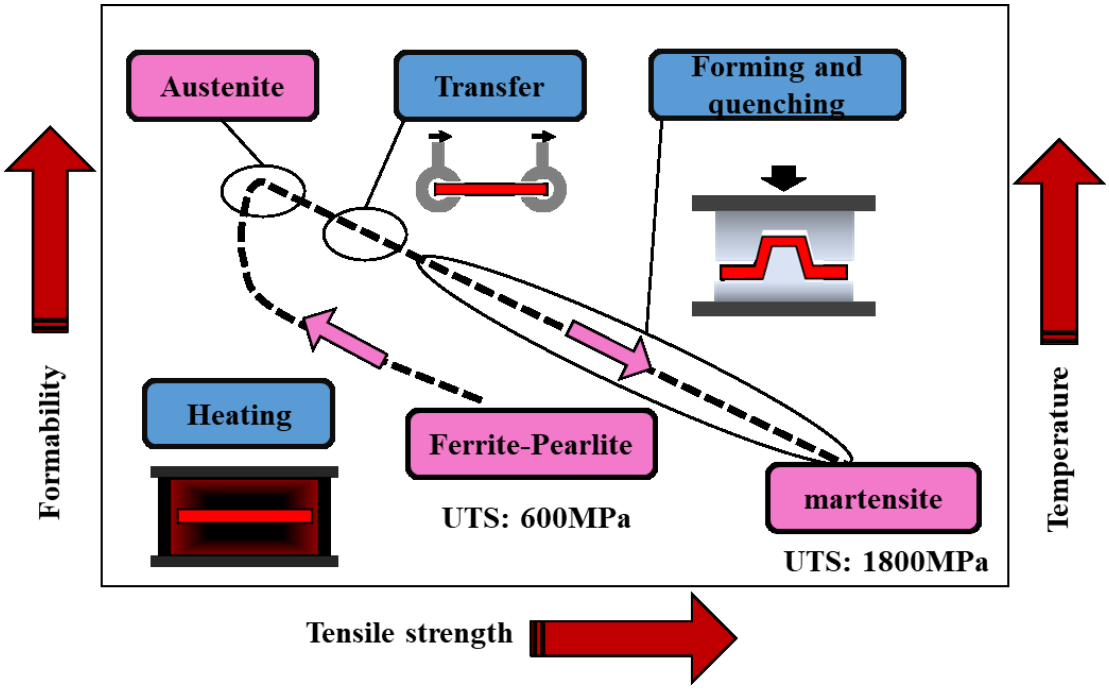

Figure 2.2 Mechanical properties and microstructure of 22MnB5 boron steel change during hot stamping process (Altan, 2007a).

A protection layer is necessary for boron steels to reduce oxidation and decarburization. One of the commonly used protective coatings of 22MnB5 is Al-Si coating. This protective layer is

transformed into an alloy layer of Fe-Al-Si during heating which is highly adherent to the substrate and has good corrosion properties (Altan, 2007a). Compared to uncoated steels, Al-Si coated blanks indicated good corrosion protection and improvement in weldability for subsequent process steps (Grigorieva et al., 2011).

2.1.3 Introduction to martensitic (MS) steel

Martensitic (MS) steel is one of the strongest AHSS grades, which is especially appropriate for weight saving applications for crash-relevant automotive components (Keeler et al., 2017). MS steel is manufactured by fast quenching low-carbon steel from the austenite phase into martensite. MS steel consists of fully lath martensitic microstructures and sometimes with low traces of ferrite, which offers a significantly improved strength-to-weight ratio compared to conventional cold rolled steels grades (Bouaziz et al., 2013). The strength of the material highly depends on the carbon content. Adding carbon element into MS steel leads to an increase in the hardenability and strengthening the martensite matrix. Figure 2.3 shows the hardness as a function of the carbon content of MS steels. The strength of MS steel increases linearly with increasing carbon content.

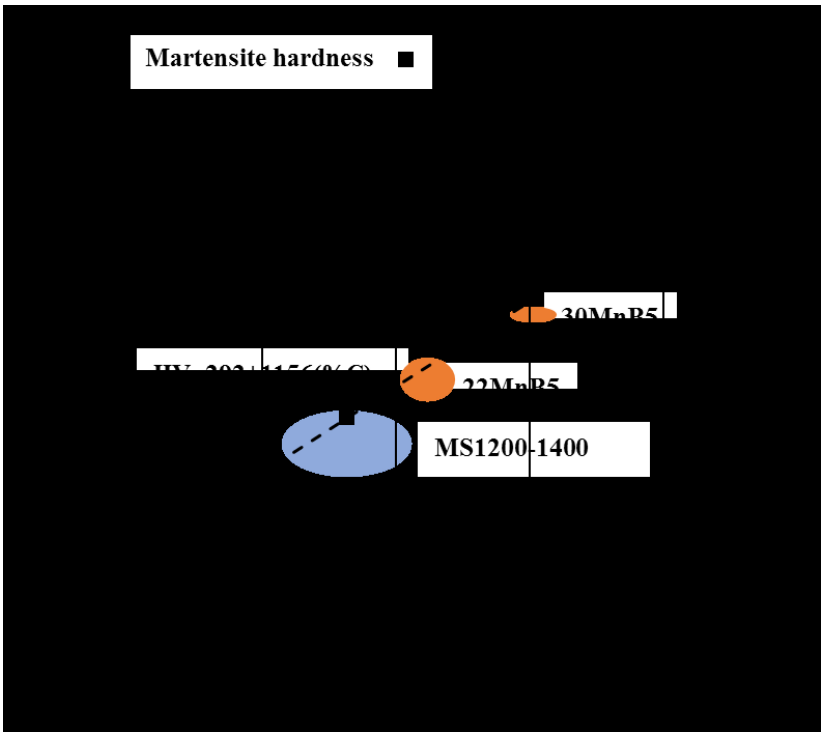

Figure 2.3 Hardness of martensitic steel as a function of carbon content (Hardy and NiobelCon, 2014).

The mechanical properties of MS steel such as ductility, toughness, hardness and delayed cracking resistance are severely influenced by heat treatment condition and alloying elements (Hardy and NiobelCon, 2014). The chemical composition of commercialized MS steel grades by ArcelorMittal is given in Table 2.2.

Table 2.2 Chemical composition of various martensitic steel grades produced by ArcelorMittal (ArcelorMittal, 2018a).

Composition	C	Mn	Si	P	S	Al
Wt%	0.13–0.35	1.20–3.00	0.50–1.00	0.02	0.025	≥0.010

MS steel is well-known due to its highest tensile strength but exhibiting the lowest ductility (Venezuela et al., 2015). The engineering stress-strain curves of MS steels and mild steel are shown in Figure 2.4. Compared to the mild steel, the MS steel grades have extremely high yield strength (1150MPa) and tensile strength (1400MPa) but low ductility (less than 5%). Currently, roll forming, bending or crash forming are widely used manufacturing operations to produce MS steel components with an ultimate tensile strength of up to 1700MPa (Thyssenkrupp, 2016). However, it is difficult to form complex shaped parts due to the poor formability at room temperature, which limits its application. Tempering is a popular method to increase the formability of as-formed MS steel but normally accomplished with a reduction in strength of material. To further expand the applications of MS steels, improved ductility whilst maintaining strength is increasingly necessary.

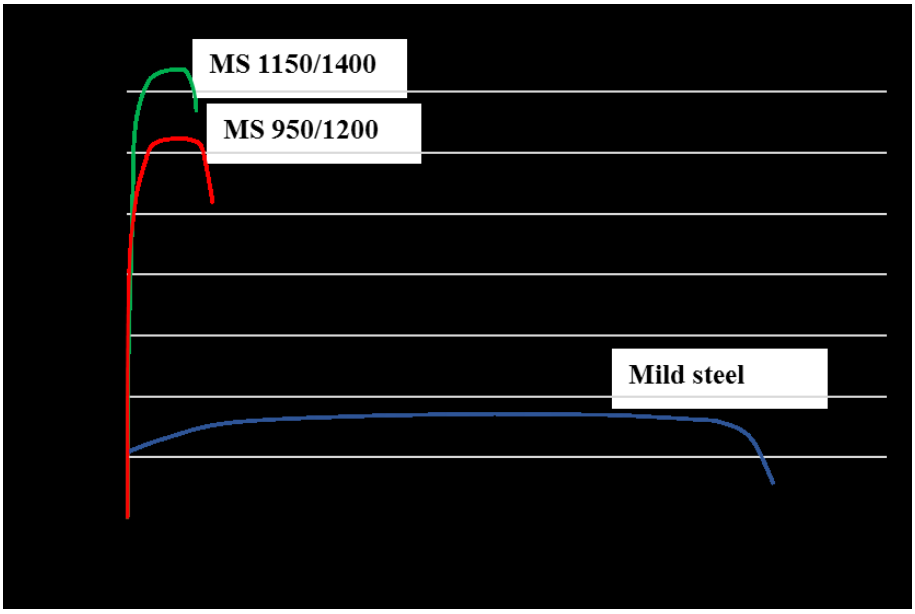

Figure 2.4 Engineering stress-strain curve for MS steels and mild steel (Keeler et al., 2017).

2.2 A review of forming technologies of AHSS

The varieties of AHSS grades exhibit extremely high strength which meets the increasing demands for weight reduction and crash safety improvement. However, the increase in strength and hardness is usually accomplished by a reduction in ductility. Conventional cold stamping is difficult for forming high strength steel sheets into complex components due to the lower formability. The other issues in cold stamping of AHSS sheets above 1.5GPa in tensile strength include excessive springback, short tool life and severe wear such as galling and seizure which need to be addressed. Hence, efficient and economical sheet metal forming techniques such as hot or warm stamping processes are preferable for manufacturing springback-free ultra-high strength steel parts having above 1.5GPa tensile strength (Mori et al., 2017).

2.2.1 Hot stamping process

2.2.1.1 Overview of hot stamping

Hot stamping (also called press hardening) was first developed and patented by a Swedish steel company, which used this process to manufacture products of high strength and wear resistance, such as saw blades and lawn mower blades (Berglund, 2008; Jonsson, 2008). The first press hardened component on automobiles was an intrusion door beam with reduced gauge and ultra-high strength, adopted by Saab Automobile AB for the Saab 9000 in 1984 (Aspacher, 2008).

In the past three decades, the hot stamping process experienced tremendous development with applications in the automotive industry. Currently, hot stamping is becoming increasingly popular in manufacturing body-in-white parts such as A/B-pillar, door beams, roof rails, and other structural members. The global production of hot stamped parts continuously increased from 3 million parts/year in 1987 to approximately 700 million part/year in 2010 (Gharbi and Palm, 2017).

A schematic diagram of the hot stamping process with temperature profile is illustrated in Figure 2.5 (Kyu et al., 2015). During the hot stamping process, the as-received sheet blank, which has a ferritic-pearlitic microstructure and medium tensile strength, is initially heated to austenitization temperature prior to forming and then soaked at that temperature for a prolonged period of time (usually 3–5 minutes) to enable the completion of austenite phase transformation. Afterwards, the blank is formed and quenched simultaneously in cold dies. The total cycle time for transferring, stamping and cooling in the die is 15 to 25s (Altan, 2007b). The quenching rate is sufficiently rapid at 50 to 100ºC/s to produce fully martensitic microstructure, which forms the basis for high strength products with strength levels above 1500MPa but a low elongation of about 5% (Hein et al., 2006).

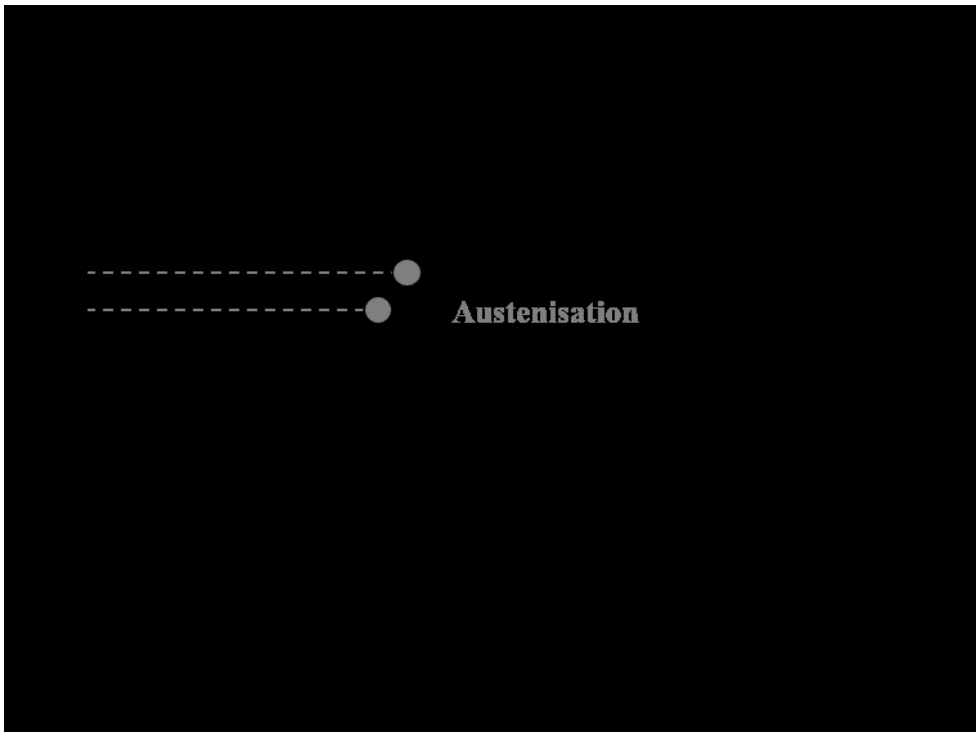

Figure 2.5 A schematic diagram of the hot stamping process with temperature profile.

The hot stamping process can be classified into two variants: direct and indirect. The processing routes of these two different stamping technologies are schematically presented in Figure 2.6. For direct hot stamping, blanks are austenitized in a furnace, transferred to the press, and subsequently stamped and quenched in cold dies. In the direct hot stamping process, the blank is formed and hardened in one tool set, which saves the cost of manufacturing and reduces the cycle time. However, this process is not necessary to form complex shaped parts, such as the inside and outside pieces of b-pillar and the inner plate of the threshold (Hu et al., 2017).

For the indirect hot stamping process, the blanks are first cold formed to near final shape in a conventional die set. The pre-forms are heated to the austenitization temperature in a furnace, followed by calibration and quenching in the pressing operation. This additional step is used to extend the forming limit of the material to produce highly complex components and reduce the abrasive wear on the die surfaces (Merklein and Lechler, 2006). The indirect hot stamping process is preferable to form complex shaped structural components.

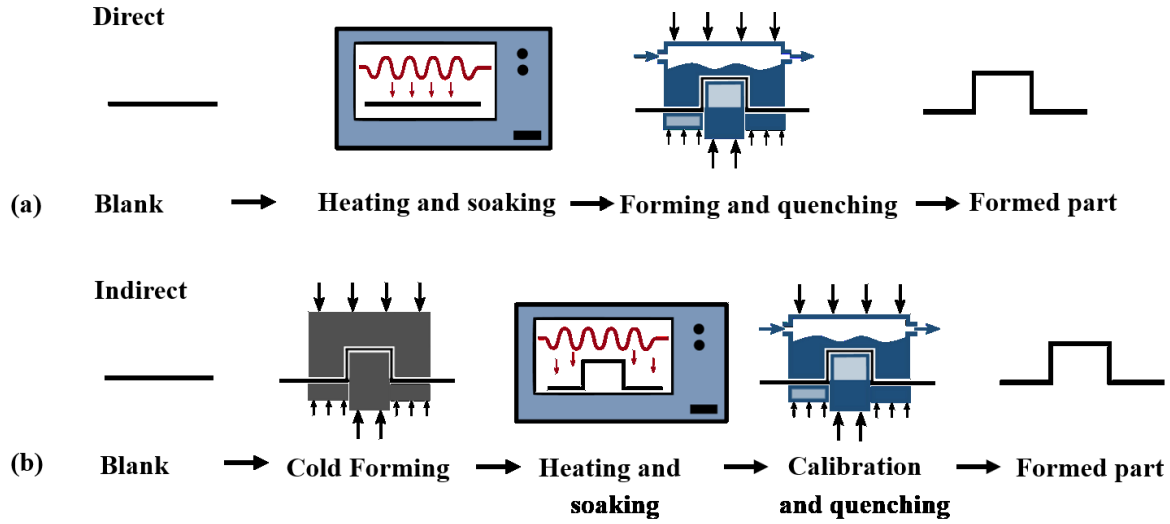

Figure 2.6 A comparison of the direct and indirect hot stamping process (Gharbi and Palm, 2017).

The hot stamping process has been extensively studied by investigating the effect of processing parameters on evaluation and prediction of thermo-mechanical properties during and after forming, design of forming tools and numerical modelling. This has also been addressed in several review papers on the hot stamping process published recently. Karbasian and Tekkaya (2010) reviewed the characteristics of hot stamping process steps by exploring thermal,

mechanical, microstructural and technological fields. Mori et al. (2017) performed a comprehensive overview of hot stamping technologies for UHSS, including quenchability, formability, heating and cooling methods and lubrication. Extensive research has been performed on the flow behaviour characterization of boron steels in the hot stamping process. Merklein and Lechler (2008) investigated the time-temperature dependent thermo-mechanical flow properties of 22MnB5 during the hot stamping process at a temperature of 500, 650 and 800ºC. Güler et al. (2014) further investigated the ductility behaviour and fracture mechanism of 22MnB5 boron steel at a broader temperature range from 400 to 900ºC. The 22MnB5 exhibited a low ductility at 700ºC which is attributed to the segregation of impurities to boundaries. Zhao et al. (2016) established an improved hot stamping process by rapidly cooling the hot blank prior to forming to 700ºC. The total elongation and the hardening exponent of 22MnB5 at 700ºC is 8.9% and 27.8% higher than at 900ºC.

The main advantage of the hot stamping process is to produce complex geometrical parts from UHSS sheet without springback and thermal-distortion. Additionally, the load required for hot stamping is relatively low with 20–40% of the load for conventional cold forming (Gucker, 2008). However, it is still challenging to further improve the production rate in hot stamping process. Productivity is limited by furnace residence time and quenching time. The increasing demand for a higher efficiency forming process inevitably results in the requirement for total forming cycle time to be reduced further (Karbasian and Tekkaya, 2010).

2.2.1.2 Heating methods

As discussed earlier, the first stage of hot stamping is heating the blank to the austenitization temperature. With current industrial technology, the roller-hearth furnaces are normally used in hot stamping production lines for continuously heating the blanks. In order to shorten the total cycle time, the furnace resistance time can be reduced by utilising fast heating technologies. Research has been carried out on developing various rapid heating approaches such as conduction (electrical resistance) heating, contact heating, induction heating and infrared heating (Mori et al., 2017).

- Resistance heating

Resistance heating is achieved by the use of an electric current to resistance heat the blank rapidly. It is mainly used for long components, such as pipes, rods and bands. Mori et al. (2005b)

developed a resistance heating equipment with a fast heating rate of 100°C/s, which has been used for hot and warm stamped UHSS parts. It was found that resistance heating attempted to maintain uniform temperature by preventing temperature reductions whilst the blank was clamped in the tool, as shown in Figure 2.7. In addition, resistance heating was found to be appropriate for partial heating of blanks for tailoring in hot stamping. Mori (2012) reported that resistance heating can minimize oxidation and enable mass production by preventing temperature reduction during transfer of the blank from furnace to die. However, rapid heating makes it difficult to control temperature uniformity for non-rectangular sheets (Mori et al., 2017).

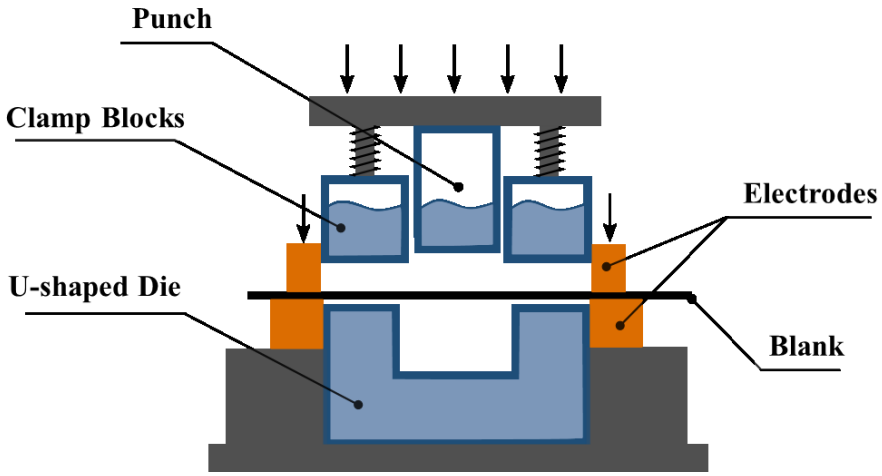

Figure 2.7 Diagram of a resistance heating method to produce rapid heating for hot stamping with a U-shaped die (Mori et al., 2005b).

- Contact heating

In the contact heating system, two large heating plates are first preheated to the required temperature by induction heating. Secondly, cold steel blanks are heated through conductive heat transfer by the lowering and contact with the pre-quenched plates, as shown in Figure 2.8. During heating, the steel blank is protected against oxidation and the temperature distribution is controlled through the optimization of contact plate temperature, contact pressure and contact time with the heating plates. Ploshikhin et al. (2011) developed this technique using an inductance heater to maintain two platens for 20–40s to complete austenitization at a temperature of 1050°C. Landgrebe et al. (2015) developed a partial contact heater for hot stamping processes with a reduced heating time of 15s to 950°C. The heating rate of contact

heating is highly dependent on the difference between platen temperature and blank temperature. A rapid heating rate is achieved when high contact pressures are applied between the blank and platen. In comparison to conventional furnace heating, contact heating offers greater energy efficiency as well as cost-savings (Mori et al., 2017).

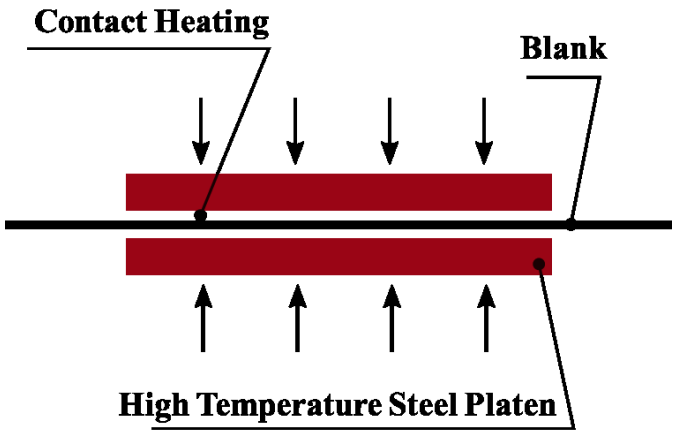

Figure 2.8 Contact heating of blank between heated plates (Ploshikhin et al., 2011).

2.2.1.3 Forming and quenching

In hot stamping, the blank is formed at a temperature close to the austenitization temperature with sufficient formability. Kusumi et al. (2014) achieved improved formability by preventing a temperature drop in the flange portions between the blank holder and the blank. Osakada et al. (2011) found that improvement of formability in hot stamping increased with increasing forming speed from 26mm/s to 149mm/s by forming a dome shaped part without fracture.

After forming, the hot austenitic blank is quenched in the closed cold tools until the entire martensite transformation of the part structure is completed. The quenching operation during the hot stamping process does not only affect the economy of the process but also the final properties of the component. The objective of the cooling duct design is to quench the hot part effectively and to achieve a cooling rate of at least 27°C/s while martensite forms (Li et al., 2014). Inevitably, an active cooling system is required to maintain low die temperatures during cooling. Figure 2.9 illustrates tool design with cool channels for hot stamping. Water has been used as cooling fluid for hot stamping to great effect. Naganathan and Penter (2012) found that tool steel with high heat conductivity is desirable to achieve rapid cooling rate.

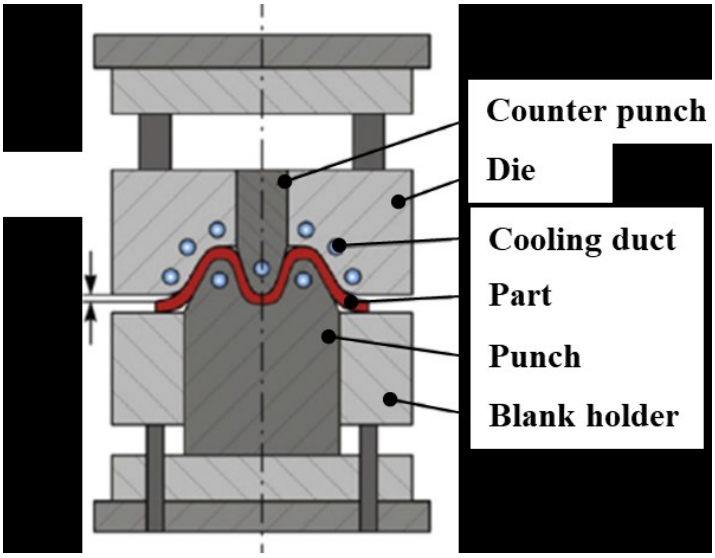

Figure 2.9 Tool design with cool channels for hot stamping process (Karbasian and Tekkaya, 2010).

2.2.1.4 Phase transformation during quenching

Phase transformation from austenite to martensite during quenching is crucial in the hot stamping process. Figure 2.10 shows the continuous cooling transformation (CCT) diagram for a typical 22MnB5 boron steel. The cooling rate for quenching is determined by the basic conditions to avoid the transformation of austenite into ferrite, pearlite, or bainite during quenching. The critical cooling rate of approximately 27 ˚C/s is shown which is the minimum cooling rate required to obtain a final microstructure that is complete martensite (Suehiro et al., 2003). The forming process must take place before the martensite start temperature is reached, otherwise crack formation due to higher strength and lower ductile yield of martensite occurs (Tekkaya et al., 2007) .

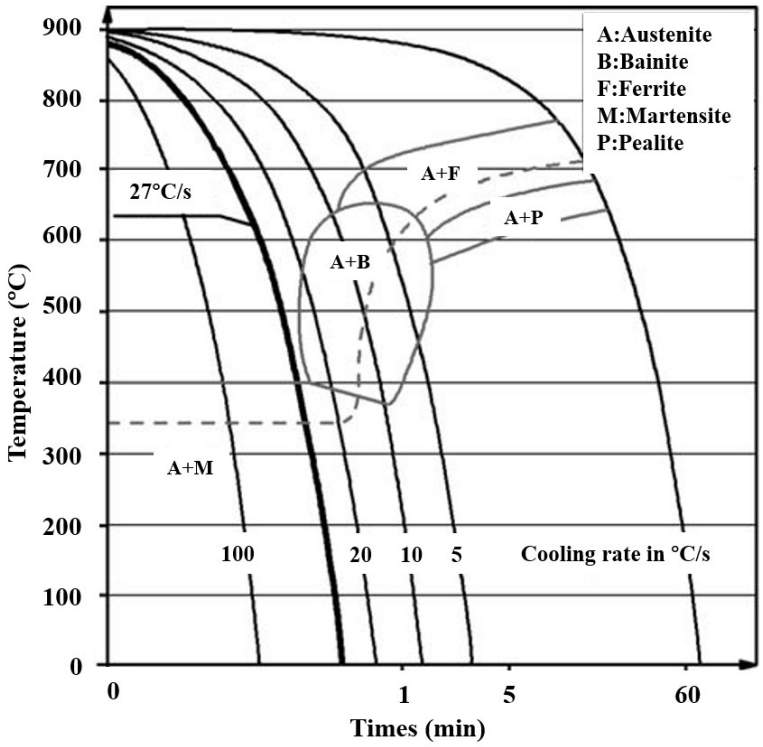

Figure 2.10 CCT diagram for a typical 22MnB5 boron steel (Tekkaya et al., 2007).

2.2.2 Warm stamping process

In the hot stamping process, blanks are commonly stamped at an initial forming temperature between 800 to 850°C. However, recent research has shown that the optimum forming temperature, at which the formability is maximised, is often 100–300˚C below the austenitization temperature (Konrad and Feuser, 2015; Zhao et al., 2016). As a result, a variant of hot stamping, called warm stamping technology has been developed which not only provides high production efficiency but also improved ductility of the hot workpiece. The temperature profile of warm stamping of steels is shown in Figure 2.10. The notable feature of the warm stamping process is to cool the hot workpieces to a certain temperature at an appropriate cooling rate usually using compressed gas or steel plate. Zhao et al. (2016) investigated a reduced forming temperature at 700–750°C of 22MnB5 at a period prior to forming. The blank exhibited superior formability and the warm-formed B-pillar showed a finer martensitic microstructure and more evenly distributed post-form strength due to a higher work-hardening exponent and ductility. Konrad and Feuser (2015) proposed a modified heat treatment process by investigating different intermediate temperatures and cooling rates to improve the ductility of 22MnB5 boron steel. It was found that the intermediate temperatures of 600°C and a fast

cooling rate of 15°C/s were beneficial for ductility and hardness. Tokita et al. (2017) investigated stretch formability of 980 MPa hot-rolled steel sheets in warm forming via spherical stretch forming tests at temperatures ranging from room temperature to 600°C. The total elongation increased from approximately 18% at 200°C to 40% at 600°C because of thermally activated mechanisms including boundary sliding and recovery became more prominent at a higher temperature.

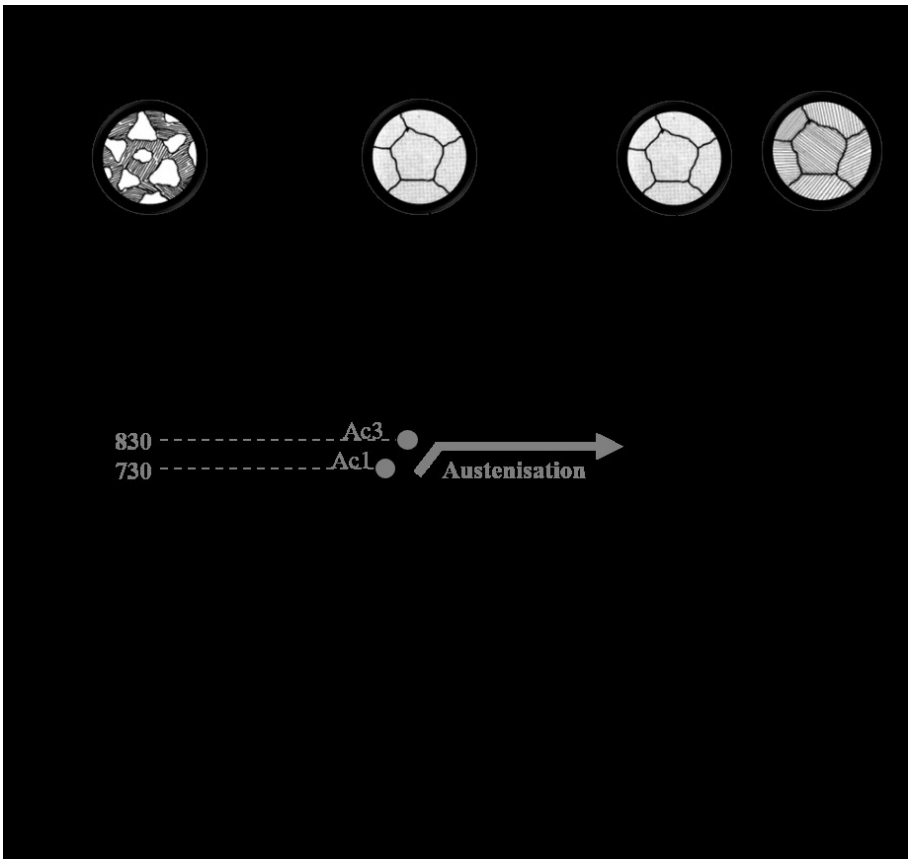

Figure 2.11 A schematic diagram of conventional hot stamping and warm processes with microstructure evolution.

Most recently, there has been extensive research regarding the hot and warm forming processes of other AHSS grades such as Medium-Mn steels (Wang et al., 2017b). Chang et al. (2016) investigated the optimal processing window for an improved warm stamping process of medium-Mn steel, which consists of austenitization temperature of 790–840°C, a soaking time of 4–7 min, an initial stamping temperature of 450–500°C, and a cooling rate of 10–60°C/s. The mechanical properties achieved by this optimised process were 1220 MPa yield strength, 1418MPa tensile strength, 11.1% elongation and 460HV post-form hardness. Li et al. (2017)

studied the characteristics of martensitic transformation and mechanical properties of medium-Mn steels and hot stamped boron steels in warm stamping processes. It was noted that final medium-Mn steel components exhibit well-balanced mechanical properties including 21.8% in tensile strength and 34.8% higher in total elongation than coated and uncoated 22MnB5.

2.2.3 Forming techniques of MS steel

2.2.3.1 Crash forming

Crash forming, a press forming method without blank holder, is an appropriate forming technology to manufacture MS steel parts. Figure 2.11 shows the schematic diagram of crash forming. In crash forming, the steel sheet is bent around the die shoulder, which is expected to reduce bending deformation that causes wall warp (Yoshida et al., 2013). However, the excessive springback and low tool life still remain as crucial problems when the MS steel is crash formed at room temperature. Calibration is integrated to improve the dimensional accuracy of the formed components (Thyssenkrupp, 2016).

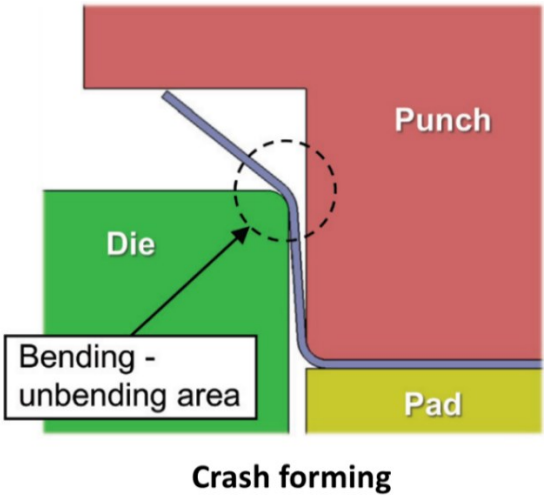

Figure 2.12 A diagram of crash forming process for MS steel without blank holder (Yoshida et al., 2013).

2.2.3.2 Roll forming

Roll forming is one of the fastest developing forming techniques to produce MS steel parts in the automotive industry. Compared to other forming operations, which have various combinations of stretching and drawing, roll forming only has a bending process using rotational tool motion to manufacture open and closed parts at ambient temperature (Kim et al.,

2017; Traub et al., 2017). Figure 2.12 illustrates the forming strategies of roll forming. In roll forming, a long strip of sheet metal passes through a series of roller dies and is progressively formed to the desired cross-sectional profile. The roller die consists of a series of stands. Every stand comprises of at least two work rolls that plastically deform the workpiece into the desired final shape by imposing bending stresses (Taylor, 2016).

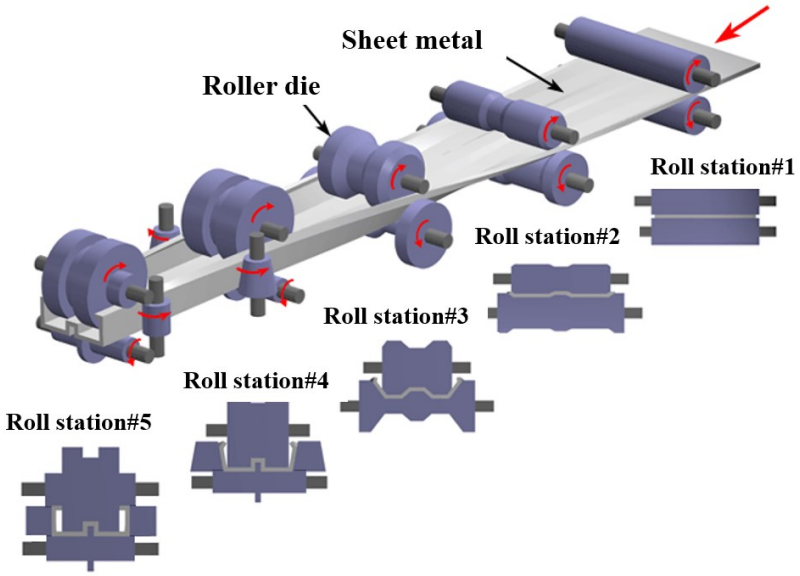

Figure 2.13 Schematic diagram of cold roll forming for MS steel products (Taylor, 2016).

Roll forming is ideal for constant-profile components with greater uniformity and consistency throughout the length of the part. Additionally, roll forming can eliminate multiple stage operations such as notching, slotting, and punching (Semiatin, 2006). Compared to the conventional stamping method, the roll forming process is a cost-effective and highly production efficient forming technology, which is an alternative solution to form UHSS to complex geometrical part with a cross-sectional profile.

2.2.4 Springback behaviour

When sheet metal is plastically deformed into a part, the shape of the formed part always deviates somewhat from the shape of the punch and die after removing the tooling. This dimensional deviation of the part is determined as springback. Springback problem is defined as one of the leading roadblocks hindering productivity of forming AHSS grades. It is undesirable which leads to misalignment in the assembly process. In order to cope with

springback, adjustment of tools is required, which leads to an increase in the die manufacturing cost and other technical problems.

Springback is caused by the elastic redistribution of the internal stresses of the metal sheets in unloading. In general, the amount of springback experienced in AHSS parts is greater than that experienced in conventional steel grades, due in large part to the progressively higher initial yield strengths and the greater work hardening rate that significantly increases the yield strength during forming.

Numerous experimental techniques and various procedures have been developed to study and characterise springback of sheet metals. The widespread methods for springback characterization are cylindrical bending, such as U-shape bending, V-shape bending and flanging (Burchitz, 2005). A standard method was established from NUMISHEET 2011 to measure the springback of a U-shaped part, as shown in Figure 2.13. The angle between bottom and sidewall θ_1 and the angle between the flange θ_2 are used for springback evaluation. Optical scanning system (ATOS system by GOM) and the contact profile measurement system (Coordinate Measuring Machine) are typical equipment to perform springback measurements with good accuracy (Bhattacharya et al., 2011).

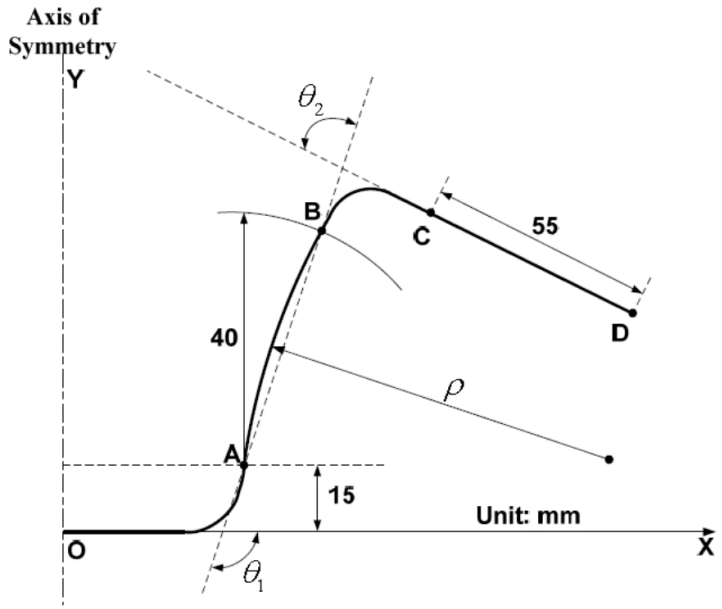

Figure 2.14 Benchmark profile and parameters of U-shaped springback (Kwansoo et al., 2011).

2.2.4.1 Effects of forming parameters on springback

Extensive research has claimed that hot and warm stamping processes for AHSS are preferable methods to overcome the aforementioned drawbacks (Yanagimoto et al., 2005). In such forming processes, the amount of springback is influenced by many factors including temperature, blank-holding force, forming speed, friction coefficient, die radius and punch and die clearance. The effects of forming temperature and forming speed are discussed in further detail below.

- Effect of forming temperature on springback

Springback behaviour for hot stamping is more complicated than that for cold stamping because of the addition of thermal effects such as thermal expansion (Nakagawa et al., 2018). It was noted that numerous studies proved springback decreased with increasing forming temperatures. Yanagimoto et al. (2005) measured the springback by performing V and hat-shaped bending tests for high strength steel sheets for different temperatures from 273K to 773K. The springback for formed components markedly decreased when the temperature was above 750K, which is approximately the critical temperature for the onset of ferrite recrystallization. Mori et al. (2007) conducted U-shaped bending tests of various high strength steels at a temperature range from 300 to 800°C. Figure 2.14 indicates the evolution of springback as a function of forming temperature. Compared to cold stamping, the springback decreased at hot/warm stamping conditions, as shown in Figure 2.14 (a). The authors' found that springback-free parts can be formed when the temperature is above 800°C due to significantly reduced strength of material.

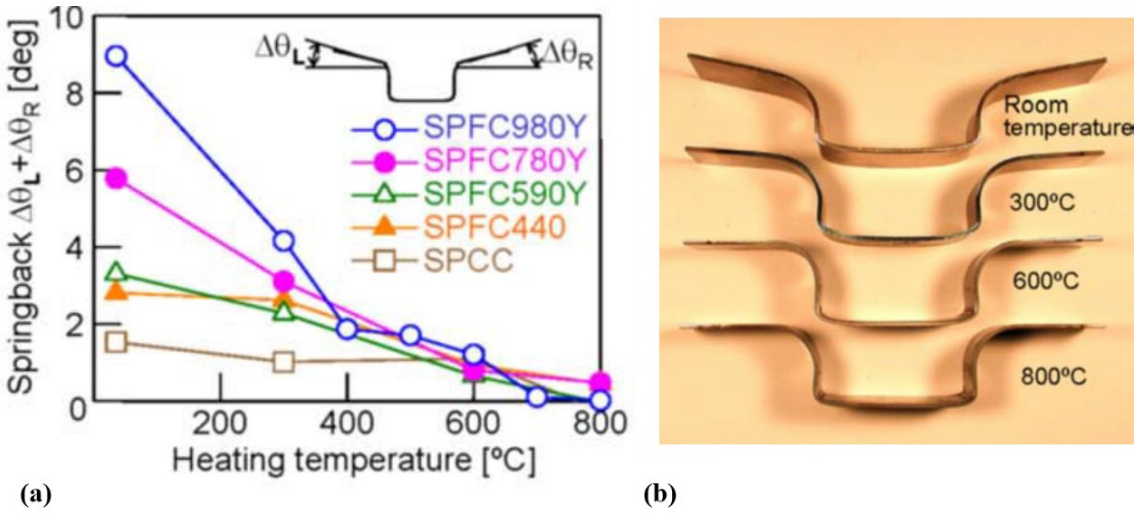

Figure 2.15 (a) Relationship between springback of high strength steel sheets and forming temperature (b) U-shaped components formed at different heating temperatures (Mori et al., 2005a)

- Effect of forming speed on springback

Forming speed is one of the key parameters affecting springback behaviour of the material. Saito et al. (2018) experimentally investigated the effects of forming speed and temperature on springback of U and V-shaped components formed from of HSS. It was found that the springback slightly increased at a higher forming speed of 10mm/s compared to 2mm/s, as shown in Figure 2.15. Choi and Huh (2014) performed tests a wider range of forming speeds (0.07, 0.7, 7 and 70mm/s) via U-bending tests of SPCC and DP780 steel sheets. The authors' reported that the amount of springback of SPCC steel decreased but springback of DP780 steel increased with increasing punch speed. This phenomenon was explained by the two steels exhibiting different strain rate sensitivity of the material. Strong strain rate hardening behaviour of DP780 steel leads to considerable springback at a higher forming speed. The effect of the forming speed on springback behaviour of HSS is not as severe compared to the effect of temperature.

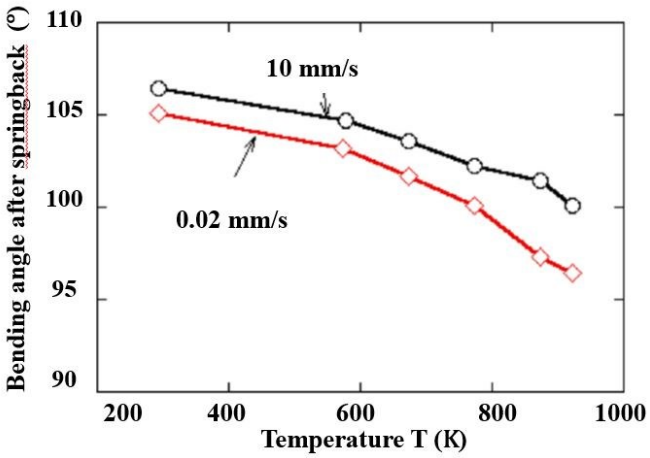

Figure 2.16 Bending angle corresponding to springback in U-shape bending (Saito et al., 2018).

2.2.4.2 Springback prediction by finite element (FE) simulation

Correct prediction of springback is becoming more important for the design of forming processes and tools by reducing the tool refining cost. Finite Element Analysis (FEA), which is a computer-based aid simulation method, has become a rapid and cost-effective tool for process and tooling design. It has been increasingly used in sheet metal forming due to a significant reduction in the development time and cost. Commercial FE simulation software such as PAM-STAMP and Autoform has been utilised to model forming processes and identify physical parameters that are sensitive to springback (Biradar and Deshpande, 2014; Wang et al., 2017a).

Extensive studies have been carried out on the basic springback characteristics of high strength steels in warm and hot stamping processes both numerically and experimentally. V and U-shaped bending of 980MPa strengthened steel sheets have been used to investigate the springback at various conditions followed by a numerical analysis using the analytical material model to determine the effects of stress relaxation and unloading crdeep (Saito et al., 2018). The springback evaluation of DP980 steel was conducted on S-rail part geometry at different forming parameters, such as forming temperatures and bending speeds, and FE simulations have shown accurate estimations of springback (Wang et al., 2017c). Shah et al. (2011) performed experimental and numerical studies on the effect of parameters such as sheet thickness, sheet anisotropy and die radii on spingback of a U-shaped part. Figure 2.16 (a) and (b) show a schematic diagram of a U-shaped component stamping tool set and developed FE

model setup, respectively. Despite recent developments in FE analyses for hot and warm stamping processes, limited work has been performed on the study of springback for MS steel at warm stamping temperatures at a fast heating rate. In this present work, both experimental and FE simulation methods have been used to investigate the springback characteristics of MS steel in U-shape bending at cold and fast-warm stamping conditions.

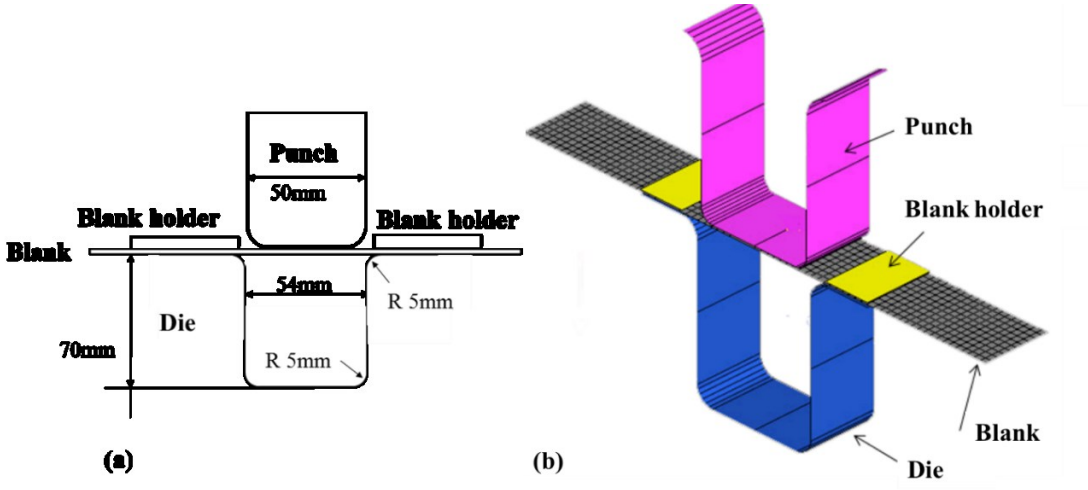

Figure 2.17 (a) Schematic diagram of the U-shaped component stamping tool set (b) FE model setup for springback prediction (Shah et al., 2011).

2.2.5 Advantages and limitations of conventional forming processes

The above-mentioned hot/warm stamping technologies can produce complex shaped UHSS parts due to the improved formability at a higher temperature. Additionally, higher geometrical accuracy is obtained in the formed parts because of the significantly reduced springback. However, despite these advances, the present hot and warm stamping processes still require a prolonged period of soaking time at elevated temperatures to obtain maximum content of martensite as well as achieve the required coating (Ormaetxea et al., 2013). It is challenging to further improve the production rate in these processes. Great efforts have been made to shorten the cycle time in the hot and warm stamping processes and it is thus extremely difficult to shorten the cycle time further (Mori et al., 2005a). In terms of roll forming, the main problem is a drastic change in the requirements and expectations of customers leading to high tool costs. Therefore, the development of new forming technology may be an alternative solution to form UHSS into complex shapes whilst reducing the cycle time.

2.3 Evolution of mechanical property and microstructure during heat treatment of martensitic steel

Martensite is a highly supersaturated solid solution of carbon in iron steel, which is the hardest phase in steels but normally very brittle. In order to suppress brittleness and enhance toughness, fracture resistance and ductility without a great loss of strength, heat treatment is generally performed on martensite in MS steel (Sauveur and Martens, 1900). This heat treatment is known as tempering, which can lead to dramatic changes in the mechanical properties of MS steels due to microstructural changes. During tempering treatment, the martensite eventually decomposes into equilibrium phases, ferrite and carbides(William Chandler Roberts-Austen, 1914). Extensive research has been performed on the influence of process variables of tempering including temperature, time and chemical composition including carbon content and alloying elements on the microstructure and mechanical properties of tempered MS steels (Bhadeshia and Honeycombe, 2017; Krauss, 2016).

2.3.1 Effect of temperature on the microstructure and mechanical property of steel

Over the last four decades, evolution of mechanical property and microstructure in the tempering has been comprehensively studied on various steel grades (Liu et al., 2016). The usual tempering temperature is between 200 and 700°C allowing for tensile strengths between 1700 and 800 MPa, an increase in toughness and ductility with reduction in tensile strength (Steve, 2001). Figure 2.17 shows the hardness as a function of tempering temperature for steel with different carbon contents tempered for 1 h (Hardy and NiobelCon, 2014). The as-quench MS steel has a martensitic microstructure and the hardness of the MS steel largely depends on the carbon content. Therefore, the highest hardness is achieved on the MS steels for alloys with 0.4 wt% carbon content. As low tempering temperatures ranging from room temperature to 200°C, it is observed that the ε epsilon carbide precipitated from patent martensite in medium carbon steels (C>0.2 wt%). During this temperature range, the carbon segregates to dislocation in low carbon steels (C< 0.2 wt%). Meanwhile, no carbide precipitation was found (Olson and W.S., 1991). The effect on the hardness of low carbon steels is negligible. When tempering temperature increases above to 200°C, the strength undergoes a rapid reduction in carbon steels

due to the fact that the solid solution of carbon content in patent martensite is continuously reduced. The ε carbide which eventually precipitated at lower temperatures is gradually replaced by rod-shaped carbide named cementite (known as θ carbide) particle within martensite crystal boundaries and prior austenitic boundaries. Krauss (2016) proved these carbides lead to a reduction in toughness and ductility. As tempering temperature increases from 400 to 600°C, spheroidization of cementite particles takes place and appreciable recovery of the dislocation substructure occurs. Finally, at 600 to 700°C, recrystallization of the martensitic substructure occurs. The final microstructure is an equiaxed ferrite containing a coarse dispersion of spheroidal cementite.

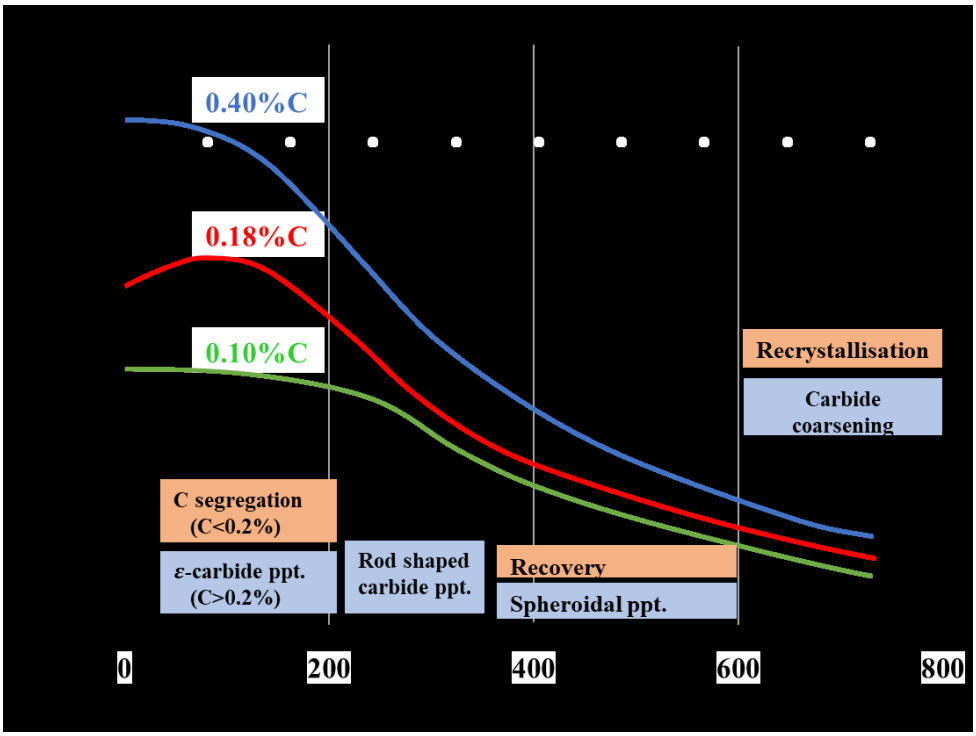

Figure 2.18 Hardness as a function of tempering temperature for various carbon content tempered for 1h (Hardy and NiobelCon, 2014).

Krauss (2014) investigated the effect of tempering temperature on mechanical properties including ultimate tensile strength (UTS), yield strength (YS) and reduction area (RA) for 4340 steel, as shown in Figure 2.18. As-quench 4340 steel was tempered for 1 hour at different temperatures from 100 to 650°C. The UTS of 4340 steel decreased linearly with increasing heating temperature since the solid solution of carbon in martensite matrix reduced. The YS increases slightly at low tempering temperature and then decreases with further increasing

temperature. The retained austenite in the steel transforms to martensite at low temperature which leads to YS increasing. The elongation of 4340 steel improved at a higher temperature.

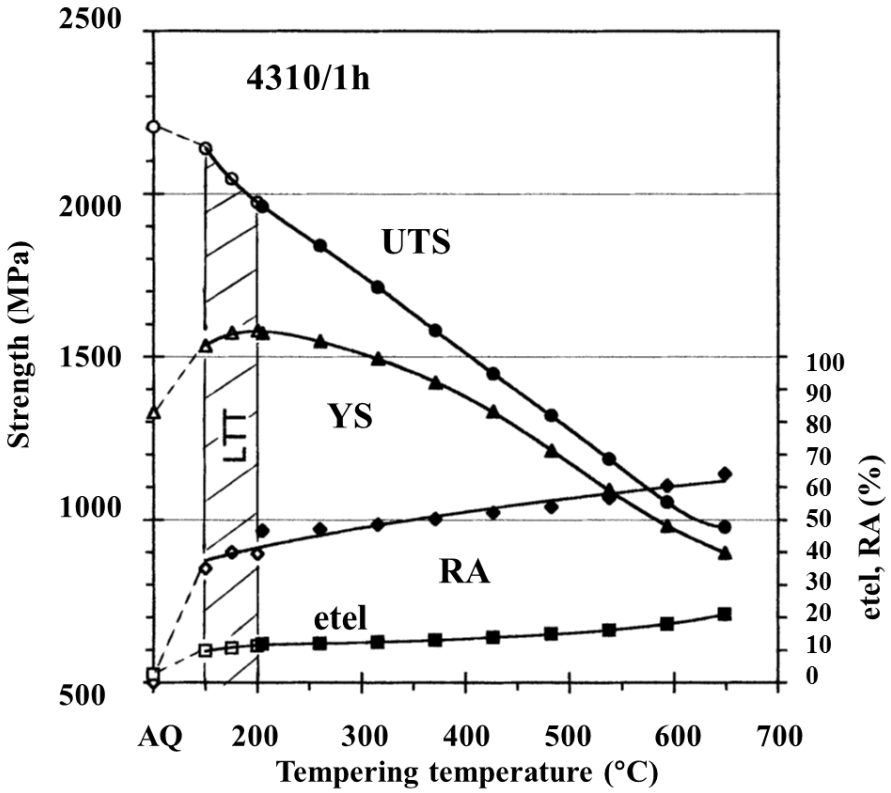

Figure 2.19 Evolution of mechanical properties of hardened 4340 steel as a function of temperature (Krauss, 2014).

Samuels (2014) explored the microstructural changes in pearlitic structures and substructures such as cementite and other carbides by using light microscopy when various steels grades were heated at subcritical temperatures. Zhao et al. (2018) systematically studied the evolution of microstructures, toughness and tensile properties with tempering temperature in the 3Mn-Si-Ni martensitic steel via transmission electron microscope (TEM) characterization. Figure 2.19 shows the TEM micrographs as the specimens were tempered at low temperature of 320°C. The parallel lath martensite can be identified clearly in the bright TEM images. The diffraction patterns show the cementite precipitated in the martensite meanwhile the retained austenite decomposed. When tempering temperature increased to 550°C, a strong recovery was found in TEM micrographs which induced the martensitic boundaries to blur and even disappear as

shown in Fig 2.20. The diameter of cementite became larger at around 20–50 nm compared to that after tempering at 320°C.

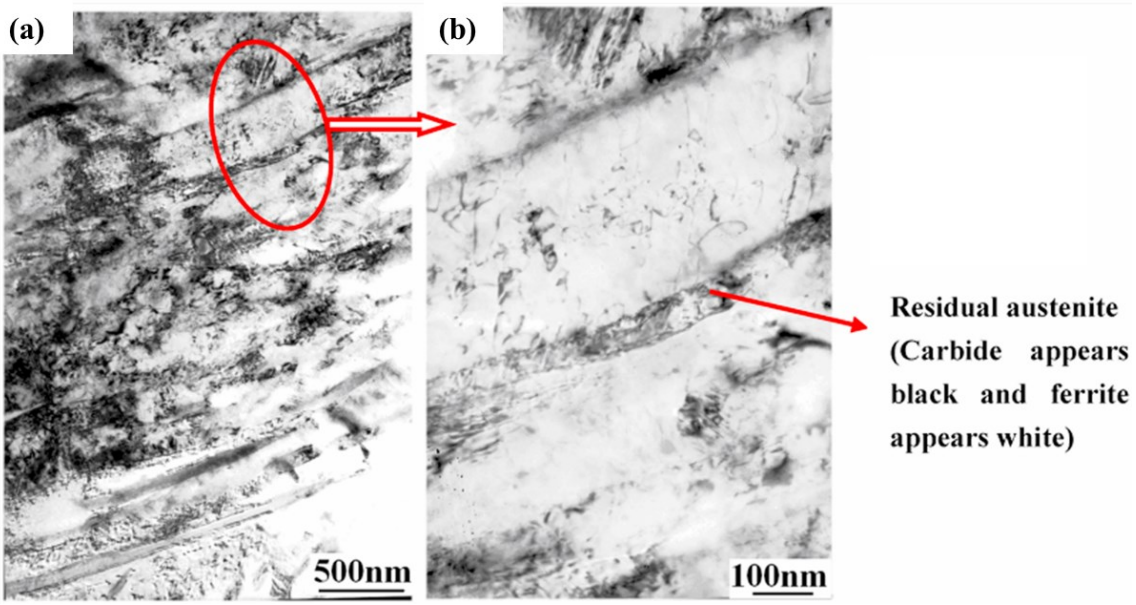

Figure 2.20 TEM images after tempering at 320°C (a) martensitic laths (b) local magnification of circled part showing cementite and decomposition of residual austenite (Zhao et al., 2018).

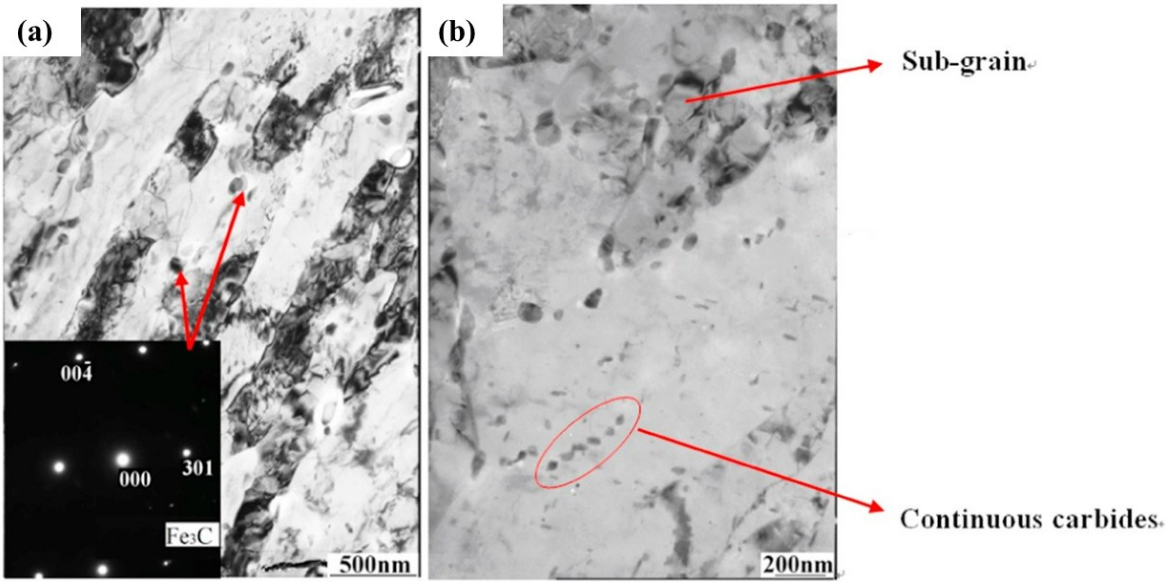

Figure 2.21 TEM images after tempering at 550°C (a) blurred martensitic laths and cementite (b) continuous distribution of carbides (Zhao et al., 2018).

2.3.2 Effect of soaking time and heating rate on the microstructure and mechanical property of steel

In general, a prolonged period (longer than 1 hour) is required in the conventional tempering process to balance the mechanical properties of steels which is time and energy intensive. Recently, rapid tempering by energy-saving manufacturing processes such as induction heating has been increasingly used. It was found that the rapid tempering process not only for reduces processing time but also refines the microstructure (Mostafaei and Kazeminezhad, 2016). Rapid tempering process can be achieved by reducing the soaking time and increasing heating rate. Saha et al. (2016) examined the various thermo-mechanical processing methods including furnace heat treatment, Gleeble heat treatment, diode laser welding and fiber laser welding on 0.24%C steel on the mechanical properties and microstructure characterization of tempered martensite. It was found that the slow heated cycles induced approximately 14.3% lower nanoscale hardness due to more microscopic structural softening.

Judge et al. (2018) achieved an improvement in strength-toughness performance in 1s short-time soaking and rapid tempering of 4340 steel compared to conventional tempering with 1h soaking. The impact toughness increased by over 43% and UTS enhanced by over 0.5 GPa. Raji and Oluwole (2012) found the YS and UTS of low carbon steel decreased with increasing soaking time which is associated with recrystallization and grain growth.

Revilla et al. (2014) found that a higher heating rate associated with short soaking time induces an improvement in hardness of 0.42%C low alloy steel. Figure 2.21 shows the residual hardness of this high strength low alloy steel increases with increasing heating rate and reduced soaking time. For each heating rate, the hardness decreases with the increasing holding time from 2 to 1260 s. Figure 2.21 (b) and (c) indicates the carbide precipitated inside the lath martensite grain and on the grain boundary. The results show that with a long soaking time and slow heating rate, the noticeable larger size of carbides is observed. For short soaking time of 2 seconds, the fast heating rate of 100°C/s improves residual hardness by over 15% compared to that heated at a slow heating rate of 1°C/s. However, using ultra-fast heating rate has not been extensively explored in flow behaviour, ductility and fracture mechanism at elevated temperatures. It is necessary to investigate these process variables and obtain a better understanding of the mechanism behind it.

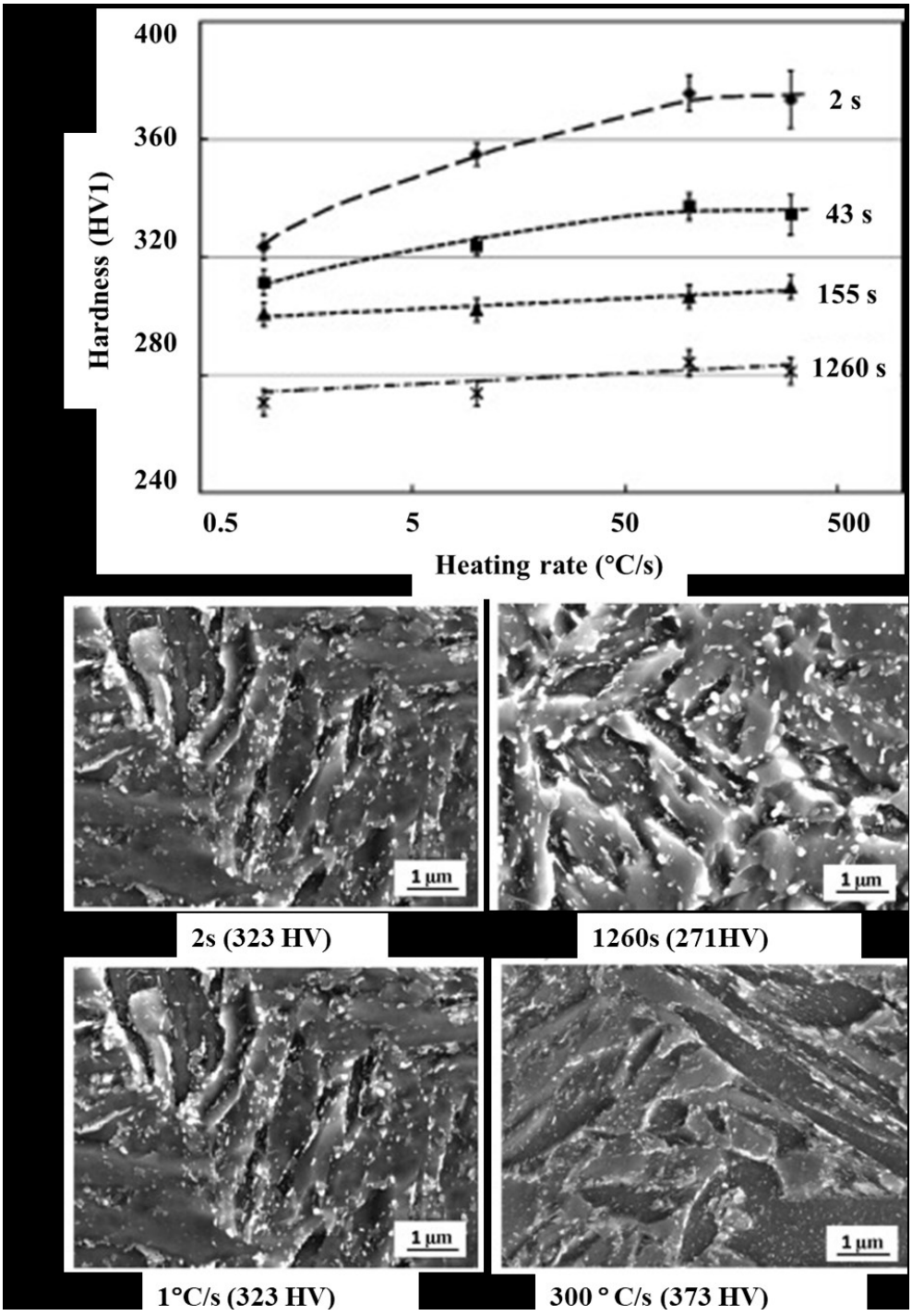

Figure 2.22 Variation of mechanical properties and microstructures of the 0.42%C low alloy steel as a function of heating rate and soaking time at the 700°C tempering treatment (a) evolution of residual hardness (b) SEM micrographs showing the carbide precipitation at different soaking periods (c) SEM micrographs showing the carbide precipitation at different heating rates (Revilla et al., 2014).

2.4 Summary

Conventional forming technologies for producing UHSS parts and the associated studies on microstructural and mechanical properties of MS steels have been reviewed. It was found that above-mentioned hot and warm stamping processes can manufacture complex shaped MS steel parts with excellent geometrical accuracy. The processing parameters including temperature, soaking time and heating rate have significant effects on microstructures and mechanical properties of MS steels. Fast heating technology is primarily utilized in hot stamping process and tempering treatment. Most research on forming MS steel components has been performed at room temperature. Limited work has been performed on the flow behaviour of MS steel at warm stamping temperatures ranging from 300-500°C at a fast heating rate, where formability of high strength steel sheets is further improved. To further expand the applications of MS steels, improved ductility whilst maintaining strength is increasingly necessary. To address this issue, a novel sheet metal forming process, entitled 'fast-warm stamping' (FWS), is developed in this research aiming to produce MS1180 steels part of complex geometry with desirable mechanical properties in reduced cycle time.

Chapter 3. Experimental programme

This chapter presents experimental work conducted on martensitic steel MS-W900Y1180T (MS1180). Firstly, the concept of the FWS process for the MS1180 is demonstrated and the FWS is compared with other conventional forming technologies. Secondly, thermo-mechanical properties characterization of the MS1180 steel were performed through uniaxial tensile tests and strength degradation tests. The ductility of the MS1180 steel was evaluated via tensile tests with variables such as temperatures, strain rates and heating rates. The strength degradation tests were conducted to characterise the post-form strength (PFS) of the MS1180 steel under the fast-warm stamping (FWS) conditions by comparing the residual hardness of heated specimens to prior to forming conditions. Finally, A forming tool set was designed, fabricated and assembled on a novel lab-scale production line called *Uni-form*, which enabled fast-warm stamping tests on the MS1180 steel to be realised and verified. Springback of the MS1180 steel was evaluated after bending at various temperature and forming speeds. Post-form strength of formed parts at different locations was characterised through uniaxial tensile tests at room temperature. In addition, metallographic characterizations were performed on as-received and deformed MS1180 steel specimens using electron microscopy to study microstructure evolution.

3.1 Testing material

The testing material for all tests was hot rolled martensitic grade (MS-W900Y1180T) steel sheet developed by ThyssenKrupp steel. The chemical composition (wt%) is given in Table 3.1.

Table 3.1 Chemical compositions of the MS1180 steel (wt%).

Composition	C	Mn	Si	P	S	B	Al	Cr
Wt%	0.25	2.50	0.80	0.06	0.015	0.005	0.015	1.20

Dog bone-shaped tensile samples were waterjet cut from as-received material. Uniaxial tensile tests were performed at a strain rate of 0.001/s on an Instron machine following the international standard ASTM E8. Mechanical properties of the MS1180 steel are presented in Table 3.2. The initial thickness of the MS1180 steel sheet was 1.6mm. The as-received MS1180 steel used for this study exhibited 930MPa yield strength and 5% uniform elongation at room temperature. Microhardness of as-received steel sheets were tested using a Vickers indenter with a load of 100N(HV10) and the mean hardness value obtained for the as-received material was approximately 400HV.

Table 3.2 Mechanical properties of as-received martensitic steel.

Type of steel	Tensile strength (MPa)	Yield strength (MPa)	Young's modulus (GPa)	Uniform Elongation (%)	Vicker's hardness (HV_{10})
MS-W 900Y1180T	1220	930	210	5	400

3.2 The concept of the FWS process of the MS1180 steel

The FWS process was expected to use ultra-fast heating of a steel blank to an appropriate temperature, whilst minimizing the major negative changes to microstructure which are detrimental to the post-form strength. Using the proposed method, a similar strength of as-received material can be retained in the formed part while the cycle time and energy costs are reduced. The feasibility of the FWS technology was initially studied on the MS1180 steel. Moreover, the proposed forming process was also verified by using other materials, such as spring steel and thermoplastic composite. The detailed results and discussion of the implementation of the FWS technology of spring steel and thermoplastic composite are presented in Chapter 6 and Appendix A, respectively.

Figure 3.1 indicates the schematic diagram of the FWS process of the MS1180 steel combined with microstructural evolution. In the proposed fast warm heating method, the MS1180 blank with desired mechanical properties and microstructures is heated rapidly at an ultra-fast heating rate to an appropriate temperature at which the formability of the blank is sufficient to form the

part. This temperature is below a critical temperature which could lead to a substantial change to the microstructure of the metal being heated. Once the blank reached the target temperature, it is transferred to cold dies immediately. The blank is subsequently stamped and simultaneously quenched with an appropriate die closing force. High forming speed is applied to avoid excessive heat loss so that the blank temperature maintains its temperature.

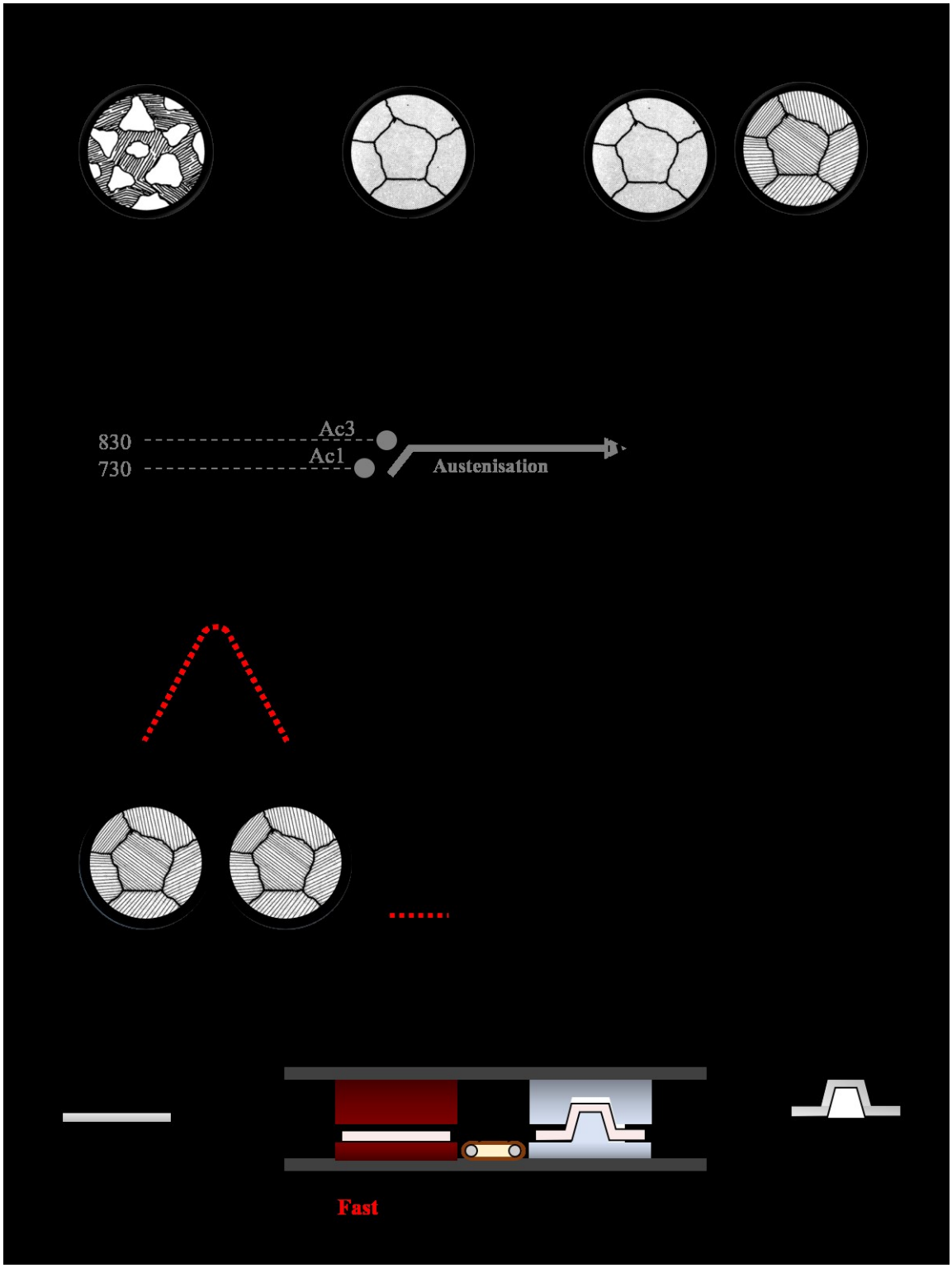

Figure 3.1 Schematic diagram of fast-warm stamping and traditional hot and warm stamping processes.

It was found that the FWS process eliminates lengthy time for austenitization prior to stamping and reduces the heating time to ensure the total cycle time for manufacturing the MS1180 parts is within 10 seconds. The ultra-fast heating rate would avoid undesirable changes to the initial microstructures of the sheet metal so that the nearly full mechanical strength of the pre-form condition can be maintained. It is due to the fact that the ultra-fast heating rate can generate finer and more uniform carbides in the rapidly heated specimens which makes a greater contribution to strengthening the matrix. On the contrary, a slow heating rate will diminish hardness and ductility because of the continuous carbides precipitation and coarsening. These coarser carbides precipitated around the grain boundary, which weaken the boundary cohesion and impair ductility. Additionally, the energy consumption/cost of this forming technology is reduced by maintaining forming temperature at the minimum level, whilst also ensuring sufficient formability to form the components. The feasibility of the FWS process is primarily conducted on the MS1180 steel.

3.3 Thermo-mechanical properties characterization under the FWS process

3.3.1 Uniaxial tensile tests

Uniaxial tensile tests at the FWS conditions were conducted using a Gleeble 3800 thermo-mechanical testing system. The test machine consists of a digital control system, a thermal system and mechanical system, which is capable of up to 10 tonnes of tension load, 20 tonnes of compression load, and a heating and quenching rate of up to 10,000°C/s.

3.3.1.1 Digital image correlation (DIC) system

Digital Image Correlation (DIC) is a state of art technique for measuring deformation and failure of the material. DIC us a full field, non-contact optical technology which is well suited for material characterization both in the elastic and plastic ranges. This technique was firstly developed by a research group in the early 1980s to measure strains by a digital camera (Peters and Ranson, 1982). Compared to using conventional strain measurements, the DIC is found to offer improved data acquisition and flexibility in terms of both spatial resolution and dynamic performance (Yang et al., 2010). Verhulp et al. (2004) further extended this work to three-

dimensions by presenting a three-dimensional digital image correlation technique for strain measurement in solid structures by using high-resolution computed tomography images.

Figure 3.2 shows the schematic for a typical two dimensional (2D) DIC test for sheet metal forming applications. A digital imaging system, usually a high-speed camera, is set up in the front of the specimen for recording images of the surfaces during the whole deformation process. DIC works by comparing digital photographs of a test piece with a stochastic coating pattern using advanced image correlation and processing algorithms at different stages of deformation. DIC software is then used for evaluating the direct acquisition of images for strain calculation. The qualities of the results are mainly dependant on two factors: resolution of the camera and quality of the speckle pattern on the specimen (Chu and Poudel, 2014).

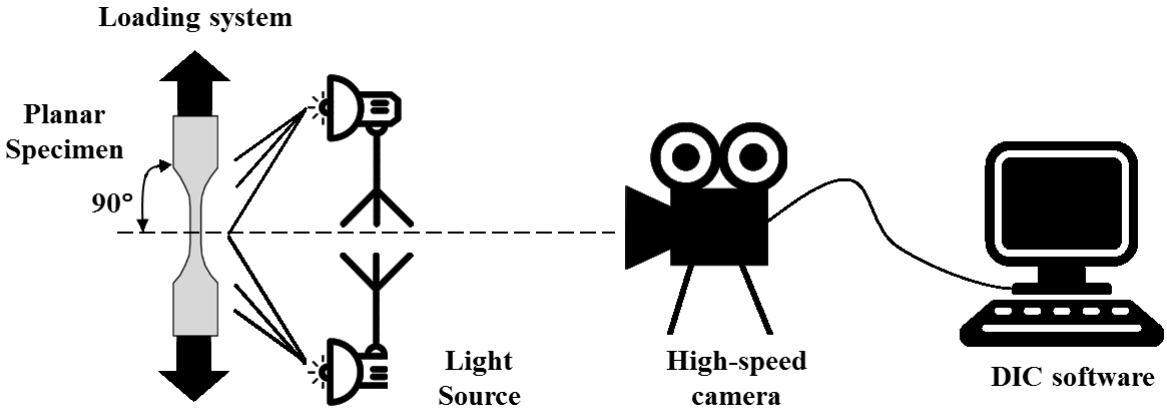

Figure 3.2 The schematic diagram of 2D DIC tensile test set up (Pan et al., 2009).

Extensive research has been performed to improve the accuracy of strain measurement. Pan et al. (2009) reviewed the methodologies of the 2D DIC for strain field measurement and extended the application of DIC for nanoscale deformation measurement by using high-spatial-resolution microscopes. Khoo et al. (2016) reviewed the development of the DIC algorithms and presented that the computation efficiency and measurement accuracy by DIC has been improved. Merklein and Lechler (2006) investigated the flow behaviour of boron steel 22MnB5 in the austenitic state by using the DIC system, but the definition of effective gauge length was not mentioned which may affect the accuracy of strain.

3.3.1.2 Specimen design and preparation

The design of dog-bone shaped specimen is shown in Figure 3.3. The width and parallel length of the gauge section were 8mm and 80mm, respectively. The specimen was clamped within low thermal conductivity stainless steel grips and fixed by two screw bolts and one dowel pin for each pair of grips. Compared to the commonly used copper grips, the steel grips would conduct less heat away from the specimen during heating, ensuring that more homogeneous temperature distribution was obtained in the deformation section. K type thermocouples were spot welded and positioned onto the specimens at mid-length, providing temperature feedback to the system. The position of each pair of thermocouples is shown in Figure 3.3 (b). T1 is the thermocouple welded at the mid-length of the specimen, and T2 with 5mm, T3 with 10mm, T4 with 15mm and T5 with 30mm away from the central position. The effective gauge length was determined after the investigation of temperature distribution on the specimen.

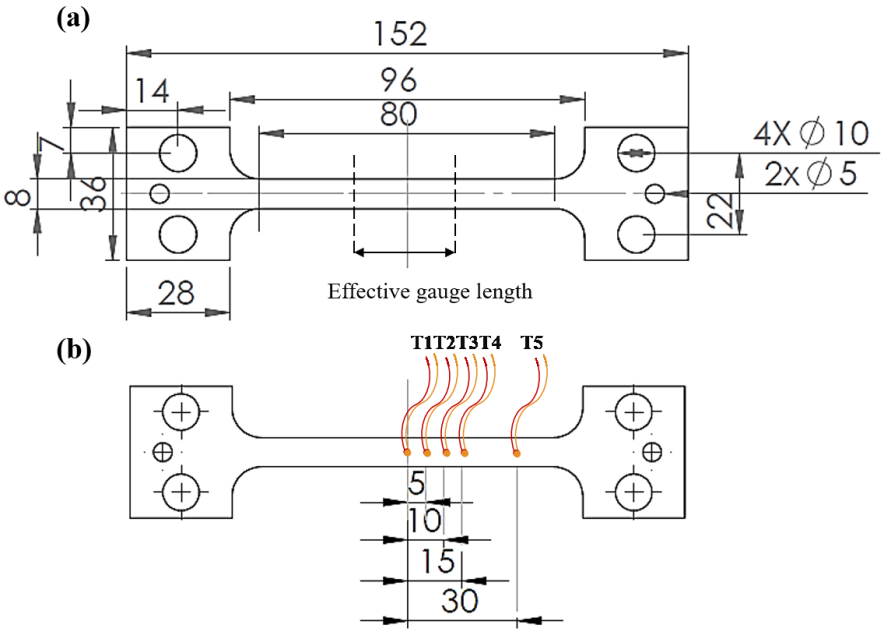

Figure 3.3 Dog-bone shaped specimen design with various thermocouple positions and effective gauge length (a) specimen design (b) the locations of five pairs of thermocouples on the specimen.

Dog-bone shaped specimens were waterjet cut from the sheet alloy. To prepare the specimen with speckle patterns for DIC, a base coat of black paint (VHT FrameProof SP102) was firstly sprayed on to the gauge length region of the specimen as a background, as shown in Figure 3.4.

A white paint (VHT FrameProof SP118) was substantially sprayed randomly as dots over the top to provide a fine contrasting speckle pattern over the surface. This paint can provide a high ductility performance during the deformation with a maximum resistant temperature of 1093°C. The paint was applied to the steel surface with the manufacturer's coating removed because the coating tended to become detached under large deformations.

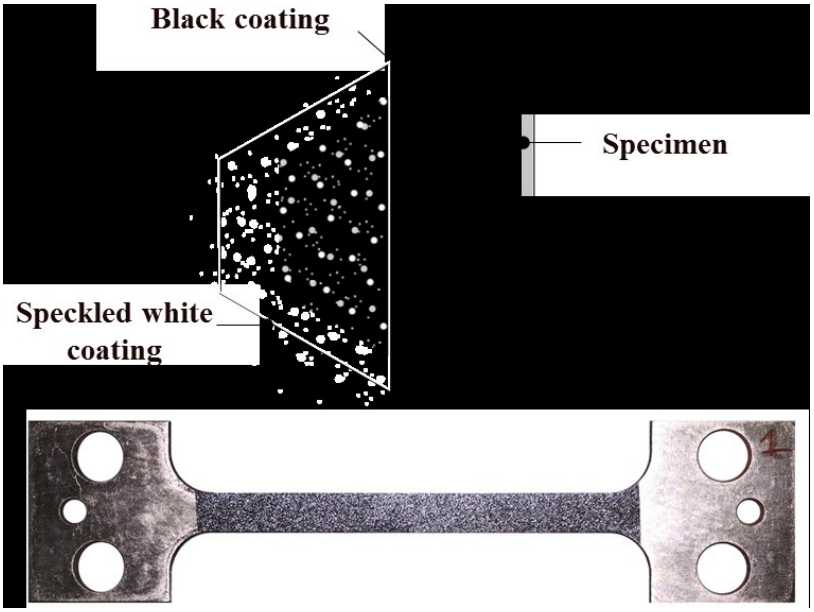

Figure 3.4 Paint spraying on the surface of the tensile test specimen

3.3.1.3 Experiment set up and programme

Figure 3.5 indicates the uniaxial tensile test set up on a Gleeble testing machine. A digital high speed camera (PHOTRON UX50) was employed in front of the test chamber and connected with the DIC software for recording the deformation of the specimen during the tensile test. The camera combines excellent resolution to frame rate performance which has full resolution of 1280×1024 pixels when 2000fps. A powerful light source was employed to eliminate interruptions from surrounding light. In the testing chamber, the specimen prepared with speckle pattern was clamped with grips and placed perpendicular to the camera lens.

Resistance heating system provided a fast heating rate of up to 200°C/s in the heating stage. During the deformation process, the actuator stretched the specimen until fracture occurred. The entire specimen was then quenched by compressed air from two flat-head quenching nozzles. Temperature was precisely controlled by the centrally welded thermocouple.

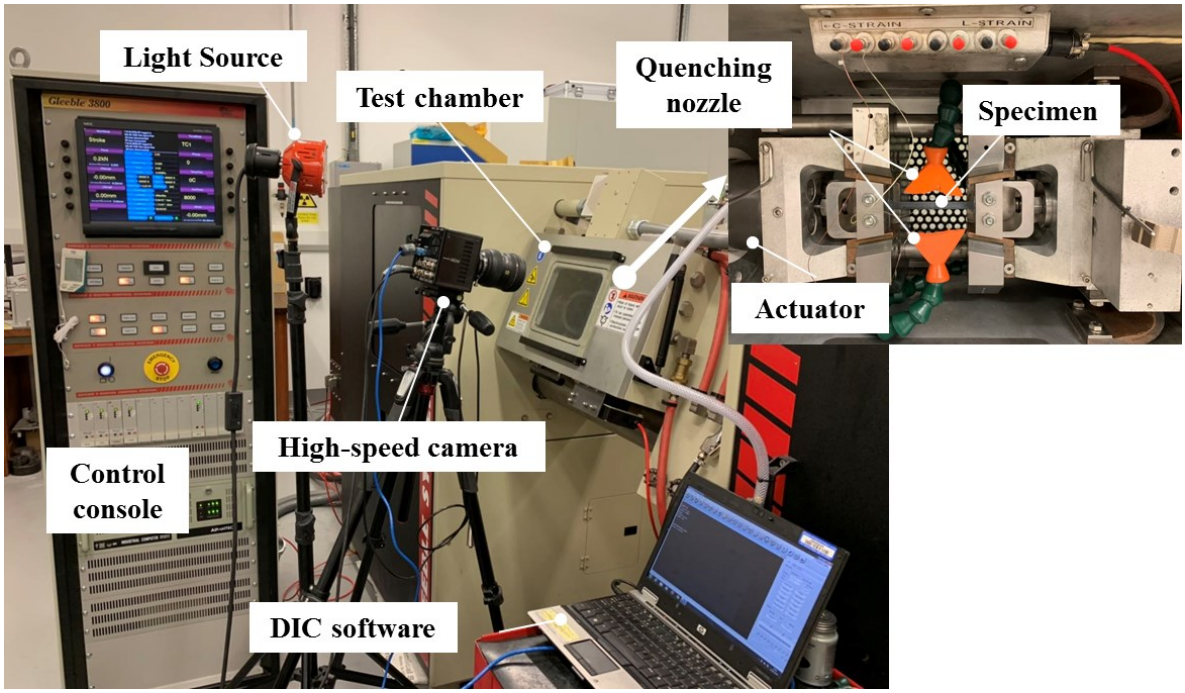

Figure 3.5 Uniaxial tensile test set up on Gleeble simulator.

The thermo-mechanical characteristics of the MS1180 steel over the range of temperatures, strain rates and heating rates were evaluated in two experimental programmes as shown in Figure 3.6. In the first group, the specimens were heated at a rate of 50°C/s to different testing temperatures of 350, 400, 450 and 500°C, which is significantly lower than the austenitization temperature of the steel, then deformed at a constant strain rate of 1/s. The elongated specimens were then cooled rapidly to room temperature at a quenching rate of 40°C/s by compressed air. To investigate the effect of strain rates on flow behaviour, another set of specimens were fast-heated to temperatures ranging from 350 to 500°C at a heating rate of 50°C/s and deformed at various strain rates ranging from 0.01 to 5/s and subsequently quenched to room temperature. In the second group, the impact of heating rates (1, 10, 25, 50, 90 and 150°C/s) was examined to determine the flow behaviour of the MS1180 steel at 450°C with a strain rate of 1 s^{-1} as shown in Figure 3.6 (b). All specimens in the second group were quenched at the same quenching rate of 40°C/s. At least three tests were performed to evaluate the flow behaviour characterization of the MS1180 steel.

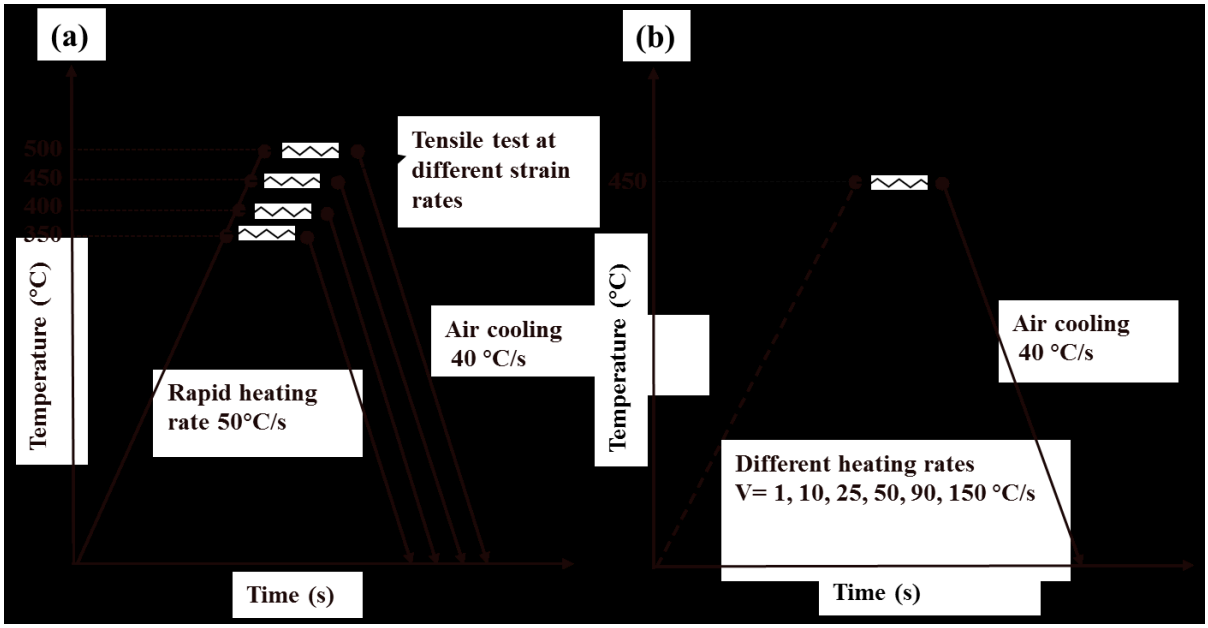

Figure 3.6 Uniaxial tensile test programme evaluating: (a) deformation temperature, strain rate and (b) target heating rate at a constant temperature.

3.3.1.4 Data processing

DIC results from a material state before fracture occurrence was used for determining critical equivalent plastic strains at fracture of the investigated steels. Figure 3.7 presented the full field of strain distribution on the MS1180 steel specimens, which was obtained by DIC analysis in the software ARAMIS system. Over 100 images were preferably utilized for strain calculation. Tensile force was measured using a load cell, fixed to the static part of the machine. The total force over the area of the specimen within the effective gauge length was used for calculating stress. An effective gauge length was defined at less than 10°C temperature differences between central position and the parallel position to calculate the strain. The engineering stress-strain curve was obtained by combining the strain and stress results and then converting to logarithmic true stress and strain to obtain the true stress-strain curve, using following equations:

Engineering strain, $e = \dfrac{(L - L_0)}{L_0}$ (3.1.1)

True strain, $\varepsilon = \ln(1 + e)$ (3.1.2)

Engineering stress, $\delta = \frac{F}{A_0}$ (3.1.3)

True stress, $\sigma = \delta(1 + e)$ (3.1.4)

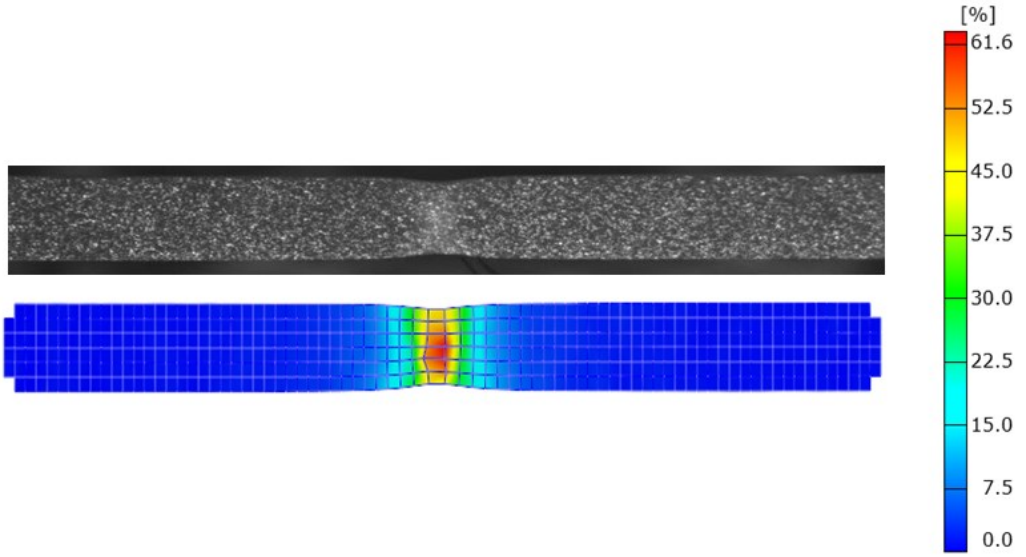

Figure 3.7 Strain distribution in axial direction of the MS1180 steel evaluated by DIC technique.

3.3.1.5 Fracture surface observation

Fracture surfaces of the uniaxial specimens after tensile testing were observed by a Scanning electron microscope (SEM) to examine the influence of heat treatment route and the correspondingly developed microstructure on the fracture behaviour and elongation. Using SEM the fracture surface was magnified by several orders of magnitude with a large depth of field, thus allowing a three-dimensional image of fracture surface to be obtained in detail and more effectively than by an optical microscope (Moore and Booth, 2015). The specimen was extracted from the end of a deformed dog-bone shaped tensile specimen. To characterise the fractography of the specimen as a function of temperature and heating rate, fracture surface observations were performed using SEM at a magnification of 2500.

3.3.2 Strength degradation tests

Strength degradation tests were established and performed on Gleeble 3800 machine and Zwick hardness indicator to evaluate post-form hardness corresponding to the FWS conditions by comparing the hardness values before and after testing.

3.3.2.1 Specimen design and experiment set up

To investigate the effect of heating rate, temperature and strain rate on post-form hardness of the MS1180 steel specimens, the hardness measurements were conducted on tensile specimens which deformed to fracture at various conditions. Vickers microhardness measurements were taken by using Zwick hardness indenter on metallographically prepared samples before and after each test which was used to evaluate the variation in post-form hardness. The hardness tester was shown in Figure 3.8, which comprises of a detector, lifter, control panel and platform. The surfaces of the specimen were ground with fine sanding paper to provide a clean surface for hardness measurement. A load of 100N (HV10) was applied with 10s dwell time for each test. The hardness was measured in the location of control thermocouples and at least 5 measurements were taken to check the repeatability.

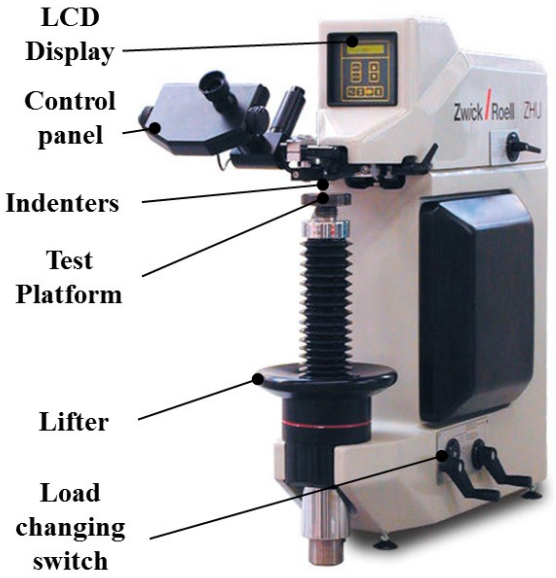

Figure 3.8 Hardness test set up on Zwick hardness indicator (Zwick/Roell, 2019).

In order to investigate the effect of soaking time and quenching rate on the hardness of the MS1180 steel specimens, the strength degradation tests were performed on Gleeble 3800 machine, as shown in Figure 3.9. The rectangular specimen was clamped between the stainless steel grips. Two quenching nozzles were adopted to perform air quenching for both sides of the specimen. Figure 3.10 shows the specimen design and the location of the welded thermocouples. The width and length of the specimen were 10mm and 120mm, respectively. The thermocouples were attached to the centre of a specimen surface.

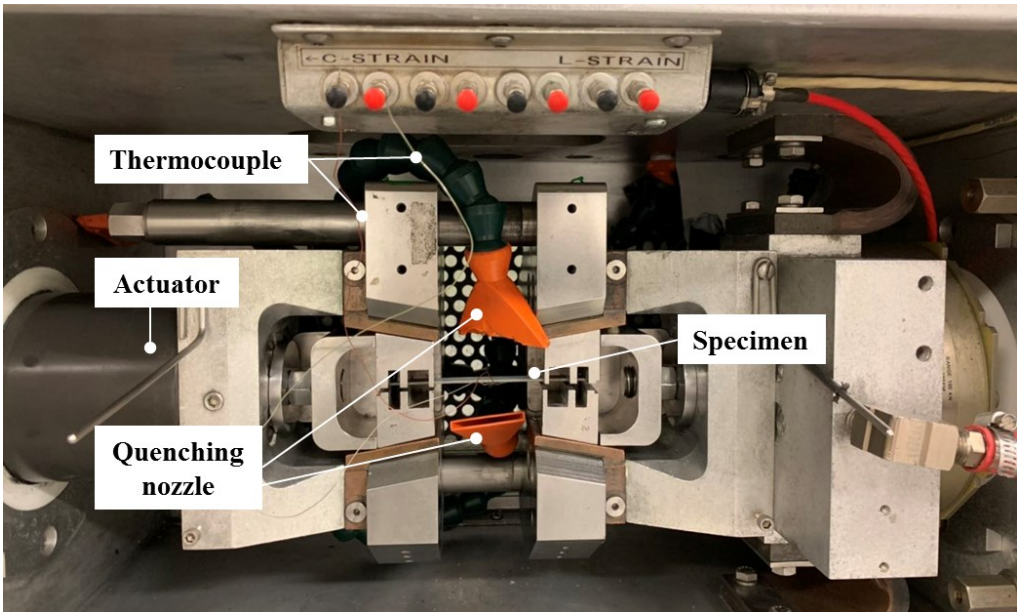

Figure 3.9 Strength degradation test set up on Gleeble.

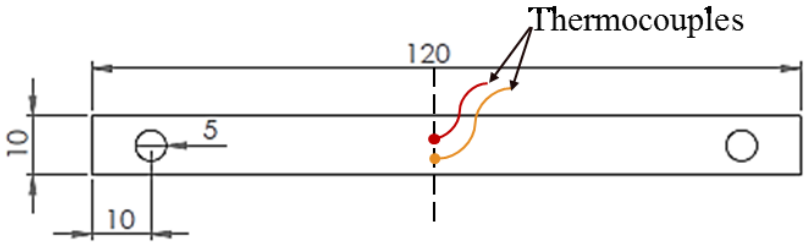

Figure 3.10 Specimen design (dimensions are in mm) for strength degradation test and a pair of thermocouples attached.

3.3.2.2 Experimental programme

Two different experimental programmes were designed to study the optimum thermal profile, as shown in Figure 3.11. In the first set of tests (Figure 3.11 (a)), the specimens were heated at a heating rate of 50°C/s up to 450°C and soaked for short periods varying from 0 to 8s. Instead of straining at elevated temperatures, after reaching target temperatures, the specimens were quickly quenched to room temperature by the air quenching at a cooling rate of 40°C/s. In the second set of tests (Figure 3.11 (b)), the specimens were heated at a rapid heating rate of 50°C/s to 450°C and subsequently quenched to the room temperature by air, die and water, respectively. A dedicated test rig IHTC-mate was utilised to conduct the die quenching. The design and experimental set up is given in Appendix B. The cooling rate of air, die and water was approximately 40, 150, 400°C/s. At least three tests were performed at the same condition to evaluate the repeatability. The detailed hardness measurements of the MS1180 steels were taken as listed in Appendix C.

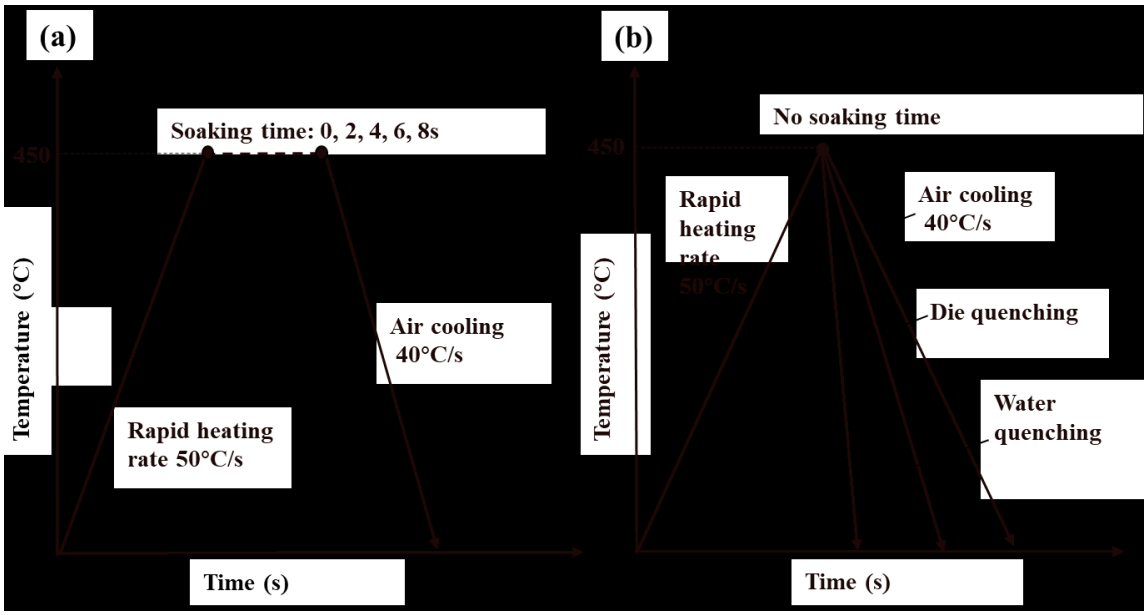

Figure 3.11 Strength degradation test programme evaluating: (a) soaking time (b) cooling rate.

3.3.2.3 Investigation on microstructure evolution via SEM and TEM

Metallographic characterization was performed on as-received and deformed specimens at the same position as the hardness measurements via the scanning electron microscope (SEM, Zeiss

Gemini Sigma 300) and transmission electron microscopy (TEM, FEI Tecnai F20), as shown in Figure 3.12. SEM and TEM observations on the MS1180 steel specimen were performed to characterise the microstructure evolution of the specimen as a function of temperature and heating rate.

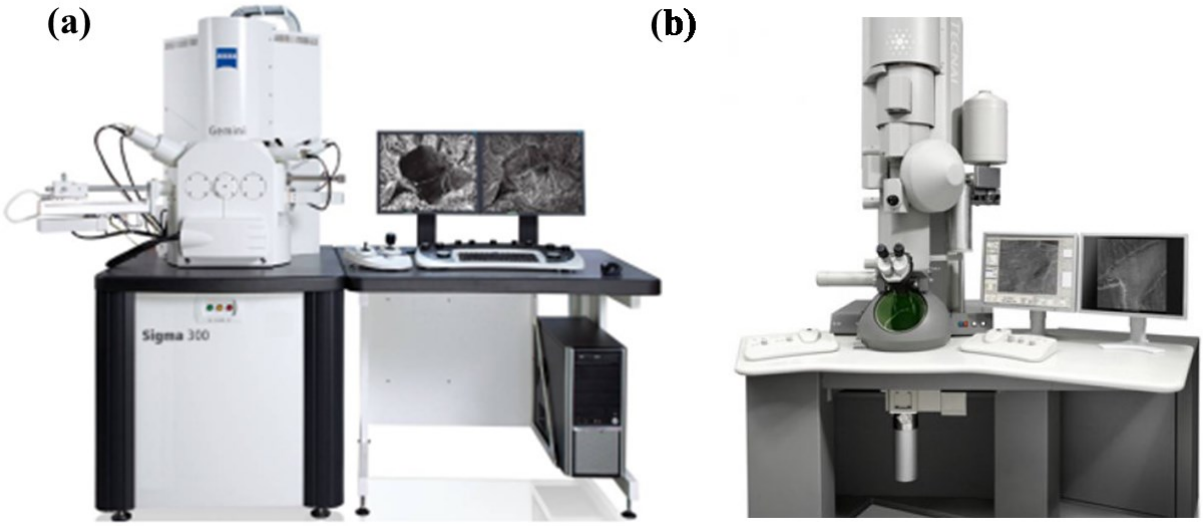

Figure 3.12 Electron microscopy for metallurgical testing (a) Zeiss Gemini Sigma 300 (SEM) (Zeiss, 2019) (b) FEI Tecnai F20 Transmission Electron Microscope (TEM) (KWIPPED, 2019).

The procedure of microstructure observation via SEM consists of cutting, mounting, grinding, polishing and etching. Firstly, the specimen was cut into the required size (normally less than 12mm in length and width) using a saw (Gwynn, 2010). Secondly, the cut specimen was hot mounted under high pressure and polymerized to form a stable material. The mounting press OPAL 410 was shown in Figure 3.13 (a). The mounting machine took 8 minutes for the heating process and 4 minutes for cooling to obtain a compact specimen. Thirdly, silicon paper with grit guide of 180, 320, 600, 800, 1200 and 2500 was used for planar grinding, as shown in Figure 3.13 (b). The surface of the specimen was cleaned and dried between each grade of silicon paper. Approximately 5–10 minutes were required for each step and surface quality of the specimen was examined in an optical microscope. Fourthly, the flat surface of the specimen was polished by automatic polisher shown in Figure 3.13 (c). The specimen was fixed on a work wheel and a small quantity of 6 μm diamond suspension was sprayed on the lapping fabric before commencing the machine. The process was subsequently repeated with 3 and 1

μm diamond suspension. The specimen was then polished by the OPUS colloidal silica solution into 0.04 μm. The pressure and time were set at 10N and 5 minutes. Afterwards, the specimen was etched with 2% nital for 25s and the surface of the specimen was cleaned and dried. Silver conductive paint was applied on at the edge of the specimen to provide a high electrical conductivity for SEM analysis, as shown in Figure 3.13 (d). Subsequently, the specimens were examined by SEM. Carbide precipitation analysis was conducted by Image J using micrographs at a magnification of 20000. At least 10^3 carbides were measured at various conditions.

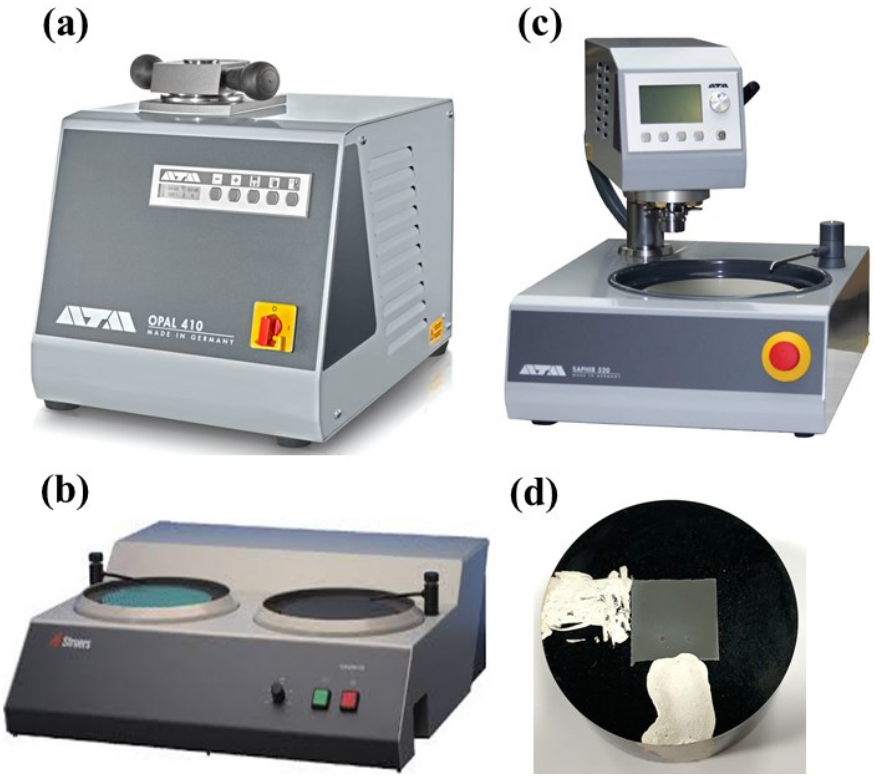

Figure 3.13 Specimen preparation for microstructure observation (a) hot press mount (Materialography, 2019) (b) grinding machine (Struers, 2015) (c) automatic polishing machine (Materialography, 2016) (d) etched specimen with silver conductive paint.

For TEM sample preparation, the specimens were initially cut off from the specimen. The specimen was then delivered to Harbin Institute of Technology for specimen preparation and performing TEM observations. Kehuan Wang helped to prepare the specimens by grinding to an initial thickness of approximately 90 μm. The specimen was subsequently cut into Φ3mm discs and then electro-polishing in a twin-jet electro-polisher with a chemical solution of 10%

perchloric acid and 90% ethanol. The TEM examinations were performed by the Kehuan Wang and follow the guidance provided by the author.

3.4 Fast-warm stamping tests

In order to validate the feasibility of the proposed FWS process for the MS1180 steel, a dedicated lab-scale pilot production line called *Uni-form* was designed and fabricated by Xi Luan, which enabled processing parameters to be realised and verified (Luan et al., 2017). The demonstration parts were fast-warm stamped using the MS1180 steel via the *Uni-form* production line.

3.4.1 Experimental equipment set up and tool design

The overall design of *Uni-form* and tool assembly are presented in Figure 3.14 (a) and (b). The *Uni-form* system comprises of a fast-heating facility, an automated conveyor system to transport the blank from heater to tool, and high rate forming tools. It is a fully automated system where forming speed, temperature and pressure can be precisely controlled and tailored to a specific manufacturing process for individual parts. A furnace was positioned on the left side close to the forming tool to enable rapid transfer of the heated specimen, thus preventing excessive heating loss. A contact heating system was chosen as the optimal heating application method which can provide an ultra-fast heating rate of up to 150 ˚C/s and a homogenous temperature of up to 600˚C. The insulation materials were applied to insulate the heaters to prevent heat loss. Two hot platens with eight inserted cartridge heaters in the heating system were pressed against the cold blank from opposing sides. Once the specimen reached the target temperature, rapidly transfer is required to minimize heat loss. The dual-belt conveyor system allows for the blank to be moved between different stages (heating, forming) automatically. The incubation chamber was designed to be structurally independent of *Uni-from*, which aims to perform further heat-treatment such as tempering or ageing as it was necessary. The combination of a precision-drive motor and accurately spaced cleats ensure that the blank is transferred with sufficient positional accuracy. A pair of small gas springs provide the clamp support plate with an adjustable blank-holding force for testing.

The FWS tests for 1.6mm MS1180 steel sheets were conducted on the *Uni-form* system fitted within the 100-Ton hydraulic testing machine, as shown in Figure 3.15. A computer with control system panel was used to set up the initial position and speed of the stroke. A spring cushion with 28 large gas-springs is positioned beneath the *Uni-form* system. The gas-spring cushions were charged to 30 bar in 2 independent circuits to adjust the stamping force. A light-gate ensured all experiments were conducted in a safe environment. An "Emergency Stop" button was embedded into the control system for safety considerations. Once the button was pressed, the furnace switched off, the hydraulic press was released and the blank transferred to the start position.

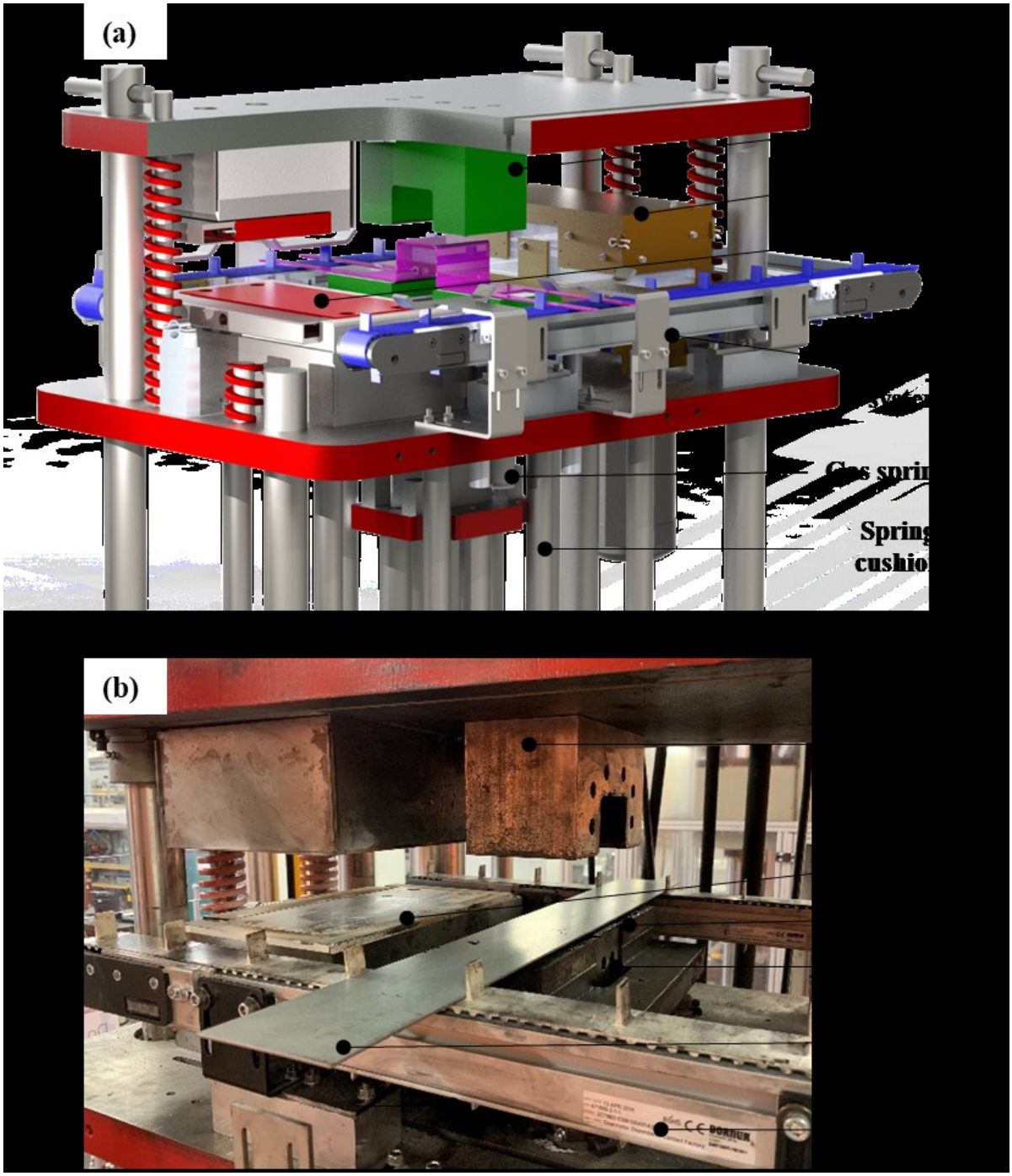

Figure 3.14 A schematic diagram of the *Uni-form* pilot production line (a) overall design of the *Uni-form* (b) tool assembly (Luan et al., 2017).

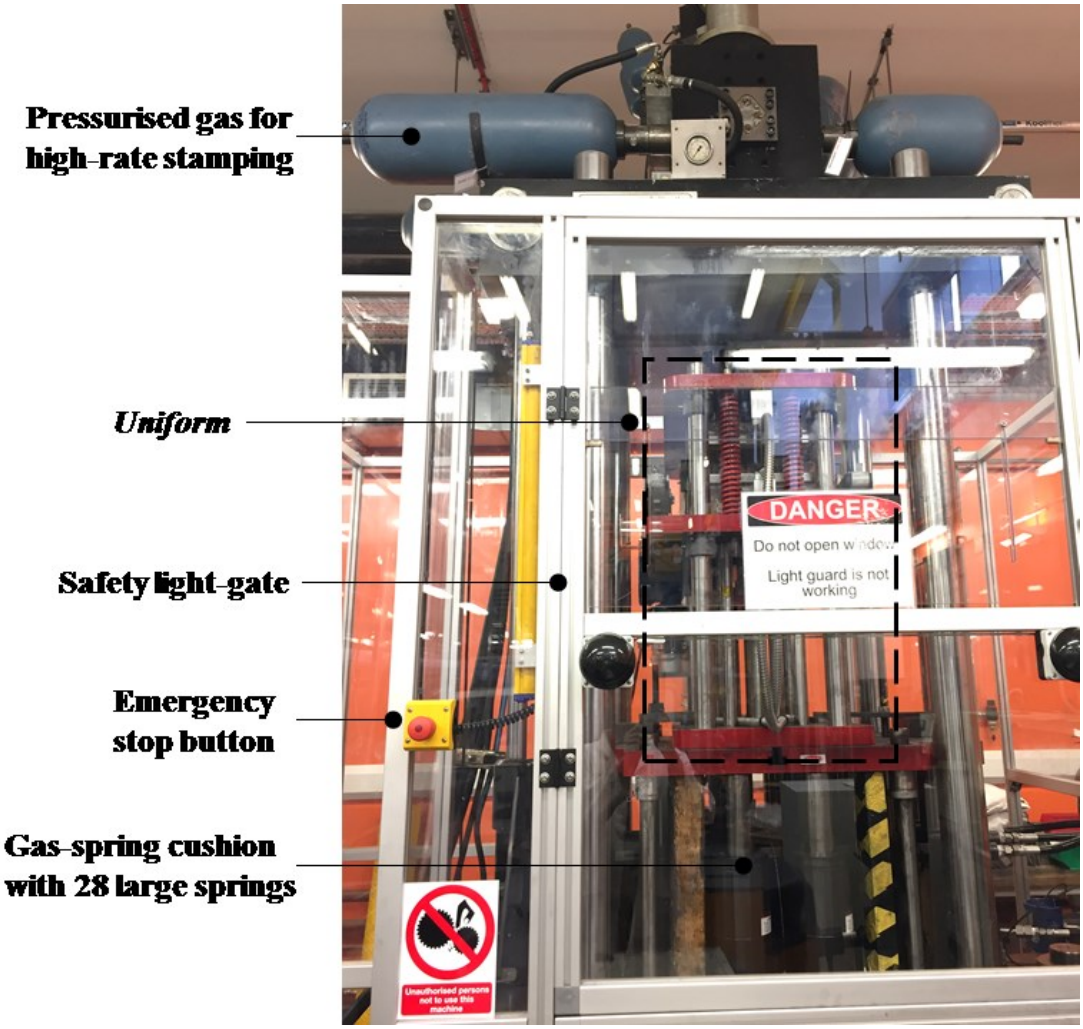

Figure 3.15 A schematic diagram of the *Uni-form* set up in 100 Ton press (Luan et al., 2017).

A warm stamping tool set was designed to be set on the *Uni-form* system for forming the demonstrator part. A U-shape tool was designed and manufactured, to evaluate the capability of the FWS process to form complex shapes. The schematic diagram of stamping tool set with important dimensions for U-shape forming tests is shown in Figure 3.16. The U-shaped die was assembled on the top frame and moved down during the forming process. The tool set was manufactured from hardened P20 tool steel which has sufficient hardness of > 50 HRC to form the MS1180 steel. The die clearance was designed to be 0.2mm (12.5%), for the work-piece of 1.6mm thickness.

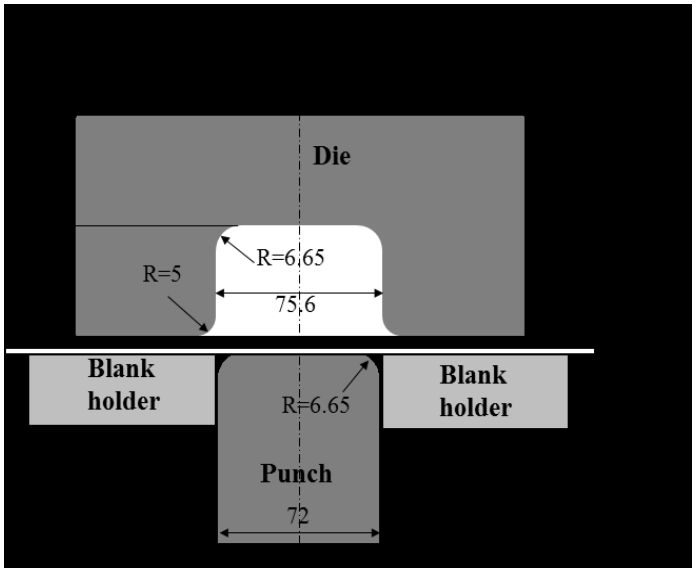

Figure 3.16 Schematic diagram of U-shaped components stamping tool set.

3.4.2 Specimen design and experimental programme

Figure 3.17 shows the specimen design for fast-warm stamping tests via the *Uni-form* system. The width of the blank was 86mm which was accurately fixed within two cleats on the belt. Two pairs of thermocouples were embedded in the mid-thickness of the blank to record the temperature evolution at the selected position during the entire process.

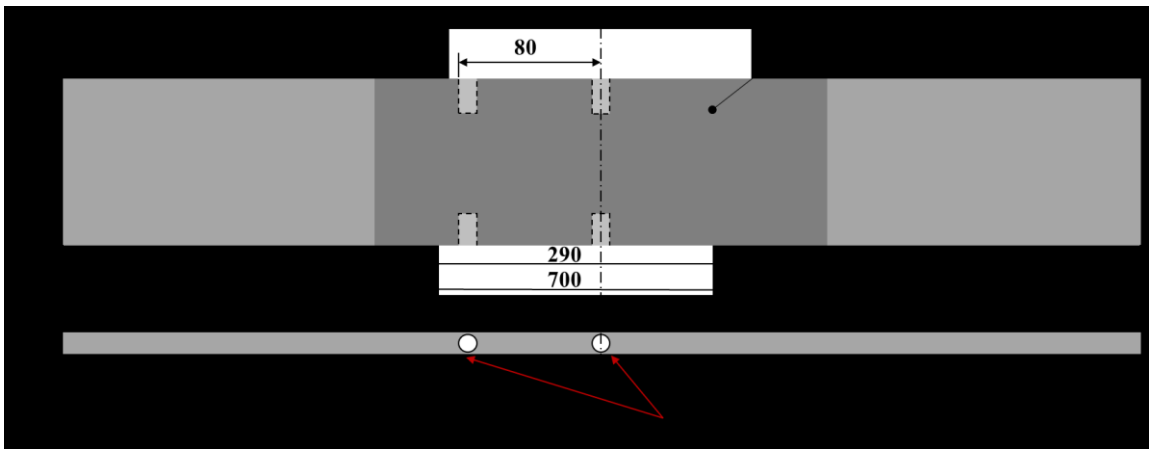

Figure 3.17 Test blank for fast warm forming with two pairs of inserted thermocouples.

The forming parameters including forming temperature, soaking time, transferring time and die closing time were set in the control program. Omega 35 was evenly applied on the surface of the contact area of the die and punch. The cold blank was initially placed between stamping

die and punch. The automatic conveyor system transported the cold blank to the furnace and heated it to the pre-set temperature. The ultra-fast heating rate about 100°C/s was performed to heat the cold blank using contact heating. Once the blank reached the target temperature, it was transferred from the furnace to the U-shaped cold die immediately via a conveyor system in 4s to avoid excessive heat loss so that the blank temperature maintained its temperature. The blank was subsequently formed at different temperatures from 300 to 450°C with a 10kN blank-holding force and was simultaneously quenched within the cold die for 5s. The frame motion in each stage during the FWS process is given in Appendix D. The effect of forming speeds at 75, 150, 250 and 380mm/s were investigated at a forming temperature of 400°C. The test matrix for FWS tests is shown in Table 3.3. The same test methodology was adopted for all the specimens at various test conditions.

Table 3.3 Test matrix for fast-warm stamping tests.

Forming speed (mm/s) /Temperature (°C)	300	350	400	450
75			√	
150			√	
250	√	√	√	√
380			√	

3.4.3 Post-form properties evaluation of formed components

In order to illustrate the uniformity of the formed part at identified optimal process variables, Vickers hardness measurements were performed on different locations along the cross-section of the formed parts. The morphology of the formed part at sidewall, bottom region and radius were examined by SEM.

To broaden the material's industrial application, mechanical properties such as post-form strength have to be confirmed on the formed parts. Therefore, uniaxial tensile tests were conducted at room temperature through the DIC system to evaluate the PFS on formed U-shaped components. Dog-bone shaped specimens were waterjet cut from the bottom region of the formed components, as shown in Figure 3.18. The gauge length width was 6mm and the parallel length was 32mm. Three tests were conducted in the same test conditions to ensure repeatability.

Prior to each test, the width and thickness of the specimen were measured at three different locations and recorded, such that the stress can be calculated during post-processing of the results. The specimen was sprayed with random speckle patterns on the surface using black and white spray paint. The test-piece was assembled in an Instron press machine for tensile testing.

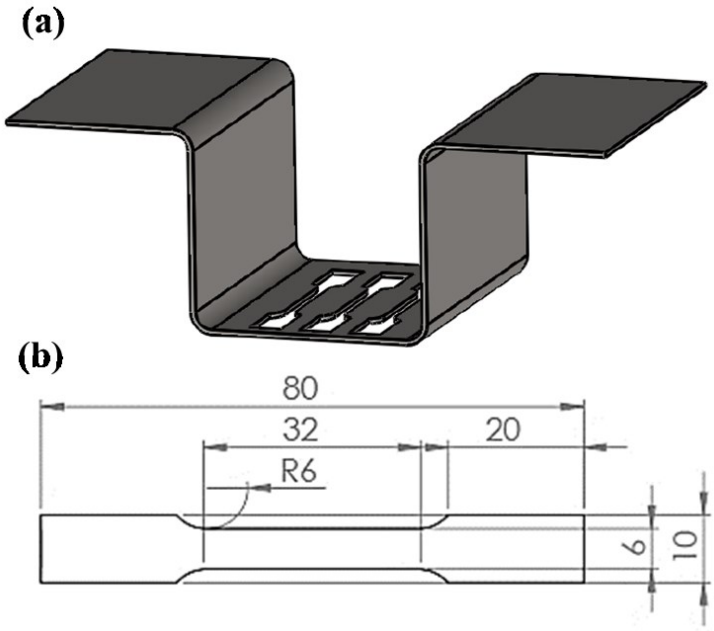

Figure 3.18 Specimen preparation for post-form strength evaluation (a) specimens machined from formed parts (b) specimen design (dimensions are in mm).

Figure 3.19 shows the experimental setup for the uniaxial tensile test on the Instron machine. The specimen was clamped by the bottom grip which was fixed firmly to the load cell to avoid any slip or slight movements. The position of the top grip was then adjusted to clamp the specimen by tightening the bolt. The load cell and displacement output port were connected to

a computer to record the full load-displacement history. The DIC system with a camera was set in the front of the sample on a stable tripod to record the deformation during testing. The frame rate of the camera was set as 1 fps for the strain rate of 0.001/s. Several adjustments were made prior to capture, namely the camera tilt angle, the focus of the camera lenses, the lighting, the aperture of the camera lenses, and the shutter time. A light source was employed for illumination. The recorded images during the deformation were imported into ARAMIS to determine the strain. The methodology for strain calculation was the same as that in the uniaxial tensile test described in sub-section.3.3.1. The value of force was read from INSTRON control systems measured by the strain gauge load cell and the corresponding stress was calculated. The engineering stress-strain curve was plotted by combining the strain and stress results and then converted to true stress-strain curves.

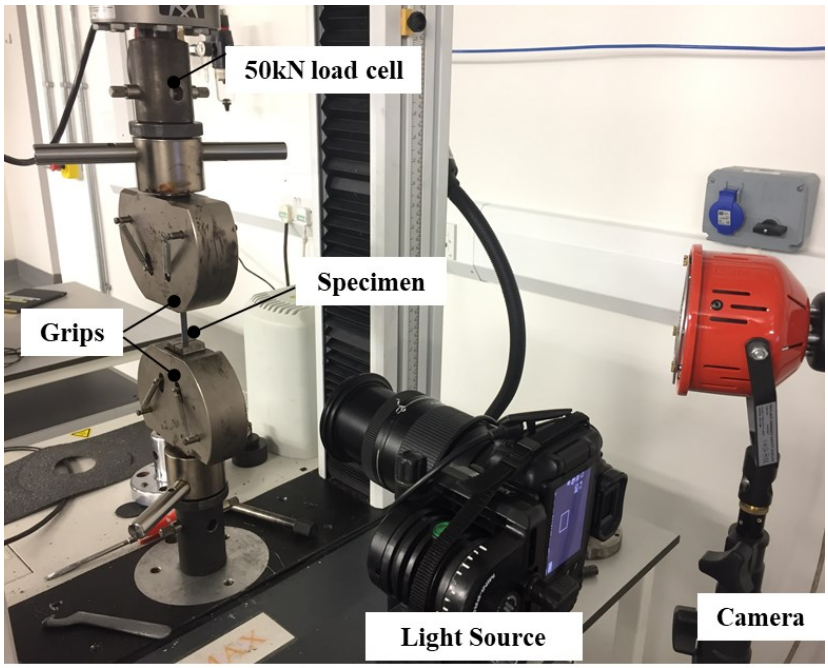

Figure 3.19 Room temperature tensile test set up on Instron.

3.4.4 Springback evaluation process

Springback of the MS1180 steel was characterized after stretch bending under various fast-warm stamping conditions. The whole profile of the U-shaped part was assessed using a scanner. The scanned profile was subsequently imported as a 2D drawing in Solidworks software and the springback of formed parts was analysed. The springback evaluation of U-shaped components was performed according to the NUMISHEET's 2011 benchmark

(Kwansoo et al., 2011). Two critical angles are defined to characterise the springback of the formed components, as shown in Figure 3.20. The angle (θ_1) is measured between the vertical line and the tangential line of the sidewall that represents the sidewall deflection. The angle (θ_2) is measured between the horizontal line and flange extensional line representing the flange springback.

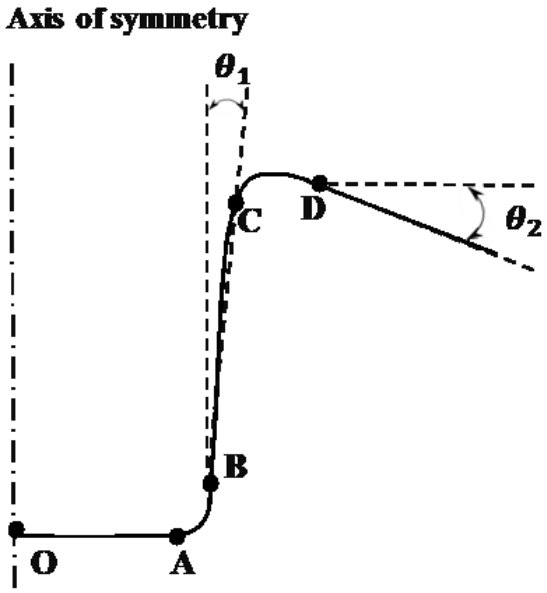

Figure 3.20 The springback angle θ_1 and θ_2 measurement of U-shaped formed components.

In order to extensively investigate the springback behaviour of the MS1180 steel under the FWS conditions, the springback of the U-shaped bending was subsequently simulated using commercial software PAM-STAMP. The FE simulations were conducted to investigate the forming temperature and forming speed on springback. Springback results from the FE simulations are validated with experimental results obtained from U-shaped bending tests.

3.5 Summary

In this chapter, a novel sheet metal forming technology, fast-warm stamping (FWS) is proposed incorporating industrial requirements for forming operations. Uniaxial tensile tests were designed and conducted to characterise the thermo-mechanical properties of the MS1180 steel under the range of temperatures and forming conditions experienced during forming. Strength degradation tests were performed to investigate the effect of temperature, heating rate, soaking

time and quenching rate on the hardness. To characterise the microstructure evolution, the SEM and TEM observations were conducted and the experimental results are discussed in Chapter 4.

The FWS process was verified via U-shaped bending tests using a dedicated automatic production line called *Uni-form*. The effects of forming temperature and speed on the post-form properties of the formed parts were studied. Springback of the MS1180 steel was characterized after U-shaped bending. These experimental results were used to verify the FE simulations results of the FWS process.

Chapter 4. Material characterisation of the MS1180 steel under FWS conditions

This chapter presents detailed results obtained from the experiments outlined in the previous chapter. Secondly, a detailed discussion and analysis are conducted to characterise the material behaviour of MS1180 steel under FWS conditions. Based on the results of uniaxial tensile tests, the viscoplastic deformation behaviour and thermo-mechanical properties of the MS1180 steel are discussed in terms of temperature, strain rate and heating rate dependence. Based on the results of the strength degradation tests, the post-form hardness evolution of the MS1180 steel under ultra-fast heating conditions is analysed. Additionally, SEM and TEM micrographs were analysed to investigate the relationship between mechanical properties and microstructures of the MS1180 steel at various temperatures and heating rates. The tensile and strength degradation test data was utilised in the development of an optimal processing window to form the MS1180 steel in complex shapes.

4.1 Thermo-mechanical properties and microstructures of the MS1180 steel at various conditions

4.1.1 Lath structured martensite of as-received MS1180 steel

The MS1180 steel contains martensitic microstructure and sometimes small fractions of ferrite or bainite. The microstructure of the as-received MS1180 steel is characterized by scanning electron microscopy (SEM) and transmission electron microscopy (TEM) as shown in Figure 4.1, in which the morphology of lath-type martensite structure was observable, with the crystallographic features of packet and blocks. Figure 4.1 (b) presents different contrast of the

Chapter 4 is based on paper work ‘‘Sun, Y., Wang, K., Politis, D. J., Chen, G., Jiang, J., Wang, L., 2019. An experimental investigation on the ductility and post-form strength of a martensitic steel in a novel warm stamping process. J. Mater. Process. Technol.’’and Sun, Y., Wang, K., Politis, D. J., Atherton, N., Pang, T., Knoerr, L. O., Captaine, H., Wang L., 2017. Flow behaviour characterization of an ultra-high strength steel under warm stamping conditions. 2nd International Conference on Lightweight Materials and Engineering Structures, 13-14 November 2017, London, United Kingdom.

parallel lath martensite variants (bright and dark bands). Different thickness of laths from approximately 0.1–1μm is visible in the microstructure which was developed during the martensitic transformation process due to the differences in transformation sequences and temperatures and the corresponding change of the austenite state (Morsdorf et al., 2015). A high dislocation density can be found within the lath martensite.

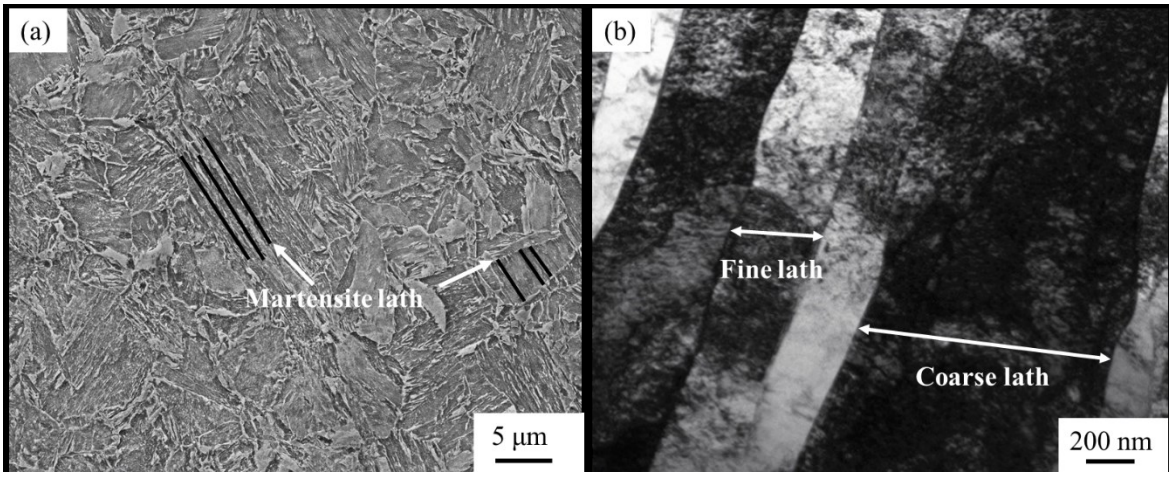

Figure 4.1 Martensitic microstructure of the as-received MS1180 steel (a) SEM micrograph of lath martensite (b) bright-field TEM micrograph of various laths with high dislocation density.

4.1.2 Deformation behaviour of the MS steel during hot uniaxial tensile test

4.1.2.1 Temperature distribution of the MS1180 steel at elevated temperature

Figure 4.2 shows the temperature distribution of the dog-bone shaped tensile specimens at different temperatures ranging from 350 to 500ºC. It can be seen that temperature distribution evolutions maintain a similar trend at various temperatures and that the temperature gradient is pronounced at the position which has the longest distance between the central point T_1. The temperature difference ΔT between T_5 and T_1 is approximately 85ºC.

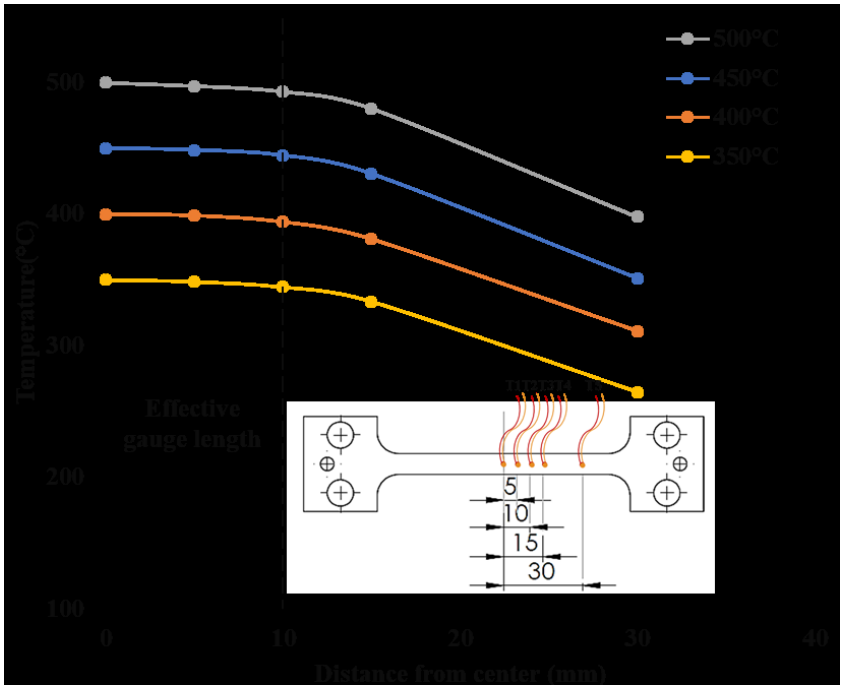

Figure 4.2 Temperature distribution in the dog-bone shaped specimen at various temperatures.

It is claimed that that a temperature difference of less than 10°C within the effective gauge length is acceptable (Shao et al., 2017). Table 4.1 indicates that the minor temperature difference between T_3 (10mm) and central point T_1. It was found that the temperature difference ΔT slightly increases with increasing temperature and all differences are maintained within 10°C. Therefore, an effective gauge length of 20mm was defined instead of using the whole parallel length to calculate the true strain. The obtained axial strain from the DIC system is synchronised with stress to plot the stress-strain curves.

Table 4.1 Temperature differences between T_3 (10mm) and central point T_1

Central temperature T_1 (ºC)	500	450	400	350
ΔT (ºC)	7.76	6.12	5.96	5.40

4.1.2.2 Flow stress-strain curves

The effects of temperature, strain rate and heating rate on the flow behaviour of the MS1180 steel were investigated at temperatures ranging from room temperature to 500°C, strain rates

ranging from 0.01 to 5/s and at heating rates from 1 to 150°C/s as shown in Figure 4.3 (a) shows the flow stress curves of the MS1180 steel deformed at different temperatures with a constant strain rate of 1/s. Both flow stress and ductility of test material were found to be highly temperature dependent. An appreciable reduction in the flow stress and an improved ductility were observed with increasing temperature. At low deformation temperatures, the true stress increased until reaching the peak value at low strain value. The gradual increase of flow stress with increasing strain is mainly associated with strain hardening, which was caused by dislocation accumulation and interactions. The flow stress subsequently decreased with increasing strain due to strain softening. Moreover, before the peak strain, work hardening was clearly observed at low deformation temperatures. The ductility of the MS1180 steel indicated by strain to failure increased from 4.2% to 14.1% as the temperature increased from 25°C to 400°C.

Figure 4.3 (b) shows the effect of strain rate on the flow properties of the MS1180 steel at 450°C. The figure reveals significant strain rate and elongation sensitivity of the flow stress. It was found that increasing strain rate led to a remarkable increase in elongation. When the strain rate increased from 0.01 to 1 /s, the corresponding strain to failure increased from 0.132 to 0.181. The improved failure to strain of the MS1180 steel at a higher strain rate is mainly attributed to the dispersed distribution of fine carbide precipitates. In addition, increasing strain rate resulted in a noticeable increase in flow stress of the MS1180 steel. The pronounced strain rate hardening effect was widely observed in the visco-plastic materials and this was caused by the tangled dislocations generated during plastic deformation. Moreover, the flow curves in the graph show that the strain hardening is more pronounced during high strain rate testing. Since static recovery is a function of time, for a higher strain rate, the shorter deformation time results in a higher dislocation density and less recovery. The plateau of flow curves at a strain rate of 5/s indicated the achievement of a steady state between strain hardening and softening.

Figure 4.3 (c) shows true stress-strain curves for the MS1180 steel obtained at different heating rates ranging from 1 to 150°C/s, with a strain rate of 1/s at 450°C. It was observed that heating rate induced a minor influence on flow stress but a pronounced difference on the ductility of the MS1180 steel. The peak flow stress increased slightly with increasing heating rate. This was due to the fact that the fast heating rate allowed less time for dynamic recovery, carbide precipitation nucleation and coarsening. In addition, the results indicate that the ductility of test

material increases with increasing heating rate from 1°C/s to 50°C/s. A rapid heating process has suppressed the detrimental precipitate coarsening at elevated temperatures, where microvoids were preferentially formed around the carbide precipitates at grain boundaries. Coarser carbides formed at grain boundaries by slow heating could weaken the boundary cohesion and impair the ductility.

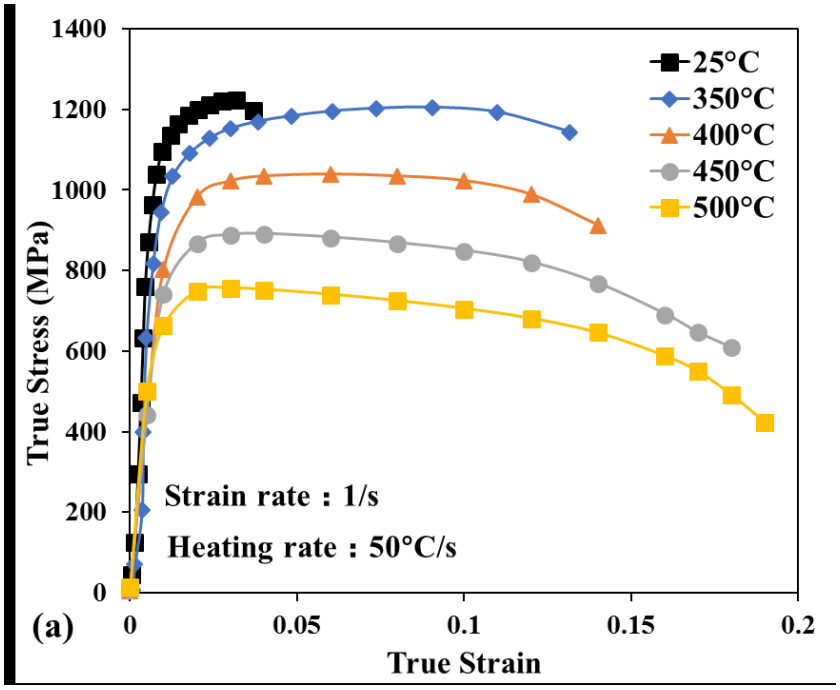

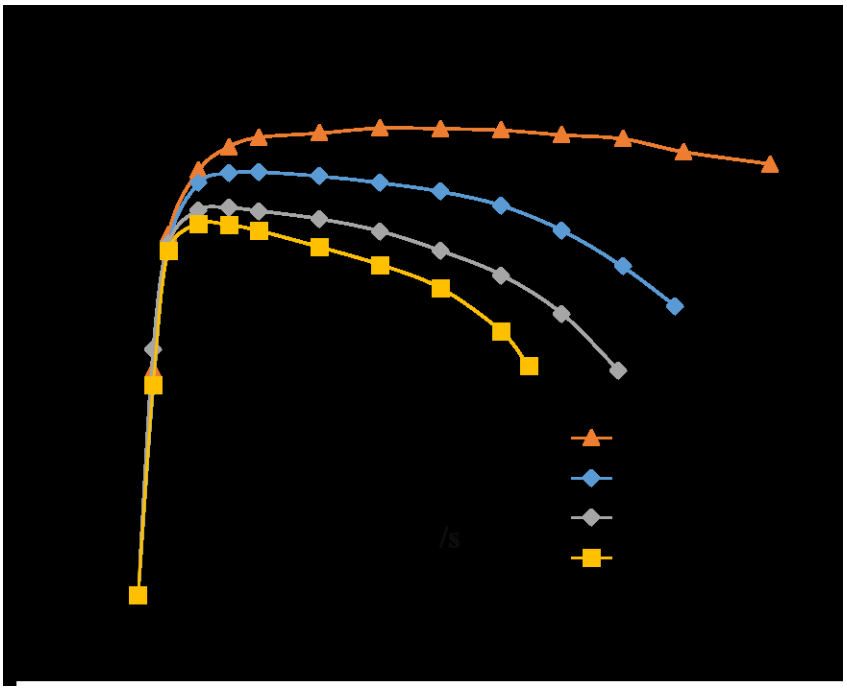

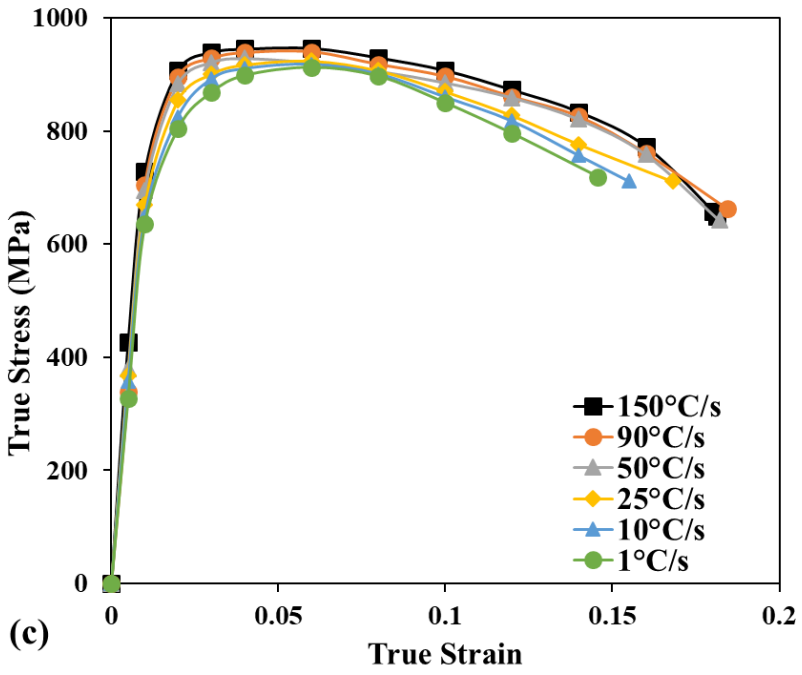

Figure 4.3 Flow stress-strain curves of the MS1180 steel tested at (a) different temperatures (b) strain rates (c) heating rates.

4.1.2.3 Effect of temperature on thermo-mechanical properties of the MS1180 steel

The mechanical properties including ultimate tensile strength (UTS), yield strength (YS) and total elongation of the MS1180 steel specimens tested at various temperatures are shown in Figure 4.4. The total elongation improved from 15.1% to 20.8% as the temperature increased from 350 to 500°C. This improvement was attributed to increased grain boundary sliding and rotation and higher dislocation mobility at higher deformation temperatures resulting in the material becomes softer and more ductile. Additionally, it was found that increasing deformation temperature induced a linear reduction in UTS and YS. The UTS of the MS1180 steel reduced by approximately 21.2% from 1100MPa at 350°C to 887MPa at 450°C. The reduction in UTS was related to material softening. The reason for softening is mainly due to the formation and coarsening of carbides and dynamic recovery during the heating and deformation processes at the temperature range from 350 to 500°C. Increasing the deformation temperatures leads to both accelerating carbide nucleation rate and dynamic recovery rate and thus the material softening is pronounced. Moreover, the decreasing strength at elevated temperature was attributed to the reduction in dislocation density. The elongation of the MS1180 steel increased steadily at temperatures ranging from 350 to 500°C. At elevated

temperatures, dislocation movement, grain-boundary sliding, diffusion and grain rotation are further activated at higher temperatures which improve ductility (Lin, 2015).

Figure 4.4 Evolution of ultimate tensile strength, yield strength and elongation of the MS1180 steel as a function of temperature.

4.1.2.4 Effect of strain rate on thermo-mechanical properties of the MS1180 steel

Figure 4.5 shows the improved total elongation from 14.2% to 22.4% as strain rate increased from 0.01 to 5/s. The improved elongation of the MS1180 steel at a higher strain rate is mainly attributed to the dispersed distribution of fine carbide precipitates. A rapid plastic deformation has suppressed the detrimental precipitate coarsening at elevated temperatures, where microvoids were preferentially formed around the carbide precipitates at grain boundaries. The coarser carbides present around grain boundaries at elevated temperatures and low strain rates weaken the boundary cohesion and impair ductility. In addition, a minor contribution of increased temperature due to heat generated during deformation could slightly increase the ductility at a higher strain rate. It was found that temperature increase at a strain rate of 5/s was approximately 3–7% and thus its contribution to ductility increase was negligible. Both UTS and YS of the MS1180 steel increases remarkably with increasing strain rate. This is mainly related to strain rate hardening, caused by dislocation accumulation and interactions.

Figure 4.5 Evolution of ultimate tensile strength, yield strength and elongation of the MS1180 steel as a function of temperature.

4.1.2.5 Effect of heating rate on thermo-mechanical properties of the MS1180 steel

The evolutions of total elongation, UTS and YS of the MS1180 steel at various heating rates ranging from 1 to 150°C/s are plotted in Figure 4.6. The results indicate that increasing heating rate initially leads to a steady increase of elongation between 1°C/s to 50°C/s, after which the total elongation remains at an eventual plateau and the effect of heating rate is negligible. The improvement to total elongation when increasing the heating rate from 1 to 150°C/s was approximately 25.7%. The improved ductility at a fast heating rate was attributed to the carbides refinement. On the contrary, coarser carbides formed at grain boundaries by slow heating could weaken the boundary cohesion and impair the ductility. Moreover, it was found that UTS of the MS1180 steel slightly increased from 855.2 MPa at a heating rate of 1° C/s to 898.5MPa at a heating rate of 150° C/s. The increased UTS is attributed to a lower state of recovery and carbide coarsening.

Figure 4.6 Evolution of ultimate tensile strength, yield strength and elongation of the MS1180 steel as a function of heating rate.

4.1.3 Fracture morphology of the MS1180 steel

4.1.3.1 Effect of temperature on fracture morphology of the MS1180 steel

The fracture surface morphologies of the MS1180 steel specimens at room temperature, 400 and 450°C at a constant heating rate of 50°C/s are shown in Figure 4.7. It can be seen from the graph that the specimen was deformed at room temperature, in which the quasi-cleavage, tearing ridges and shallow dimples morphology can be observed, as shown in Figure 4.7 (a). The quasi-cleavage fracture describes a brittle fracture surface indicating low energy absorption, that combines the characteristics of cleavage fracture and dimpled fracture (Chang et al., 2016). At 400°C, the tensile fractographs demonstrated typical ductile fracture with obvious small dimples and microvoid characteristics, as shown in Figure 4.7 (b), indicating improved plastic deformation prior to fracture. Figure 4.7 (c) shows the size of dimples increased with increasing temperature at 500°C, which corresponds to peak ductility. These observations further justified the stress-strain results obtained from the tensile tests.

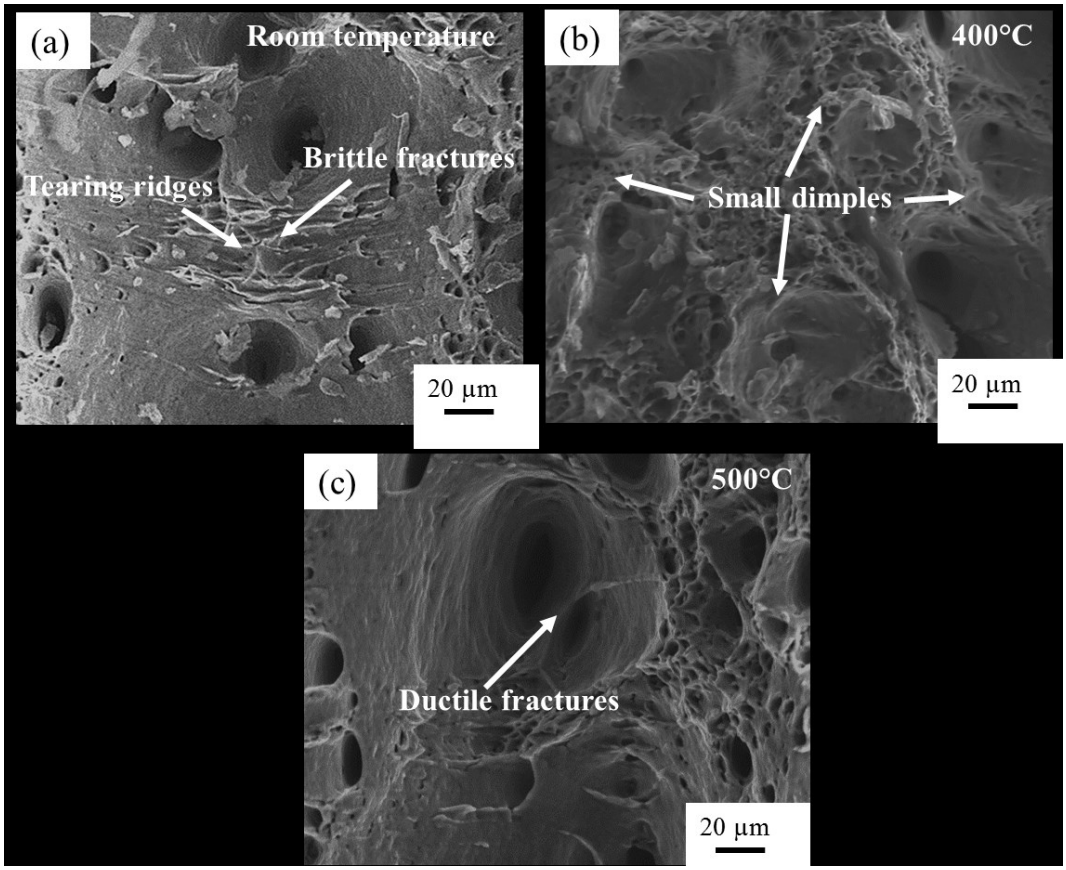

Figure 4.7 Morphology of the fracture surface of uniaxial tensile specimens at (a) room temperature, (b) 400°C and (c) 500°C.

4.1.3.2 Effect of heating rate on fracture morphology of the MS1180 steel

Figure 4.8 (a) shows the fracture morphology of specimens heated at a slow heating rate of 1°C/s, which indicates relatively low ductility. Deeper and larger dimples and microvoids are found for specimens at a heating rate of 50°C/s, as presented in Figure 4.8 (b), indicating a greater amount of plastic deformation before fracture. As the heating rate increased further to 150°C/s, it can be seen from Figure 4.8 (c) that the pattern of dimples is similar to that observed at a heating rate of 50°C/s, which is consistent with the stress-strain curve results. Once heating rate is greater than 50°C/s, the effect of heating rate on the ductility of the material was negligible.

Failure normally occurs by void nucleation and growth in most ductile metals. These voids and cracks preferentially occurred around coarser carbides at grain boundaries during the hot deformation of the MS1180 steel specimens. The difference observed in Figure 4.8 can be

explained by the size of carbide precipitates and growth within the grain boundaries due to the diffusion of carbon at various conditions. The different carbide particles nucleated, grew and merged during the heating and deformation processes. Carbide precipitates formed under fast heating rates generally are finer and dispersed. This result is consistent with the research results of Sackl et al. (2016) in a heat treatable steel 42CrMo4. Coarser carbides formed at grain boundaries by slow heating could weaken the boundary cohesion and impair the ductility. Therefore, finer carbide precipitates formed by rapid heating can induce a greater strain which leads to an improved ductility.

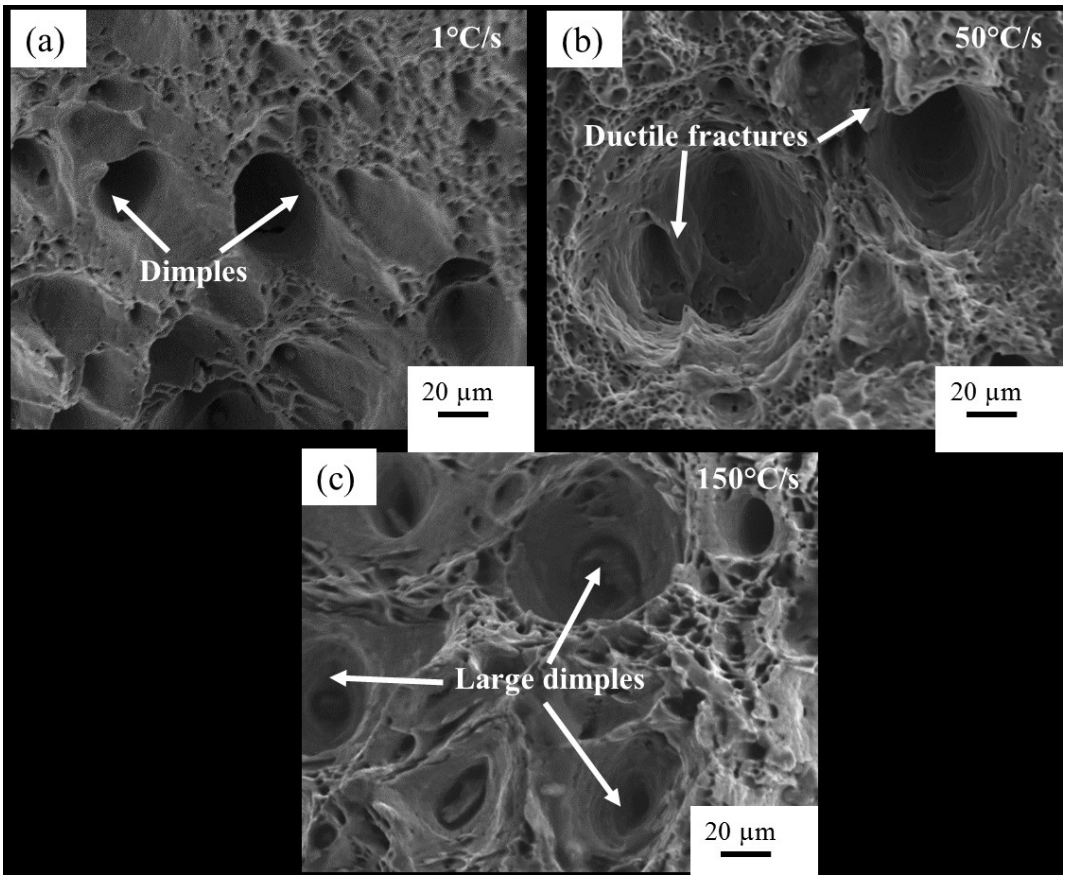

Figure 4.8 Morphology of the fracture surface of uniaxial tensile specimens at (a) 1°C/s, (b) 50°C/s and (c) 150°C/s.

4.1.4 Post-form hardness (PHS) evolution of the MS1180 steel under different conditions

4.1.4.1 Effect of temperature and strain rate on PHS and carbide precipitation of the MS1180 steel

Apart from elevated temperature deformation behaviour, post-formed strength behaviour was also affected by forming processing parameters. Figure 4.9 shows the variations of the post-form hardness (PFH) of the MS1180 steel as a function of temperatures. The PFH of testing material decreased with increasing forming temperature, where PFH is expressed as a percentage of the hardness of the MS1180 steel prior to forming. For reference, the hardness value of the as-received material was approximately 400 HV. It is clear that temperature plays a significant role in the PFH of the MS1180 steel. The PFH of the specimen decreased linearly with increased heating temperature. The PHS of 370.2 HV was achieved at a lower heating temperature of 350°C, which was only reduced by approximately 6.4% compared to the original hardness. A considerable reduction in hardness at temperatures above 350°C was observed, where a 17.2 % reduction was found at 500°C. The gradual reduction of hardness was due to the fact that the higher heating temperatures accelerates the decomposition of martensite phase and the nucleation and coarsening of carbide precipitates. In addition, the contribution of solid-solution strengthening of carbon in martensite reduced with increasing temperatures and hence induced a lower PFH.

Figure 4.9 Evolution of the post-form hardness as a function of temperature.

Figure 4.10 Evolution of the post-form hardness as a function of strain rate.

Figure 4.10 shows the PFH evolution of the MS1180 steel at 450°C as a function of strain rate. It was observed that the PFH of the MS1180 steel increases with increasing strain rate. The hardness value was 27.6% greater at a fast strain rate of 5/s compared to that of the specimen deformed at a strain rate of 0.01/s. The reason is believed to be that the slow deformation rate allows a lengthy deformation period at elevated temperatures which leads to a reduction in hardness due to considerable softening of the steel. The observed decrease in hardness was attributed to the formation of coarser carbides at lower strain rate conditions. This coarser distribution of carbides at low deformation speeds leads to a lower PFH. Moreover, the stronger recovery of dislocation at a low strain rate led to a reduction in the dislocation density, which diminishes the PFH.

Following tensile testing, the microstructures of deformed specimens at various conditions were evaluated by SEM and TEM. Figure 4.11 exhibits the SEM micrographs of the MS1180 steel specimen at 350 and 500°C with a heating rate of 50°C/s. It can be clearly seen that the lath martensite structure within prior austenite grain was observed, as shown in Figure 4.11 (a). As the temperature increases to 500°C, parallel martensitic laths were distinguishable as the carbides precipitated within laths, as shown in Figure 4.11 (b). The grain boundaries were clearly identified for fast-heated specimens at 500°C. It can be concluded that the martensitic structures for the fast-heated specimens remained similar to the preheated material.

In order to gain an understanding of the microstructural behaviour, such as carbide precipitation within laths at elevated temperatures, SEM scans were performed, as shown in Figure 4.11 (c) and (d). Figure 4.11 (c) indicated that the carbide precipitation was located within lath boundary at 350°C. The coarser carbides were observable for the specimens at a higher temperature of 500°C as shown in Figure 4.11 (d). This result is consistent with those reported by Zhao et al. (2018) for 3Mn-Si-Ni martensitic steel.

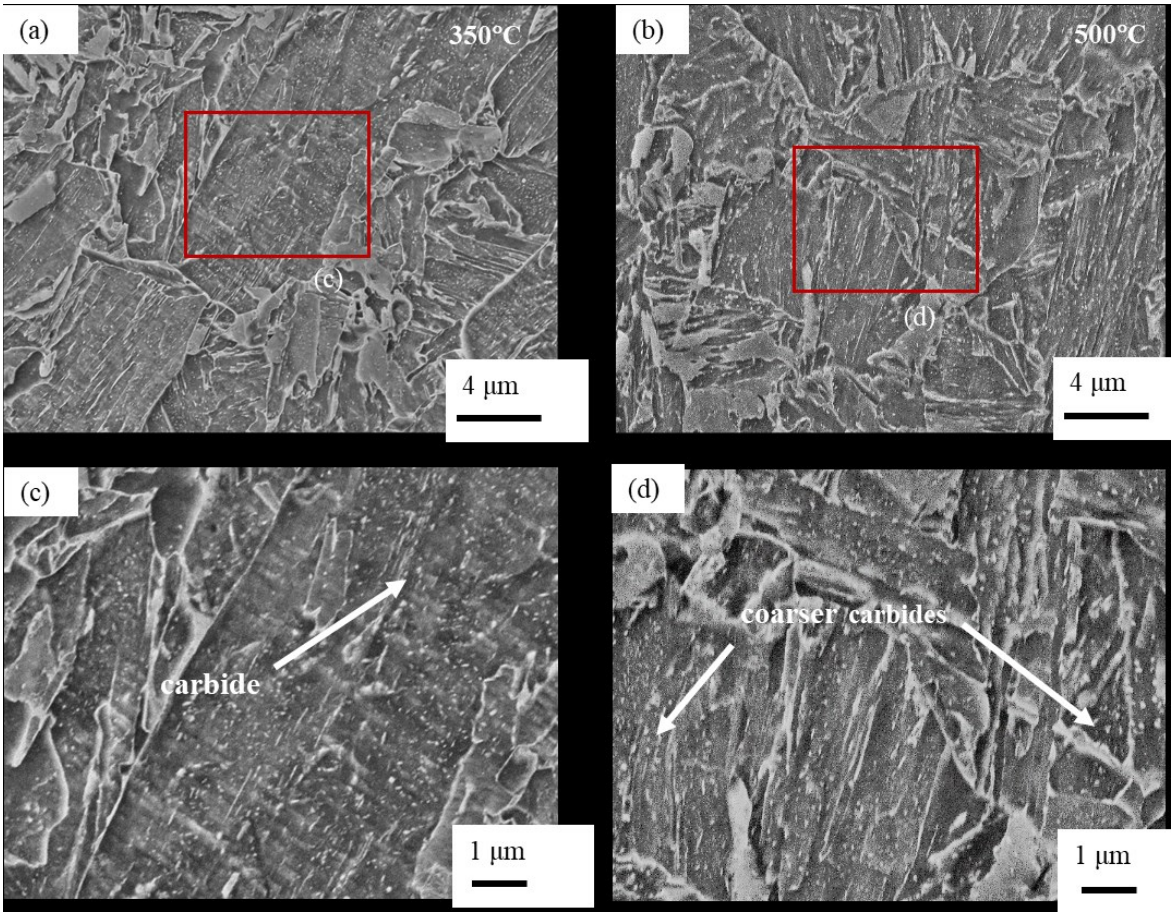

Figure 4.11 SEM micrographs showing the effects of temperatures on the microstructures of the MS1180 steel (a) 350°C, (b) 500°C, (c) local magnification of carbides precipitates at 350°C (d) local magnification of carbides precipitates at 500°C.

4.1.4.2 Effect of heating rate on PFH and carbide precipitation of the MS1180 steel

In terms of post-form hardness (PFH), as observed in Figure 4.12, increasing the heating rate resulted in a consistent increase in hardness. Compared with a slow heating rate of 1°C/s, the PFH at an ultra-fast heating rate of 150°C/s improves by approximately 5%. It was found that the ultra-fast heating rate was not only beneficial for ductility but also PFH of the MS1180 steel at an elevated temperature of 450°C. It is believed that a prolonged period of heating and soaking of the MS1180 steel will diminish hardness due to the continuous carbides precipitation and coarsening. Finer and more uniform carbides in the rapidly heated specimens made a greater contribution to strengthening the matrix which induced a higher strength. Additionally, fast heating rate retards the annihilation of dislocations by recovery. A lower state of recovery at fast heating rate results in a higher dislocation density which induced an

improved PFH. Moreover, the contribution of solid-solution strengthening of carbon in martensite increased with increasing heating rate. These results are consistent with those reported by Revilla et al. (2014) in low alloy steel. Therefore, a heating rate over 50°C/s at 450°C is favourable which would be beneficial for maintaining the PFH and simultaneously improving the ductility of the material.

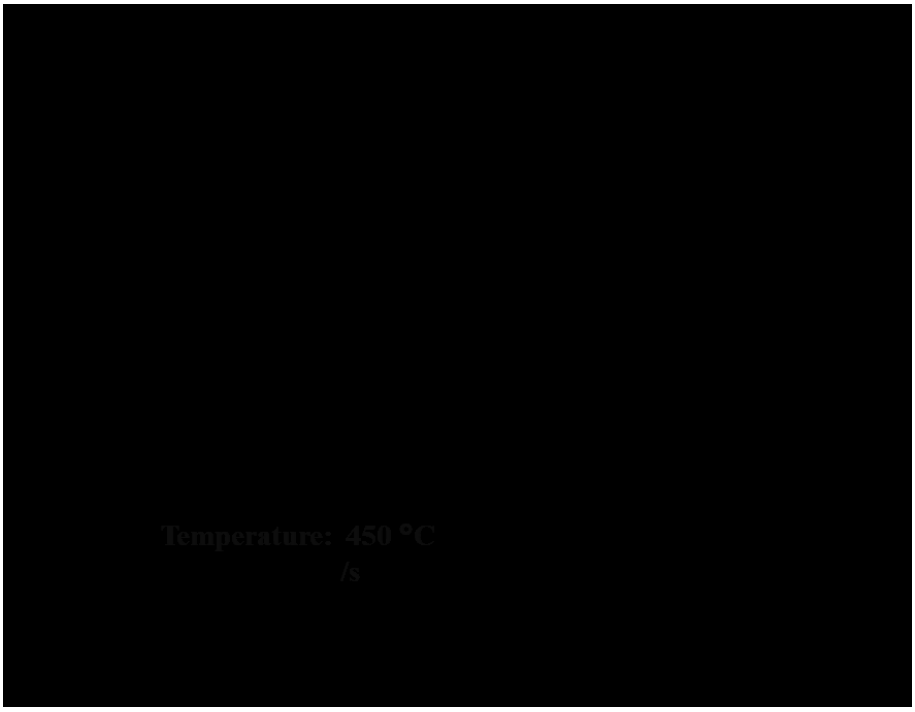

Figure 4.12 Evolution of the post-form hardness as a function of heating rate.

Figure 4.13 shows the SEM micrographs of the specimens that were heated to 450°C at various heating rates. The carbides precipitating inside the grain and on grain boundaries were visible as shown in Figure 4.13 (a)-(d) at a heating rate of 1, 10, 50 and 150°C/s. It can be seen that the density of carbide increased with increasing heating rate from 1 to 150°C/s. The carbide precipitation is finer at a fast heating rate of 150°C/s. These carbides were cementite which was gradually transformed from ε-carbide during the heating process when the heating temperature is higher than 250°C (Massardier, 2014).

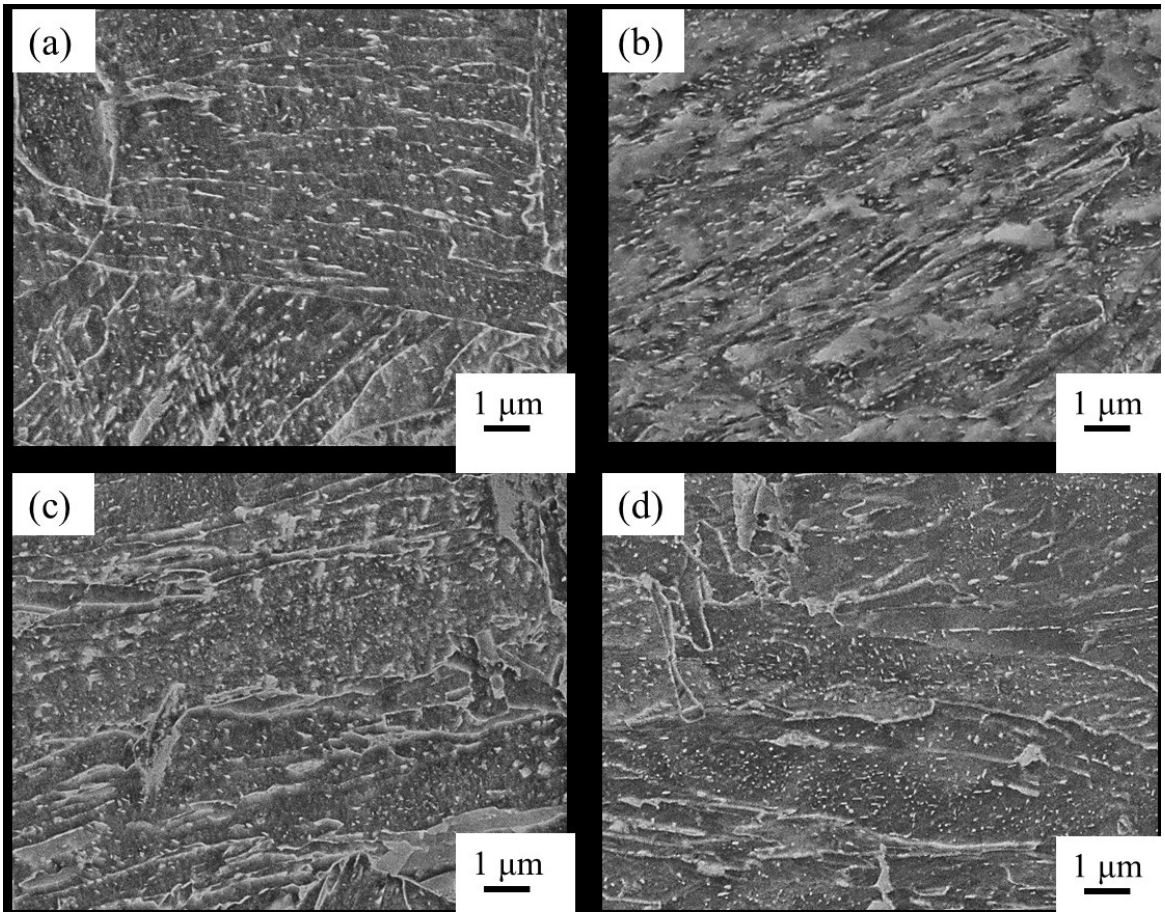

Figure 4.13 SEM micrographs showing the effects of heating rate on the carbide precipitates of the MS1180 steel (a) 1°C/s, (b) 10°C/s, (c) 50°C/s and (d) 150°C/s.

TEM observation was performed on specimens heated at different heating rates, which can be used to distinguish the pattern of cementite formed in lath martensite more precisely. Figure 4.14 (a)-(c) shows that needle-shaped cementite was clearly observed around the lath boundary or prior austenite boundary. At the heating rate of 1°C/s, the growth and coalescence of cementite are easily identified as shown in Figure 4.14 (a). The results indicated that with increasing heating rate, the density of cementite increased and the refinement of cementite structure was observed, as shown in Figure 4.14 (b) and (c) suggesting that the ultra-fast heating rate is beneficial for the refinement of carbides.

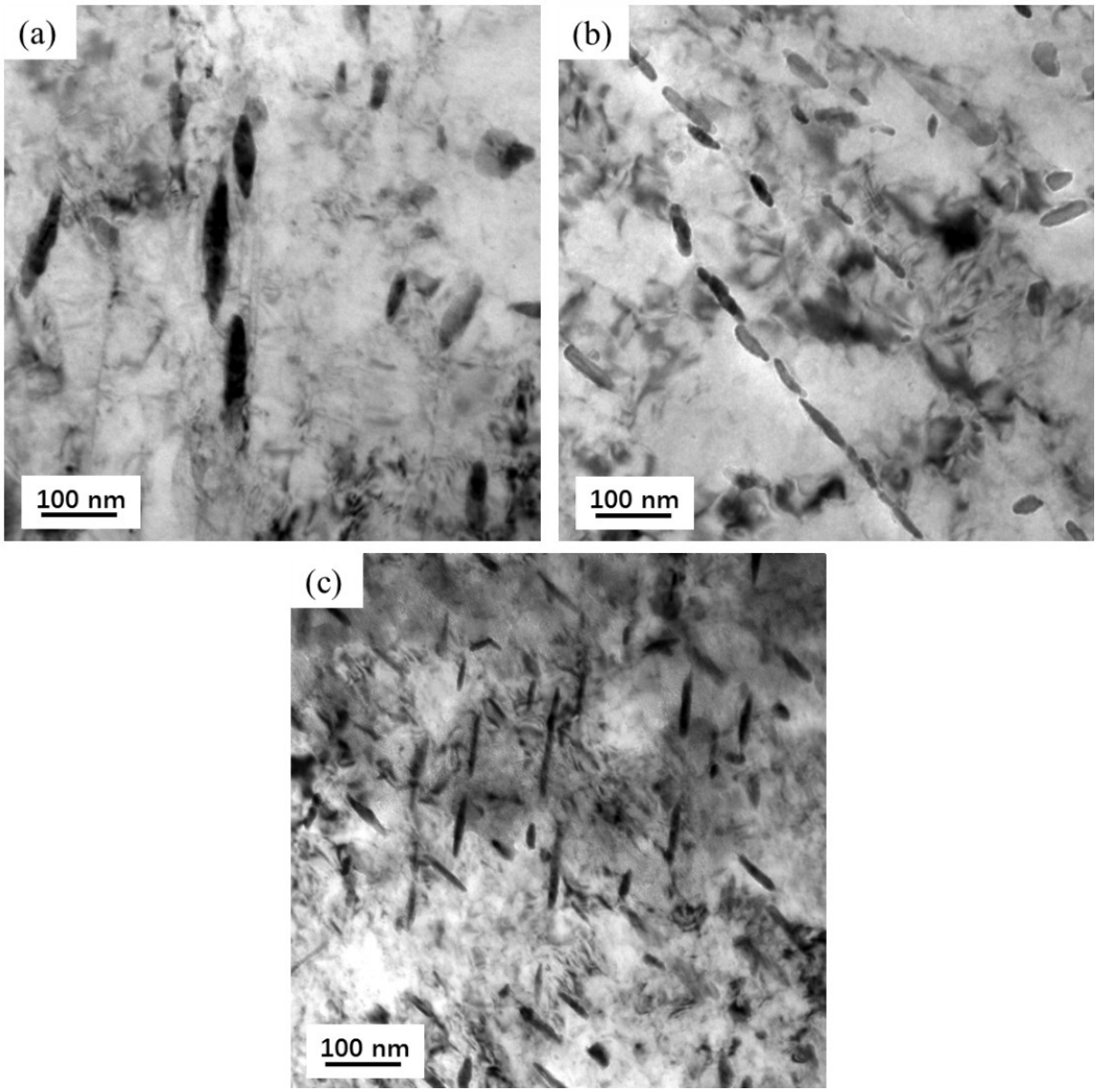

Figure 4.14 TEM micrographs showing carbides of the MS1180 heated at different heating rates (a) 1°C/s, (b) 50°C/s and (c) 150°C/s.

Carbide precipitation analysis was subsequently carried out by Image J using micrographs at a magnification of 20000. At least 10^3 carbides were measured at various conditions. The evolution of carbide volume fraction and size distribution are plotted in Figure 4.15 as a function of the heating rate. The equivalent diameter of carbides was defined using the cross-sectional area of each carbide. At least 10 micrographs were used to calculate the equivalent diameter of carbides. It can be seen that the carbides are smaller than 200nm. The size of carbide reduces with an increase in heating rate. During the continuous heating process, a lower heating rate would lead to a prolonged heating period, which led to the coarsening of carbides.

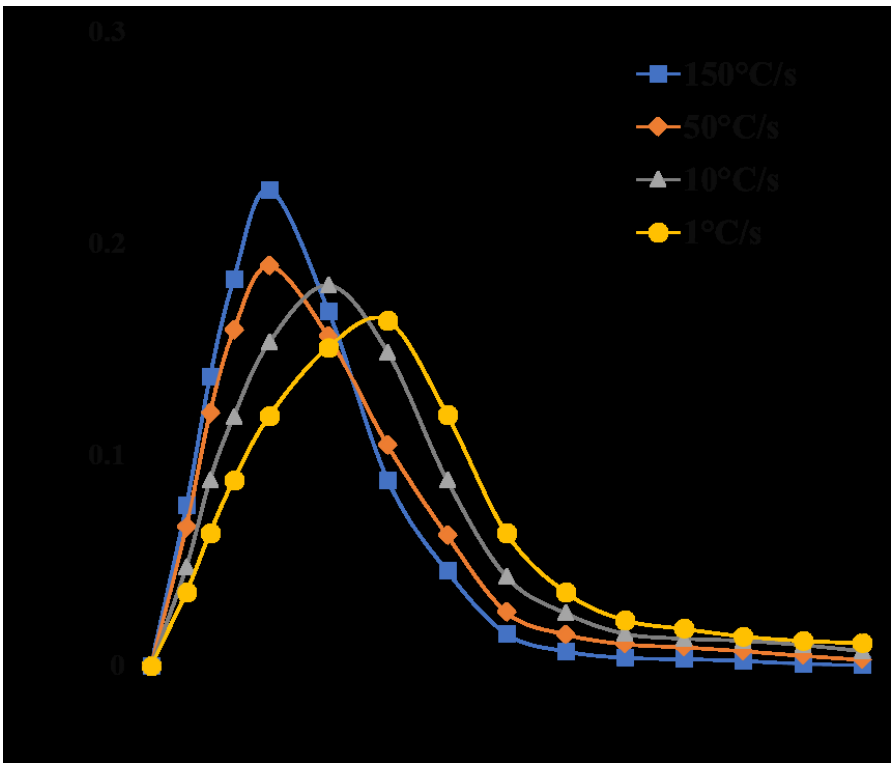

Figure 4.15 Effect of heating rate on the carbide size distribution.

The relationship between the equivalent diameter of carbide and residual hardness was plotted in Figure 4.16. For a lower heating rate of 1°C/s, the result shows the mean carbide diameter was approximately 62 nm, leading to a low hardness of HV375. It was found that for higher heating rates, a slight increase of hardness was observed due to the refinement of carbide. Compared to the slowly heated sample at a heating rate of 1°C/s, the mean size of carbides at a high heating rate was smaller at approximately 48nm which leads to a roughly 5% increase in hardness. The ultra-fast heating rate stimulates a higher nucleation rate, which enables fine and more copious precipitates to be obtained. These finer precipitates exhibit better strengthening effect compared to coarser precipitates and thus induced a higher post-form hardness (Xie et al., 2016). An additional strengthening mechanism is the contribution of remaining carbon in the solid solution of martensite, which increases with heating rate and hence induces a residual hardness enhancement.

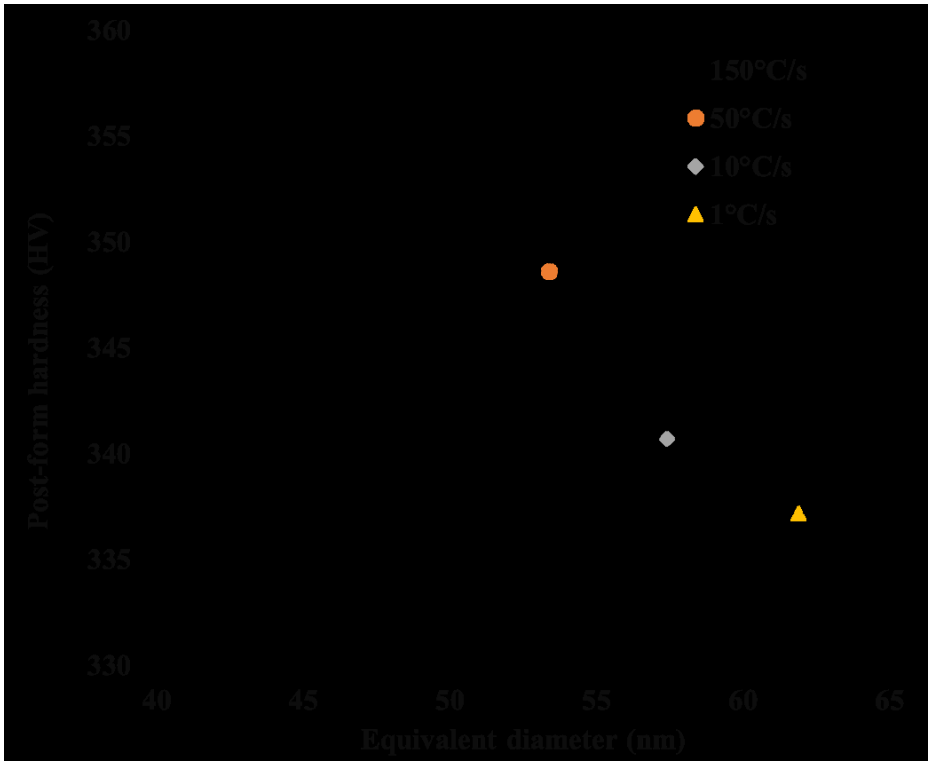

Figure 4.16 The relationship between carbide size and residual hardness.

Figure 4.17 indicates a schematic illustration of the carbide precipitation of deformed samples at various heating rates. The microstructure of as-received material, lath martensite structure, is composed of laths, blocks and packets within a single prior austenite grain. These packets are further subdivided into blocks containing laths with similar crystal orientations. The blocks and packets in the microstructure contribute to the mechanical properties of lath martensite, such as toughness and strength. A high density of dislocation was found within lath martensite which hinders the lattice movement, thus, inducing the high strength of the MS1180 steel. When the specimen was heated at a slow heating rate to elevated temperatures and deformed to fracture, larger carbide precipitates in needle-shape tend to nucleate within laths and on the lath boundaries. For an ultra-fast heating rate, the carbide is finer and dispersed and thus higher dislocation density is retained. It is found that some dislocation was newly formed due to plastic deformation occuring concurrently with the annihilation of dislocations by recovery. The recovery phenomenon of reduction dislocation in induced density is one of the major reasons for reducing the strength of the MS1180 steel at elevated temperatures (Krauss, 2001). In conclusion, the carbide precipitation influences the change of strength and ductility of the material significantly.

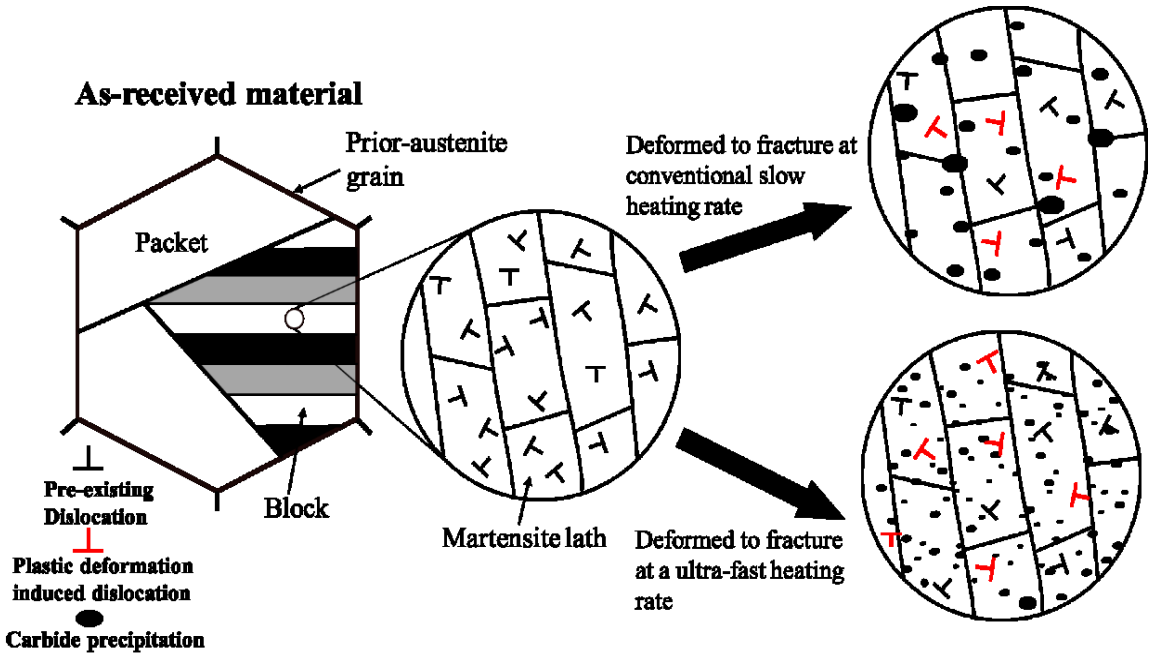

Figure 4.17 Schematic illustration of the carbide precipitation of deformed samples at different heating rates.

It was apparent that temperature and heating rate significantly affect the microstructure and mechanical properties. With the increase of the heating temperature, the carbide gradually precipitated from the martensite matrix. The supersaturation of martensite decreased with increasing temperature, which means the solid-solution strengthening of carbon in martensite was further reduced and thus a reduction in residual hardness occurred. At higher heating temperatures, the carbides undergo coarsening and the recovery is more pronounced. Therefore, a lower heating temperature is preferred to maintain a higher residual strength of the MS1180 steel.

It was found that the fast heating rate can simultaneously enhance ductility and PFH of the MS1180 steel. The reason is believed to be that the rapid heating rate retards the annihilation of dislocations by recovery and accelerates the precipitation kinetics of carbides. As a consequence, a combination of more copious and finer carbides and high dislocation density are obtained at a fast heating rate which contribute more to strengthening the matrix, and thus improves PFH of the MS1180 steel. In addition, the PFH increase is directly related to solid solution strengthening by carbon. The residual carbon content is higher at rapid heated samples which induced a greater contribution to strengthening martensite. On the contrary, slow heating

induces the growth of carbides and as a consequence, coarser carbides precipitated around the grain boundary, which weaken the boundary cohesion and impair ductility.

4.1.4.3 Effect of soaking time and cooling rate on hardness of the MS1180 steel

Figure 4.18 shows the hardness evolution of rapidly heat-treated specimens as a function of the soaking period. It was found that a longer soaking time leads to a steady reduction of strength for specimens heated to 450°C. Compared to the specimens without soaking, the hardness of specimen soaked at 8s decreased by approximately 2.9%. The prolonged soaking time led to coarsening of carbides and stronger recovery of dislocation, and consequently, the residual strength decreased. Figure 4.18 (b) shows the hardness of the specimens quenched by different media. It was found that water quenching resulted in approximately 3.1HV increase in hardness compared to air quenching. The super-fast cooling rate achieved via water quenching minimized the carbide coarsening and recovery process and thus the water-quenched specimen exhibited a slightly higher hardness. In order to minimize the strength reduction, short soaking time and fast quenching rate are preferred for the FWS process.

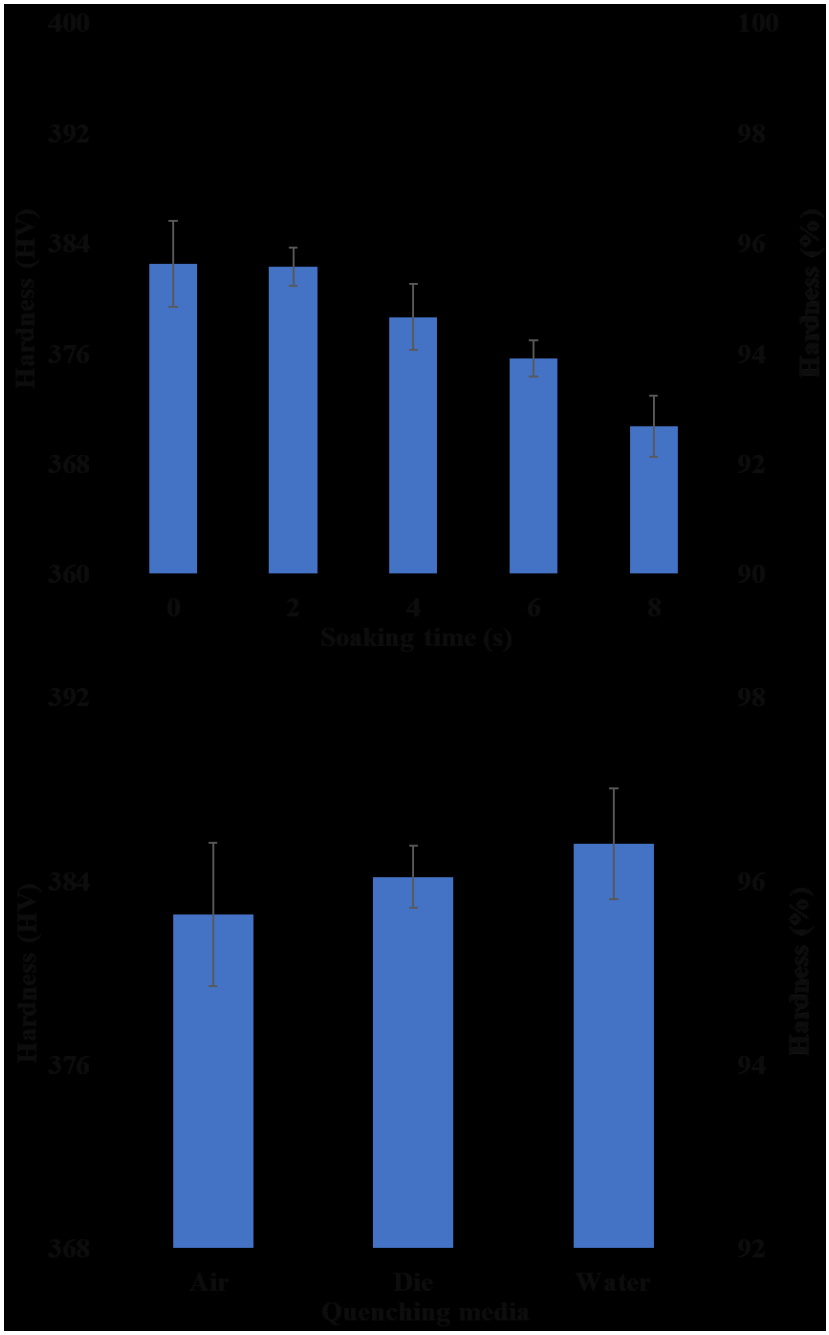

Figure 4.18 Evolution of the hardness as a function of (a) soaking time (b) quenching media.

4.2 Development of an optimal processing window for the FWS process

The process variables in FWS including temperature, strain rate and heating rate can significantly affect the thermo-mechanical properties and microstructures of the MS1180 steel.

Based on these experimental results, an optimal processing window must be developed for FWS technology.

Figure 4.19 shows the processing window for FWS by defining the processing parameters on cementite nucleation and ductility of the MS1180 steel. The elongation of specimens at different conditions was utilised to plot the background colourful map. It is found that the cementite precipitation tends to occur earlier at a lower heating rate. The cementite nucleation period is shorter at a fast heating rate. The trend of the start and end formation of cementite was predicted according to the micrographs which shown in a dash line. The nucleation of carbides during the continuous heating process is unavoidable unless the heating rate is extremely high. The optimal temperature was defined at 450°C which has a balanced ductility and post-form hardness. Additionally, the elongation of the MS1180 steel was shown in Figure 4.19, which increased with increasing temperature and heating rate. Since the uniaxial tensile tests have not been covered with the superfast heating rate above 150°C/s and slow heating rate below 1°C/s, the data are predicted by using interpolation based on the existing results, which is shown in light grey colour.

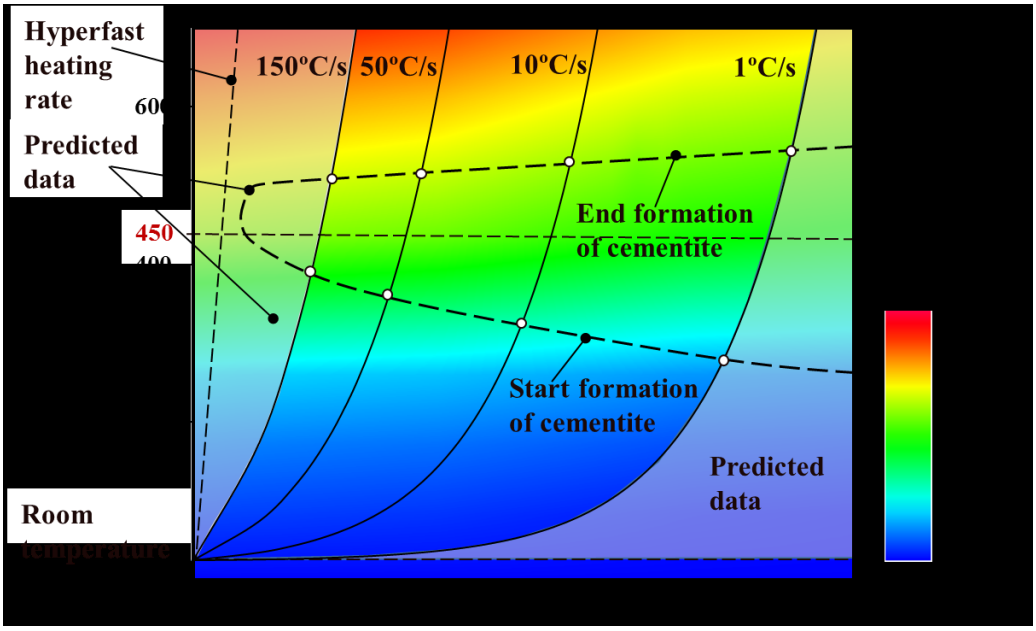

Figure 4.19 Development of processing window of fast-warm stamping by defining cementite precipitates nucleation and elongation of the MS1180 steel at various conditions.

As presented in section 4.1, the peak ductility of the MS1180 steel was achieved at 500°C although the PFH was significantly reduced. The peak PHS can be obtained at a lower forming temperature although the material is less ductile. Therefore, the optimal processing window for fast-warm stamping of the MS1180 steel was suggested to be a forming temperature range of 400–450°C with a heating rate of at least 50°C/s and no soaking time, which can provide superior strength-ductility combinations. These optimal forming parameters not only enhanced the ductility of material but also minimized the recovery process and carbide coarsening and thus the reduction in PFS was diminished. Additionally, high forming speed is preferred for FWS technology which is not only beneficial for excellent PHS and ductility but also for a short cycle time.

4.3 Summary

The flow behaviour and ductility the MS1180 steel has been characterised by uniaxial tensile tests under different temperatures, strain rates and heating rates. A roughly threefold improvement in ductility was found as temperature increased from 25°C to 450°C. The total elongation increased from 14.2% to 22.4% as strain rate increased from 0.01 to 5/s. Additionally, ultra-fast heating rate enhanced the ductility of the MS1180 steel at 450°C by 25.7% when the heating rate increased from 1°C/s to 150°C/s. The improved ductility at higher strain rate and heating rate is mainly attributed to the dispersed distribution of fine carbide precipitates.

The effects of temperature, strain rate and heating rate on the post-form hardness of the MS1180 steel have been investigated. The PFH decreased from 370.4 HV to 331.2 HV as the temperature increased from 350 to 500°C. The gradual reduction of hardness was due to the fact that the higher heating temperatures accelerated the decomposition of martensite phase and the nucleation and coarsening of carbide precipitates. Moreover, the contribution of solid-solution strengthening of carbon in martensite reduced with increasing temperature and hence induced a lower PFH. Compared with a slow heating rate of 1°C/s, the PFH at an ultra-fast heating rate of 150°C/s improves by approximately 5%. The slow heating rate will diminish hardness due to the continuous carbide precipitation and coarsening. Additionally, a lower state of recovery at fast heating rate results in a higher dislocation density which induced an improved PFH. SEM observations show that martensitic structures were still distinguishable

as the carbides precipitated within the laths or on lath boundaries at 500°C due to the ultra-fast heating. The SEM and TEM observations performed at various heating rates indicated that the carbide is finer and dispersed at an ultra-fast heating rate.

The optimal processing window for fast-warm stamping of the MS1180 steel was suggested to be a forming temperature range of 400–450°C with a heating rate of at least 50°C/s and no soaking time, which can provide superior strength-ductility combinations.

Chapter 5. FWS tests and finite element (FE) simulation of the FWS process

In this chapter, forming trials for the proposed FWS process were conducted through the dedicated pilot production line *Uni-form*. The post-form hardness and microstructural distribution at different locations of formed U-shaped components under optimal forming conditions were presented. Moreover, the effect of forming temperature and forming speed on springback of formed components was investigated. Additionally, the FWS process for the MS1180 steel U-shaped component was simulated using the FE commercial software PAM-STAMP. The setup of FE model was developed and the FE simulation results were experimentally validated according to the proposed process. These simulations were subsequently used to analyse the mechanics of springback under various forming conditions.

5.1 U-shaped formed component via the FWS process

5.1.1 Mechanical properties and microstructure of formed components

In this research, the proposed FWS process was validated by producing U-shaped components from a 1.6mm MS steel sheet blank at a forming temperature from 300 to 450°C and a forming speed from 75mm/s to 380mm/s. A demonstrator U-shaped part was successfully formed at 400°C and forming speed of 250mm/s, as shown in Figure 5.1, following the developed optimal processing window. No crack or localized necking was visible in any region of the formed part.

Chapter 5 is based on paper work ‘‘Sun, Y., Cai, Z., Politis, D. J., Luan, X., Chen, G., Wang, L., 2019. Springback characteristics of UHSS for warm u-shape bending: experiments and FE simulation. 38th International Deep-Drawing Research Group Conference. 3-7 June 2019, Enschede, Netherlands.’’ and patent ‘‘Sun, Y., Ji, K., Luan, X., Liu, X., Fakir, O. EL., Cai, Z., Wang, L., 2017. Fast warm stamping of ultra-high strength steel sheets’’.

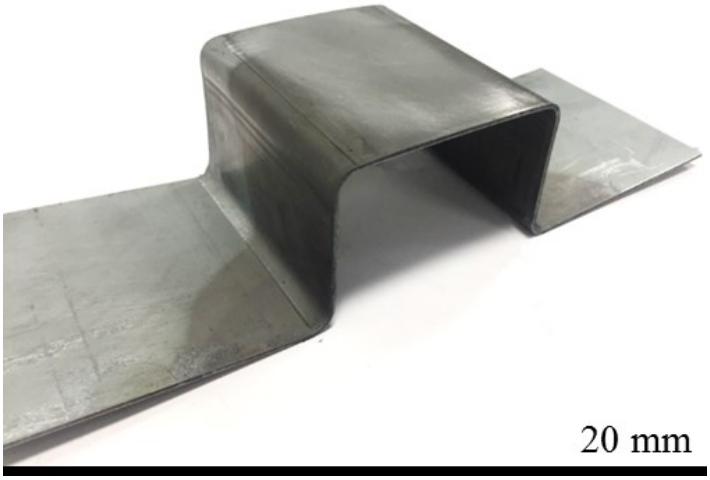

Figure 5.1 Fast-warm stamped demonstrator U-shaped part from MS1180 steel sheet.

Hardness testing was conducted at 8 different positions along the cross-section of the formed component, as shown in Figure 5.2. The formed part exhibited an evenly distributed hardness values of approximately 370±10 HV, throughout the cross-section. It was found that the formed parts exhibited about 92% of the original as-received MS1180 steel hardness. Moreover, the hardness of the formed parts is consistent with the hardness of the specimens in degradation tests at the same conditions, as mentioned in section 4.1.4.

Figure 5.3 shows the microstructural characterization of fast-warm formed components at locations 5, 6 and 8. It can be observed that uniformity of lath martensite microstructure existed in the selected areas resulting in the formation of uniform post-form hardness. Additionally, the martensitic microstructure was retained in the fast-warm stamped part and thus the PHS of the formed part was almost identical to the as-delivered material. To further characterize the morphologies of carbide precipitation, a close view of fine carbides is presented around and inside grain and on grain boundaries, as shown in Figure 5.3 (d). The fast-warm stamping process was found to suppress the detrimental precipitate coarsening and maintain the as-received microstructure. This result is consistent with SEM micrographs which were obtained from the fast-heated specimen in section 4.1.4.

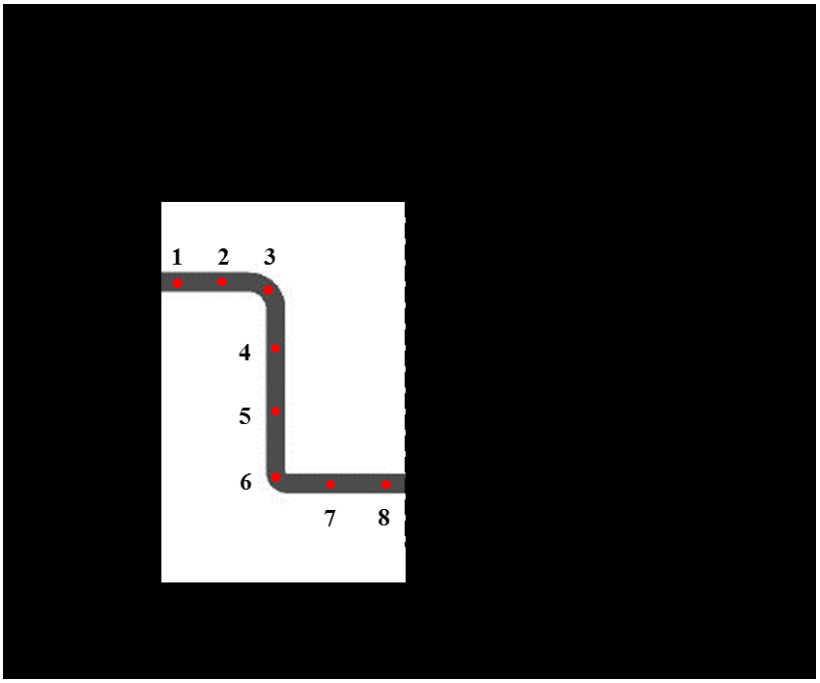

Figure 5.2 Vickers hardness distribution through a cross-section of U-shaped parts at 400°C.

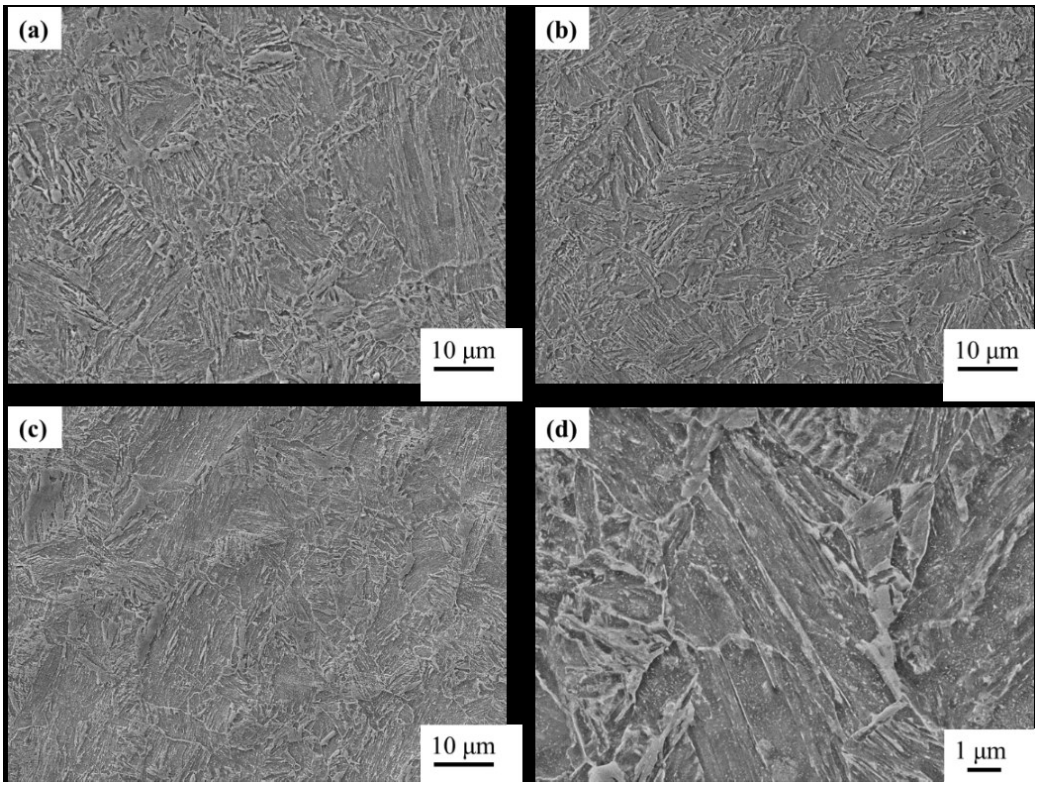

Figure 5.3 Microstructure of fast-warm stamped part at (a) location 5, (b) location 6, (c) location 8 and (d) magnification of carbide precipitates at location 5.

Dog-bone shaped specimens were cut from the bottom region on the formed U-shaped components and tensile tests were performed at room temperature to examine the mechanical properties. Figure 5.4 indicates the effects of forming temperature on the flow behaviour of the MS1180 steel deformed at a fixed strain rate of 0.001/s. It was observed that an appreciable reduction in the flow stress occurred as the forming temperature increased. The ductility of the MS1180 steel indicated by strain to failure slightly improves by approximately 15.2% compared to as-received material. This is because elevated temperature enables more activated recovery and carbide precipitation resulting in a softer material.

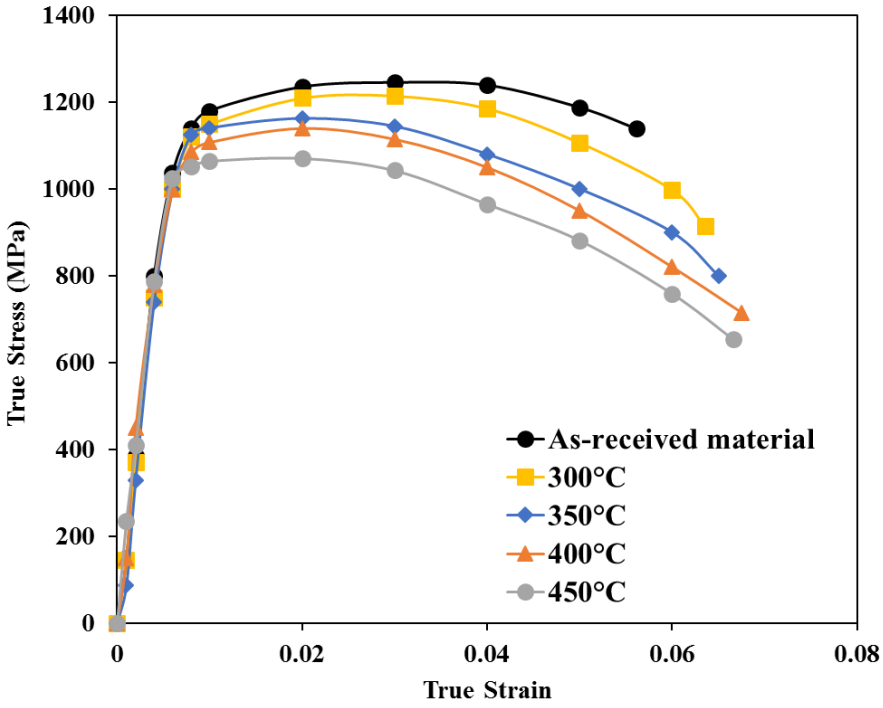

Figure 5.4 Flow stress-strain curves of formed parts at various temperatures.

Figure 5.5 shows the variation in mechanical properties of U-shaped components formed at different temperatures ranging from 300°C to 450°C. The hardness recorded was the average value measured at various locations on the surface of formed parts. Figure 5.5 (a) shows the evolution of the PFH is a function of forming temperature. An excellent PFH of approximately 394.0 HV was achieved at forming temperature of 300°C, which is only reduced by approximately 3% compared to the original hardness. The PFH of the MS1180 steel decreased gradually with increasing forming temperature. The hardness of formed components at 450°C was approximately 370.4 HV, which is nearly 92% of the as-delivered strength of material.

Additionally, a similar tendency could also be found in the evolution of the PFS, as shown in Figure 5.5 (b). Increasing the forming temperature resulted in a continuous decrease in the PFS due to a tiny portion of martensite that was inevitably dissolved during the fast-warm stamping process. The evolutions of PFH and PFS at various temperatures show a close agreement with the results in Section 4.1.4.1. Nevertheless, it can be confirmed that a fast-warm stamped part at 400°C exhibited over 92% mechanical strength of the original as-received material consisting of 1140MPa UTS and 370HV hardness.

The total manufacturing cycle time of the proposed forming technology was within 10 seconds. The reduced cycle time leads to a higher production rate and lower energy consumption. Additionally, the post-form strength and microstructure of the MS1180 steel for the formed part can be maintained close to the supplied material via the FWS process. These benefits enable this forming technique to be an alternative solution to form high strength components.

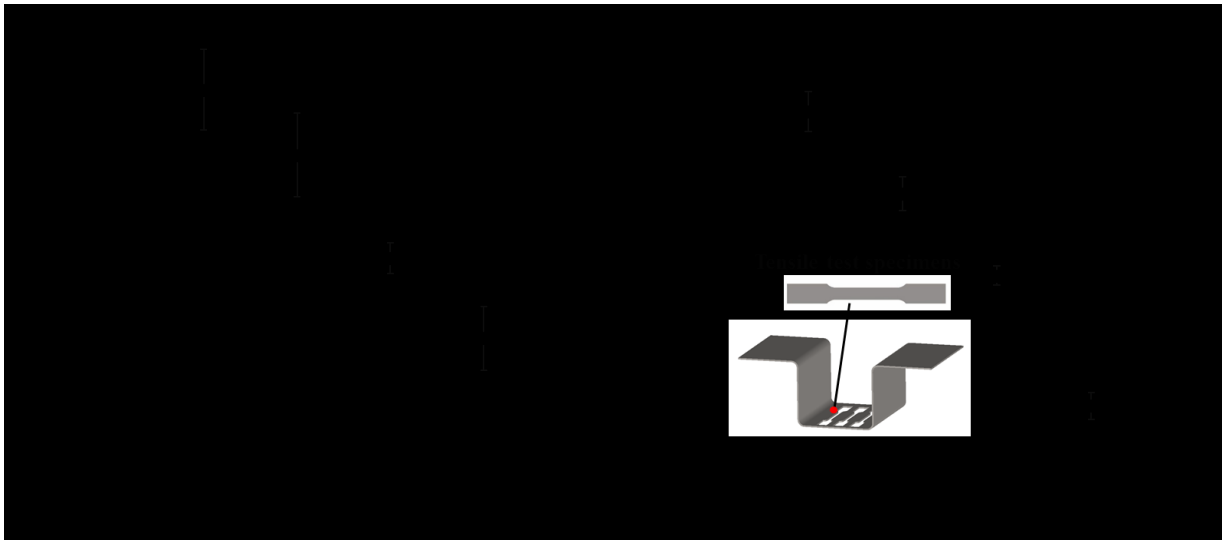

Figure 5.5 Effect of temperature on the mechanical properties at the examined location of U-shaped parts: (a) post-form hardness (b) ultimate tensile strength.

5.1.2 Springback analysis of U-shaped components

The geometries of formed MS1180 steel sheets for different forming temperatures are shown respectively in Figure 5.6. It can be seen that the final geometry formed at 300ºC has considerable springback at the sidewall and flange area. The springback decreased at a higher forming temperature of 400ºC and was nearly eliminated at a temperature of 450ºC.

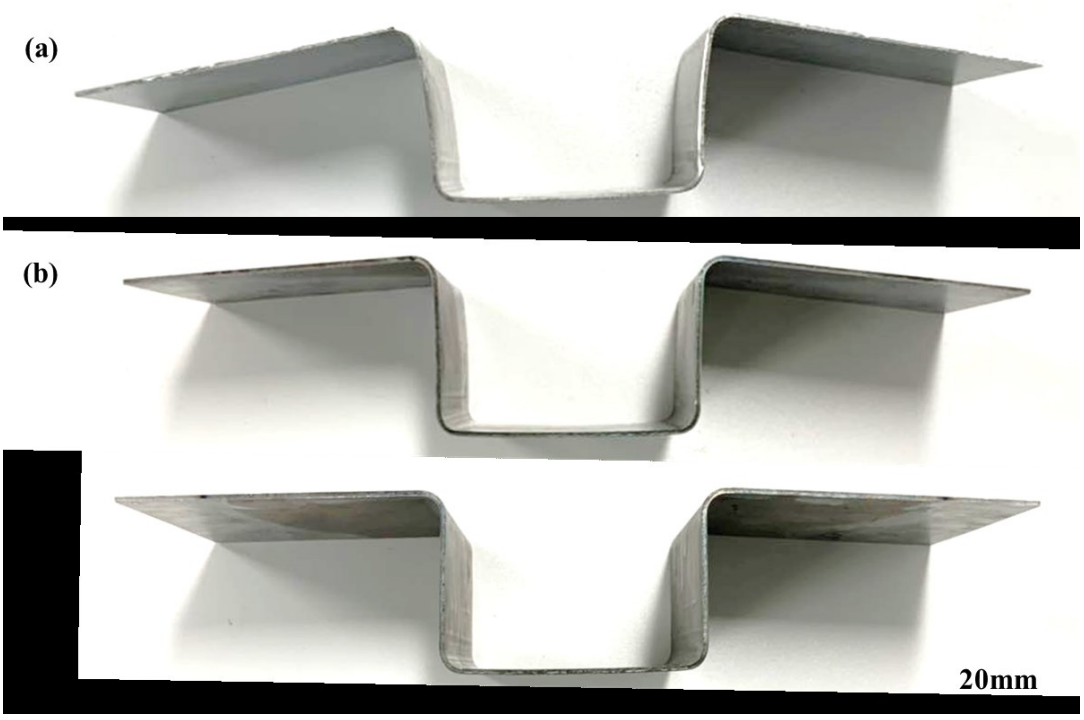

Figure 5.6 Three formed U-shaped components with MS1180 steel at different temperatures (a) 300ºC (b) 400ºC (c) 450ºC.

Figure 5.7 illustrates the effect of stamping temperature on springback angle for MS steel components formed by FWS and cold stamping. It was observed that the extent of springback decreased significantly as the temperature increased from room temperature to 300°C and was subsequently followed by a linearly drop as the stamping temperature increased above 300°C. The magnitude of springback angle θ_1 dramatically decreased by 60.7 % from 8.36° to 3.28° as the stamping temperature increased from 25 to 400°C. The springback angle θ_2 showed a similar tendency by decreasing by approximately 62.3% over the same temperature range as the springback angle θ_1. The primary reason for reduction of the springback is the lower residual stress at elevated temperatures. When the blank was formed at room temperature, the high strength and material draw-in from the blank holding area lead to a significant springback. At elevated temperatures, the reduction of flow stress is considerable, subsequently reducing material draw-in and increasing the tensile deformation. Moreover, the lower yield strength at a higher temperature results in lower deformation resistance. It can be deduced that the FWS process for MS steel is an effective method in minimising springback.

Figure 5.7 Springback angle of U-shaped component as a function of forming temperature.

Figure 5.8 shows the experimental results of the effect of forming speeds (75, 150, 250, 380 mm/s) on springback angle at a stamping temperature of 400°C. The results of both springback angles showed a similar trend where increasing the forming speed initially leads to a steady reduction in springback angle, where after 250mm/s, the amount of springback remains nearly constant and is hence unaffected by forming speed. The reduction of springback angles θ_1 and θ_2 when forming speed is increased from 75 to 380 mm/s is 20.9% and 38.6% respectively. Compared to θ_2, the angle θ_1 was less sensitive to temperature. This springback reduction with speed phenomenon can be explained by the difference of the tangential stress in the top and bottom surfaces of the blank after forming. A smaller through-thickness stress gradient was normally accompanied by lower level of springback. Higher forming speeds induced higher tensile stress in both top and bottom surfaces resulting in lower through-thickness stress gradient of the formed parts, and thus springback decreased. The stress gradient distribution of formed part was generated by FE simulations and presented in section 5.2.3 for further discussion. Higher forming speeds also reduced the period of the forming stage, which led to a higher temperature as well as lower flow stress remained by the blank from contacting the

punch until fully deformed by forming tools. These findings are consistent with the results reported by Wang et al. (2017a). It can be concluded that a combination of high stamping temperature and a fast forming speed in the FWS process were beneficial in reducing springback as well as improving the formability of the MS1180 steel.

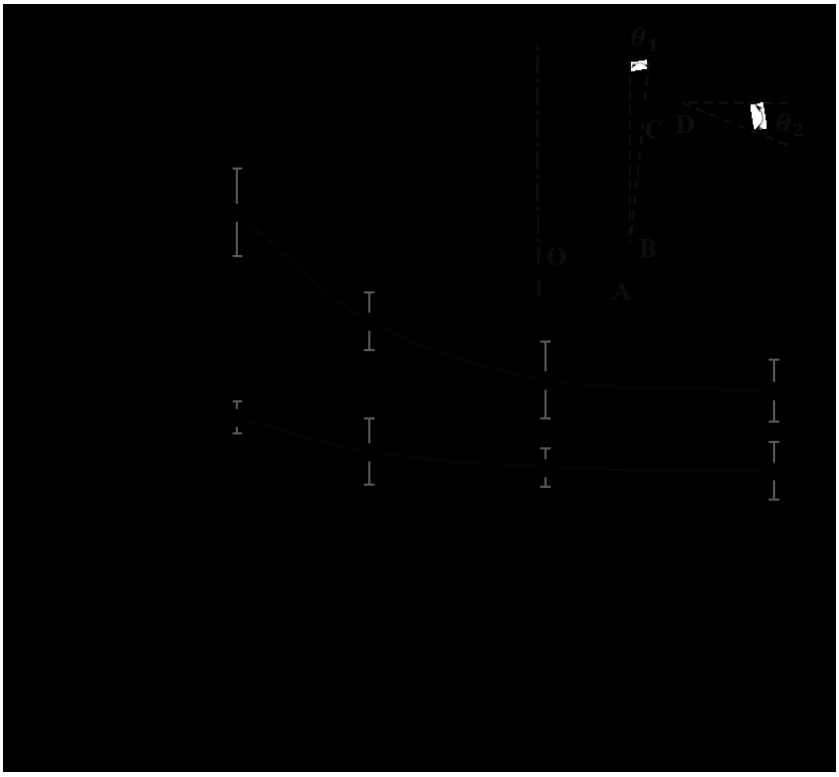

Figure 5.8 Springback angle of the U-shaped component as a function of forming speed.

5.2 Finite element simulation of FWS process

5.2.1 FE model setup

The final form of a part is changed by springback, which makes it difficult to produce the part accurately. The PAM-STAMP is a software package that is specialised for sheet metal forming processes, especially for warm and hot stamping processes. To effectively predict springback behaviour, FE simulations were performed to simulate the entire fast-warm stamping process for a U-shaped part of similar geometry to the components formed experimentally. The aim of the FE simulation software can not only detect springback, which also be beneficial for minimizing the risk of costly changes to refine tools.

In setting up the simulation, the 'hot-forming module' was initially selected to enable the thermal and mechanical effects to be modelled during the forming process. The CAD geometrical forming tools were created by the commercial software Solidworks and then imported as IGES files into PAM-STAMP. The forming tools were defined as a rigid body as tool distortion during the whole process was negligible. The imported forming tools were subsequently meshed using DeltaMESH tool. The FE model set-up for U-shaped forming tests is shown in Figure 5.9. For simplicity, the tool geometries are all symmetrical thus only half of the component was simulated via a symmetry plane condition.

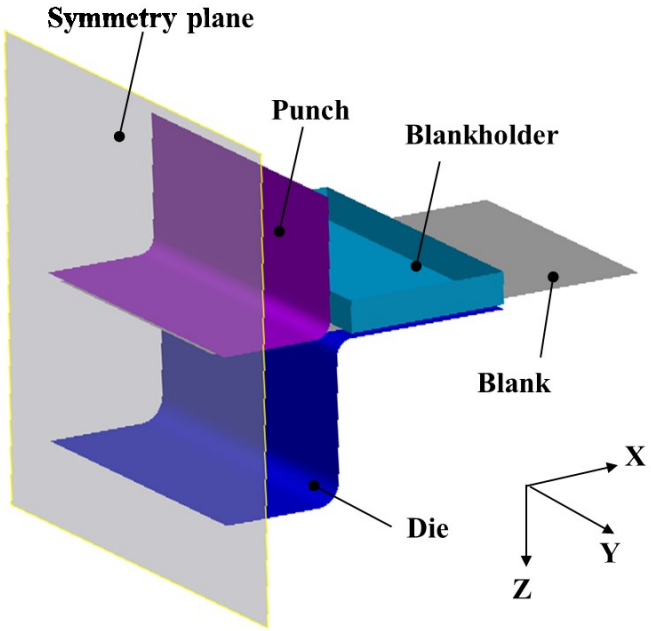

Figure 5.9 Demonstration of forming tools, blank and their coordination frame set up.

The initial element sizes, the level of mesh refinement and in particular, the final element sizes are one of the most important parameters for calculation speed and quality. This applies especially for a high-quality simulation. The size of the elements for the blank must be small enough to analyse precise phenomena like surface defects or springback. Size of elements corresponding to half the radius of the die entry fillet is usually used. In this study, shell elements with a finer mesh size of 1.6 mm were used for the blank which is corresponded to the element size used for the blank. The smaller mesh size allows the blank can be deformed freely during forming. The mesh size of 1.6 mm was considered as the convergent value, and 1.6×1.6 mm^2 quadrangle thermal shell elements were used to mesh the specimen to optimise

the computational time. The blank with 1.6mm mesh size is shown in Figure 5.10. The effect of type and the number of elements on FE simulations would be considered in the future study.

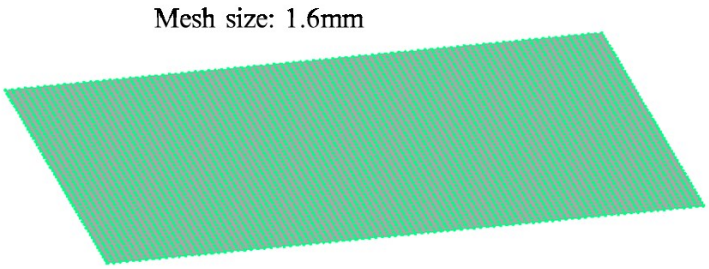

Figure 5.10 Blank meshing with 1.6mm mesh size.

The FE simulation of the U-shaped part forming process was divided into 5 stages in PAM-STAMP, namely gravity, holding, stamping, quenching and springback, as shown in Figure 5.10. In the gravity stage, the blank was firstly placed on the bottom blank holder without contacting the die and the punch. In the holding stages, the blank holder moved downwards and contacted the blank. A constant blank-holding force of 10kN was applied on the blank. In the stamping stage, the punch moved towards the blank at the selected forming speed, continuously drawing the blank into the die. In the quenching stage, the formed component was subsequently quenched within the cold tools for 5s at a constant die closing force of 170kN. During the stamping and quenching stages, the heat transfer between the blank and the tool led to a considerable drop in the blank temperature. In the final stage, springback was simulated using a 'One Step Springback' unloading scheme, which eliminates all the constraints simultaneously and forces the blank to attain equilibrium within two numerical increments. The 2D sectional view of springback for the U-shaped part was subsequently measured using Solidworks. The physical parameters of the blank and tools are provided in Table 5.1. The friction coefficient of 0.2 between the workpiece and the tooling elements was assumed to remain constant, which based on the work by Liu et al. (2020). The thermal boundary conditions were applied to this FE model. The thermal exchange of air is used in the FE simulations which was defined at a temperature of 20°C. The thermal exchange between tools and blank was subsequently defined by determining the interfacial heat transfer coefficient (IHTC) at different conditions.

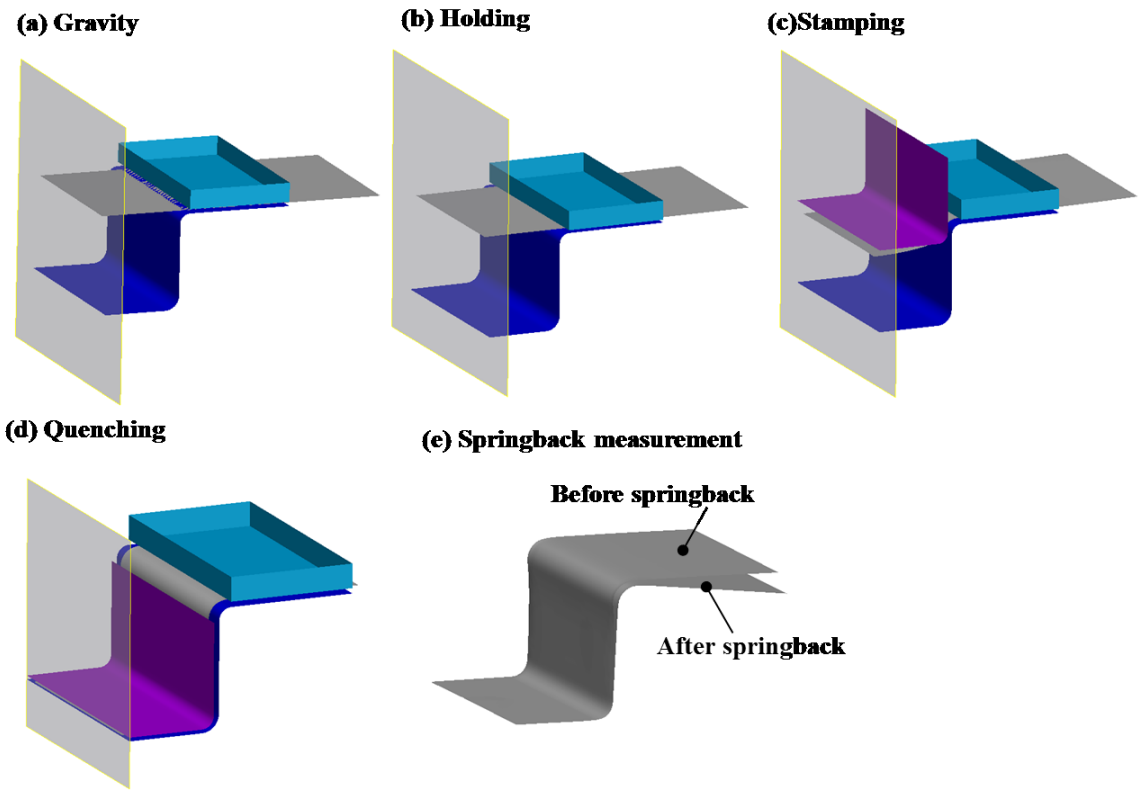

Figure 5.11 Schematic diagram of the FE model setup and springback measurement.

Table 5.1 FE model parameters for U-shaped forming tests.

Forming parameters	Value
Initial tool temperature (°C)	20
Forming temperature (°C)	25, 300, 350, 400, 450
Forming speed (mm/s)	50, 150, 250, 380
Blank-holding force (kN)	10
Die closing force (kN)	170
Quenching time (s)	5
Friction coefficient	0.2
Lubricant	Omega-35

The IHTC between warm blank and cold tools is an important thermophysical parameter in the hot/warm stamping processes, which affects the post-form properties and springback of formed components. An experiment facility call IHTC mate was designed by Xiaocan Liu which has been utilised to perform IHTC tests (Liu et al., 2020). The IHTC tests were conducted at 450°C

and the IHTC evolution with contact pressure for the MS1180 steel as shown in Figure 5.11. It can be seen that the IHTC values increase considerably from 0.6 to 11.0 kW/m^{2}K when contact pressure increased from 0.5 to 30 MPa. The rate of increase of IHTC reduced as the contact pressure increased from 30 to 40MPa. When contact pressure reached 40MPa, the plateau in the IHTC value was found at a value of approximately 12 MPa. This was attributed to the real contact area between the specimen and tools, which approached the peak value and thus the plateau of the IHTC occurred.

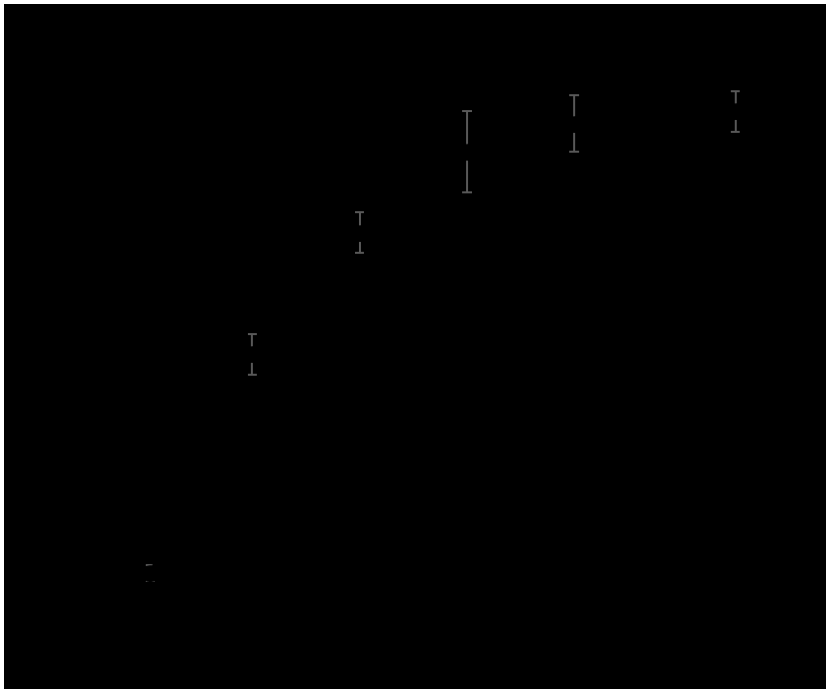

Figure 5.12 The interfacial heat transfer coefficient (IHTC) as a function of contact pressure for the MS1180 steel.

5.2.2 Material model setup

The material properties of 1.6mm MS steel blank such as the flow behaviour of the MS steels at different temperatures (25, 300, 350, 400 and 450°C) and at various strain rates (0.01, 0.1 and 1/s) were utilised as input data, which were characterised from uniaxial tensile tests via a thermo-mechanical simulator Gleeble 3800. Currently, material softening behaviour is not acceptable for state-of-the-art commercial FE software and it is assumed that the stress remains nearly constant once reaching the peak value. Figure. 5.12 shows the modified flow-stress curve of MS steel at different temperatures and strain rates. These curves were imported into

PAM-STAMP as discrete data points. It was found that the maximum strain obtained by forming a U-shaped component was less than 0.02 at a forming speed of 250mm/s. Therefore, the flow stress-strain curves used in the FE simulation ensured good accuracy for the simulation results. The thermal properties of the MS1180 steel blank used in this FE analysis are given in Table 5.2. The dissipation factor describes the percentage of internal work which will be converted to temperature. The default value dissipation factor is 0.9 (ESI, 2015). The thermal conductivity and specific heat of MS steel at elevated temperature were based on work by Huang et al. (2007).

Figure 5.13 Flow stress at different strain rates at a temperature of 450ºC.

Table 5.2 Material properties of MS steel blank (Huang et al., 2007).

	Temperature (°C)				
Property	25	300	350	400	450
Young's modulus (GPa)	210.0	185.6	169.8	160.3	148.7
Thermal conductivity (W/(m·K))	24.5	27.9	28.0	28.1	28.2
Specific heat (J/(kg K))	431	573	599	626	660
Poisson's ratio	0.3				
Dissipation factor	0.9				

5.2.3 Verification of the FE simulation results

The FE simulations were verified for both temperature and thickness distribution by comparison between the FE simulation and experimental results. During the U-shape bending process, the temperature of the blank at two selected positions, the bottom region and sidewall, were recorded and experimentally validated to ensure the FE simulation accurately captured the temperature change during deformation. Figure 5.13 shows the comparison of temperature evolution between the FE simulations and experiments. A close agreement was achieved between the FE simulation and experimental results. It was found that the temperature dropped slightly from approximately 400°C to 393°C during the first 0.2s. This was attributed to the blank not being contact with the cold die until the end of the stamping. In the quenching stage, the temperature reduces considerably at the bottom region due to the cold tools combined with a large die closing force resulting in a rapid quenching process. The temperature evolutions were thus successfully captured in the experiments and accurately predicted by the FE simulation.

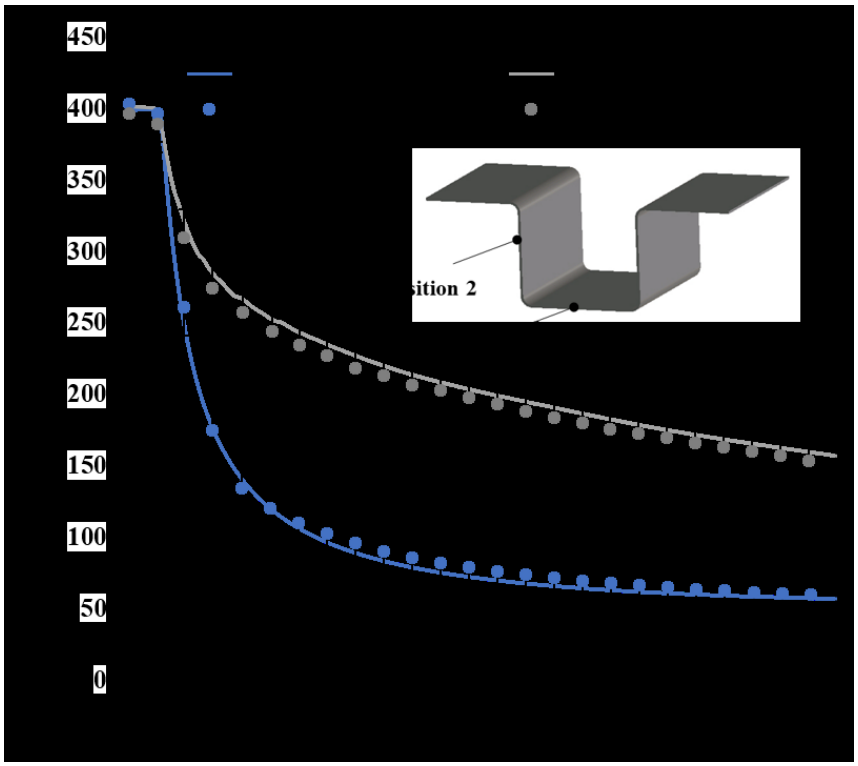

Figure 5.14 Temperature evolution comparison between experiments and simulations for the MS1180 steel.

Figure 5.14 indicates the normalized thickness distribution comparison between the experimental results and the FE simulations along the curvilinear distance of the U-shaped formed component. As shown in the figure, a close correlation between the experimental results and the FE simulations was achieved. The normalised thickness distribution evolutions shown in the curve are within the error bars of the experimental results. Good agreements were achieved for both the temperature evolutions and thickness distribution, verifying that the FE simulation was conducted accurately and was suitable for further use to evaluate the springback effects.

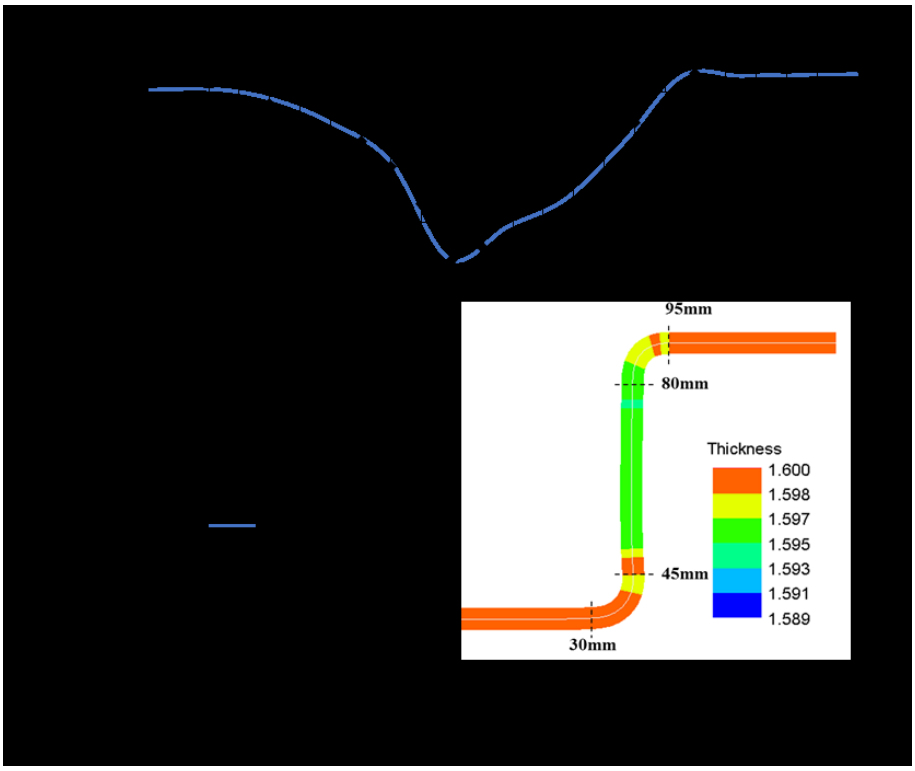

Figure 5.15 Normalised thickness distribution comparison between the experiment and simulation along the curvilinear distance of the formed U-shaped part.

Figure 5.15 shows the experimental and simulated results of springback angle as a function of temperature (Figure 5.15 (a)) and forming speed (Figure 5.15 (b)) for the formed MS1180 steel components. The springback prediction from FE simulations at various temperatures and forming speeds are within the error bars of the experimental results at a reasonable error of approximately 5.1% and 6.1% for both springback angles θ_1 and θ_2, respectively. It can be confirmed that good agreements were achieved between the experimental results and the FE

simulation ones. To further investigate the effect of temperature and forming speed for springback, stress distribution across the upper and lower layer of a formed part was examined by defining a local coordinate system in the FE model at the end of the quenching stage.

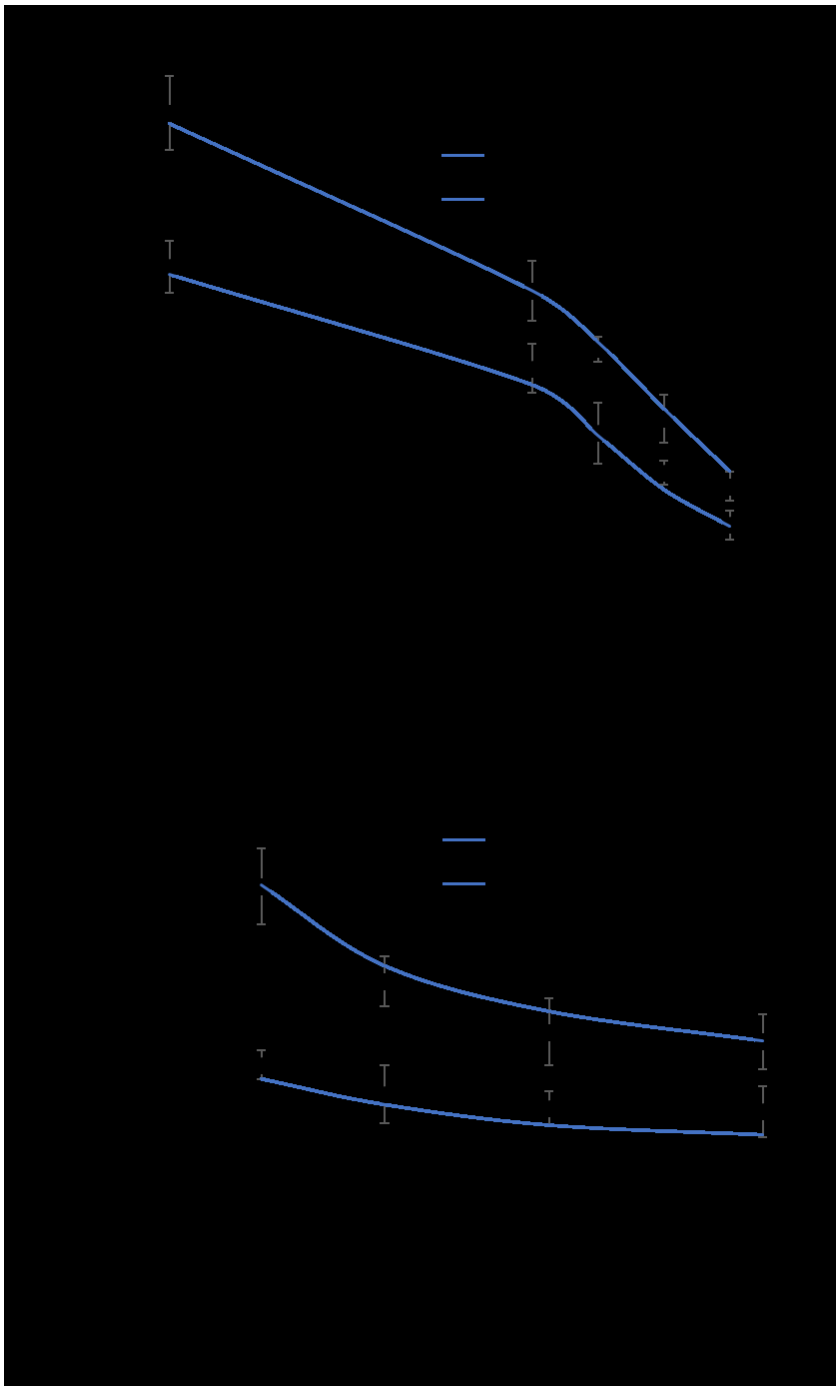

Figure 5.16 Comparison between experimental data and the FE simulations results of springback of U-shaped parts on the effect of (a) forming temperatures (b) forming speeds.

The stress distributions along the upper and lower layers of the formed component at room temperature and 400°C are shown in Figure 5.16 in four tooling regions (OA: punch bottom, AB: the punch corner, BC: sidewall, CD: die corner). In region OA, the blank was subjected to tensile stress in the upper layer and small compressive stress in the lower layer. It was found that pronounced stress differences were obtained between the upper and lower layers of the formed part for cold stamping condition. At elevated temperature, the reduction in mechanical strength leads to excessive blank material draw-in from blank holding areas. In punch corner region AB, the blank experienced a transition from tension to compression in the upper layer and a transition from compression to tension in the lower layer due to the combination of plastic stretching and bending over the punch. For the element in the sidewall region BC, the blank was subjected to bending, unbending and reverse bending during the forming process. The blank was drawn into the die while straightened by the sidewall in region BC. For cold stamping conditions, the stress characteristics resulted in a large bending moment and thus greater springback in this region. At 400°C, it was observed that the stress distribution differences between the upper and lower layers decreased due to the reverse bending effect. Therefore, the curvature of the sidewall was reduced. In the die corner region CD, it was found that the stress distribution changed from compression to tension in the lower layer and tensile to compression in the upper layer. This was attributed to the bending of the blank taking place at the exit to this region (point D), and the reverse bending at the entrance of the sidewall region (point C). The decreased stress distribution differences at point C and D at 400°C led to a reduced springback for θ_2.

Figure 5.17 shows the stress distribution for two various forming speeds of 75mm/s and 250mm/s. A small variation of stress distributions was found in the punch corner and die corner region (AB and CD), suggesting the material was already drawn in at selected speeds which limited the extent of plastic deformation in these regions. In the sidewall region BC, larger stress distribution differences in the upper and lower layers were found when the blank formed at high forming speed. The higher forming speed reduces the period of the forming stage and thus the blank were maintained at higher temperature as well as lower flow stress level. The blank was drawn in the die cavity earlier at higher forming speed and thus decreased the sidewall curvature. These results were consistent with the findings reported by Kim and Koç (2008).

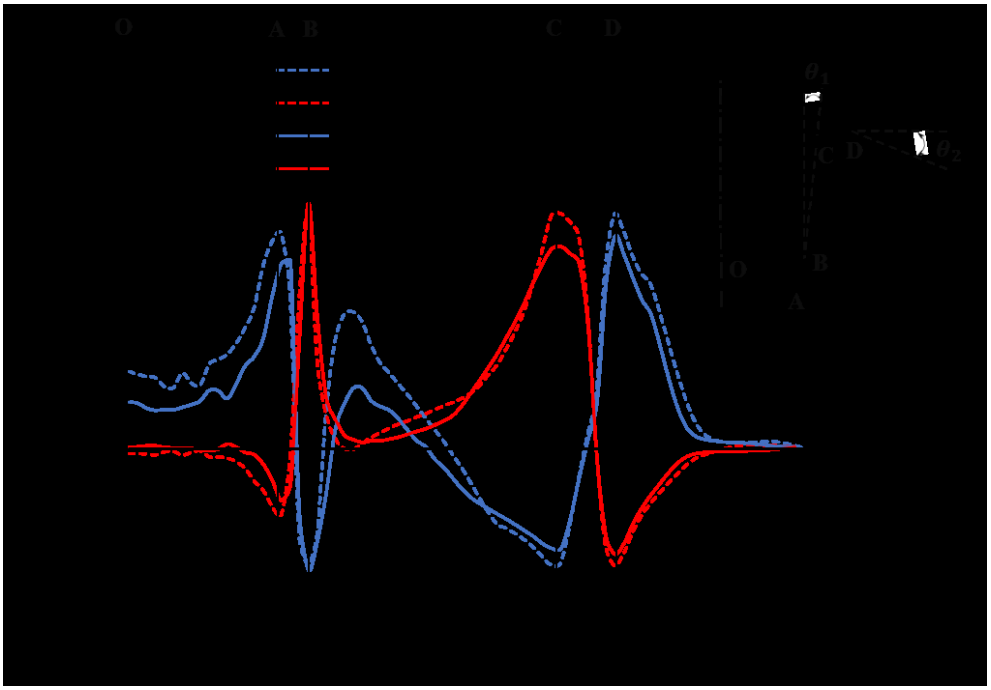

Figure 5.17 Stress distribution on the upper and lower layers of the formed part at room temperature and 400°C.

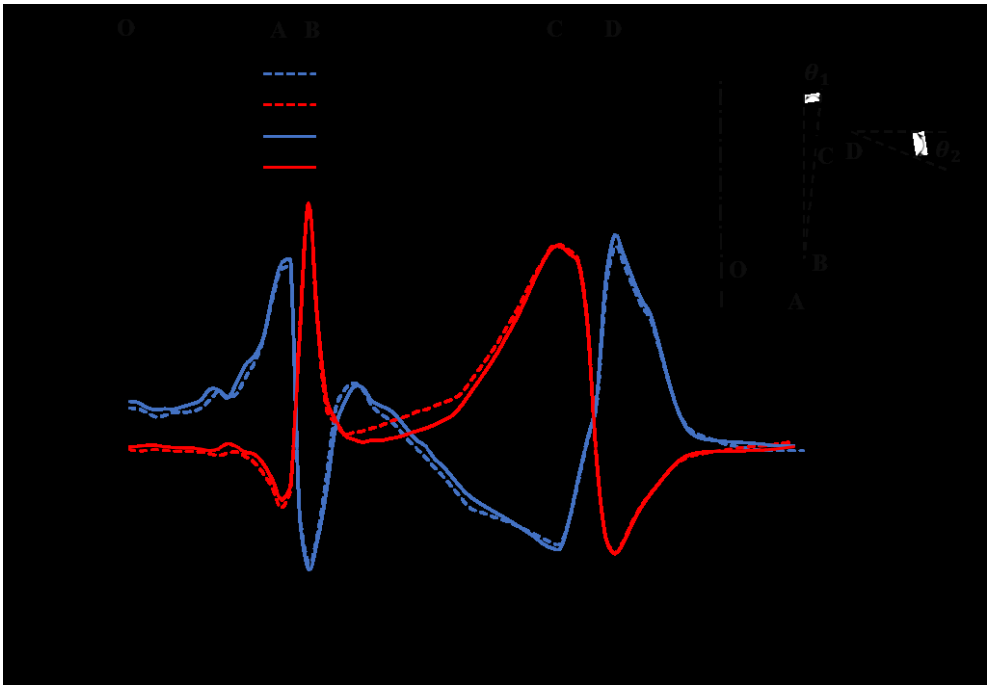

Figure 5.18 Stress distribution on the upper and lower layers of the formed part at various forming speeds.

5.3 Summary

In this chapter, the validation of the FWS process was conducted by forming U-shaped components through the dedicated pilot production line *Uni-form*. It was confirmed that the fast-warm stamped part at 400°C exhibited over 92% mechanical strength of the original as-received material consisting of 1140MPa UTS and 370HV hardness. Moreover, the lath martensitic structure remained was almost identical to the microstructure of the as-delivered material. The overall manufacturing cycle time in the FWS process was within 10s. Springback under FWS conditions was successfully characterised, and it was found that a higher blank temperature and a fast forming speed reduced the amount of springback in the formed component. The magnitude of the sidewall springback angle reduced by 60.7 % as the stamping temperature increased from 25 to 400°C. This was attributed to the overall reduced flow stress level in the blank with increasing forming temperature. Higher forming speeds were also found to minimize the springback. Therefore, the optimal processing window for fast-warm stamping of the MS1180 steel was suggested to be at higher forming temperature range at 400-450°C with faster forming speed, which is potentially to produce a complex shape with minimized springback. An FE model of the FWS process of a U-shaped component was successfully generated and verified by comparing with the results of experimental forming trials. A close correlation was obtained for both the temperature and thickness variables. The FE predictions for springback of the formed part were in good agreement with the experimental measurements with errors less than 6.1.

Chapter 6. Case study: Implementation of the FWS technology for spring steel

The FWS process is a promising technology to form AHSS into complex shapes with the required post-form properties while reducing the total cycle time. Feasibility studies on the FWS of the MS1180 steel were conducted by forming a U-shaped demonstrator. Additionally, the concept of the FWS process was not limited to AHSS for automotive applications. In this chapter, the FWS was proposed for manufacturing the disc springs of spring steel. The processing window of disc springs was developed through a set of thermo-mechanical experiments. A warm stamping tool set was designed, fabricated and integrated into the *Uni-form*. Disc springs were formed under optimal heating conditions with desired mechanical properties. The overall quality of the formed disc spring was evaluated by checking the dimensional precision, post-form hardness, surface roughness and load capacity.

6.1 Introduction for disc spring

Disc springs, sometimes named Belleville springs or washers, are used in a variety of applications across a broad range of industries where there is a requirement for a high force within limited space. Disc spring is defined as a circular component that deforms to a reduced height when subjected to a load along the axis of symmetry. Disc springs are classified into different types depending on the shape and usage(International industrial springs, 2019). Figure 6.1 shows the most commonly used disc spring products manufactured from various materials (Dharan and Bauman, 2007). This study concentrates on the conventional disc springs manufactured by spring steels.

Chapter 6 is based on paper work ‘‘Sun, Y., Wang, K., Politis, D. J., Cai, Z., Wan, L., Wang, Y., Wang, L., 2018 A novel stamping process of 60Si2Mn steel disc springs. 4th International Conference on Advanced High Strength Steel and Press Hardening, ICHSU 2018, 20-22 August, Hefei, China.’’

Figure 6.1 Common disc springs manufactured by different raw materials (MW Industries, 2019).

In accordance with manufacturing group classification (DIN2093, 1992), disc springs are classified into 3 groups depending on the thickness:

- Group 1: Disc thickness less than 1.25 mm
- Group 2: Disc thickness from 1.25 mm to 6 mm
- Group 3: Disc thickness over 6 mm up to 14 mm

Figure 6.2 shows the schematic diagram of group 1 and 2 disc springs with thickness less than 6mm. The spring disc geometry consists of five parameters namely inner diameter (D_i), outer diameter (D_e), thickness (δ), cone height (h) and overall height (OH). The axial load is applied on the inner circumference whereas the outer circumference is supported on a rigid surface (Mastricola et al., 2017).

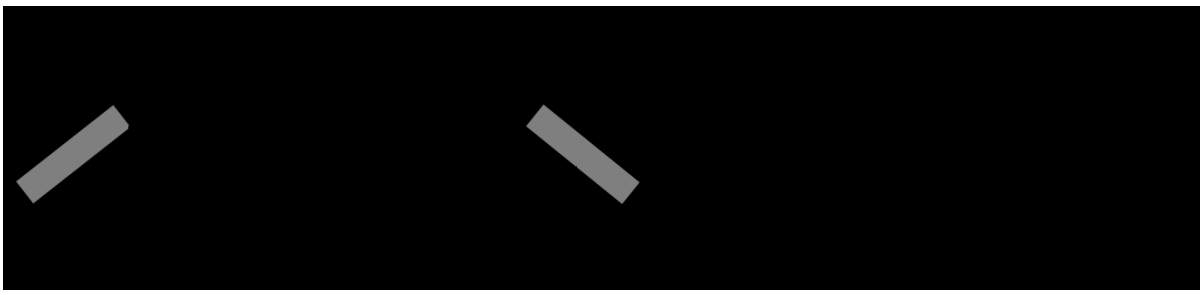

Figure 6.2 Cross-section details and designations of group 1 and 2 disc spring (Patangtalo et al., 2016a).

Disc springs offer a well-developed solution to many engineering problems (Foard et al., 2019). The biggest advantage of disc springs in applications is the good flexibility by configuring them in stacks to achieve the desired performance (Dharan and Bauman, 2007). Figure 6.3 shows different disc spring combinations including parallel stack, series stack and parallel-series stack. Figure 6.3 (a) shows disc springs assembled in the parallel stack which can increase the maximum load allowance with each added washer. The assembly for stacking series as shown in Figure 6.3 (b) indicates that the disc springs are arranged in the opposite direction which increases the amount of available travel. The combination of both parallel and series washers allows specific spring characteristics for desired application requirements (Foard et al., 2019).

Compared to the helical coil springs, the conical shape design of the disc spring makes it stronger, stiffer and more resilient (Patangtalo et al., 2016b). Disc springs have been extensively used in the fields of aeronautics, astronautics, metallurgy and machinery (Zheng et al., 2014). Recently, disc springs have been used in precision instruments such as medical equipments, nuclear reactors and satellites which have strict requirements for their dimensional precision and performance (Raj et al., 2018).

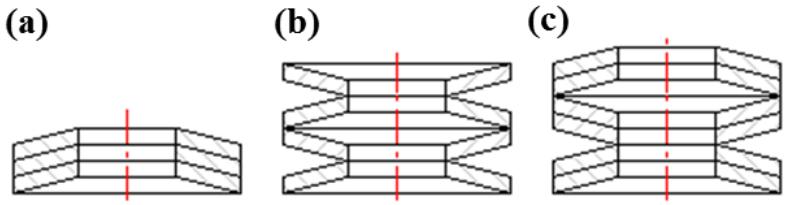

Figure 6. 3 Different disc spring combinations (a) parallel stack (b) series stack (c) parallel-series stack (Scherdel, 2019).

6.2 Development of the FWS process of disc spring

6.2.1 Conventional manufacturing processes of disc springs

Cold stamping followed with customizable heat treatment processes is the traditional production method of manufacturing disc springs, as shown in Figure 6.4 (a). In the conventional manufacturing process, the initial blank is cold stamped within tooling. The formed parts are subsequently heated to austenitization temperature in a furnace and soaked,

followed by oil quenching to minimize the residual stress in the components. Compared to water quenching, oil quenching is preferred to reduce the risks of distortions or cracks. The as-quenched disc spring microstructure consists of martensite and in some cases a small portion of bainite and thus it has high compressive strength although toughness. Further heat treatment (tempering) is subsequently performed to obtain the desirable post-form properties such as toughness and hardness, which is highly dependent on temperature and soaking time (Li et al., 2011). Customised tools are utilised to mount the disc springs during the austenitization and tempering processes to reduce thermal deformation.

Hot stamping process has increasingly been utilized for manufacturing disc springs. Compared to the conventional cold stamping process, the initial blank is heated to austenitization temperature and subsequently formed and quenched simultaneously between cold dies. The hot stamped parts are full martensitic microstructures and tempering is subsequently conducted on the formed parts to achieve an improved toughness. However, deformation of the formed disc springs during tempering may still occur, which not only affects the performance but also reduces fatigue life (Patangtalo et al., 2016a). The forming tools and process involved for producing disc springs to required dimensions are costly, and thus the development of a cost-effective forming technique to manufacture disc springs is in great demand.

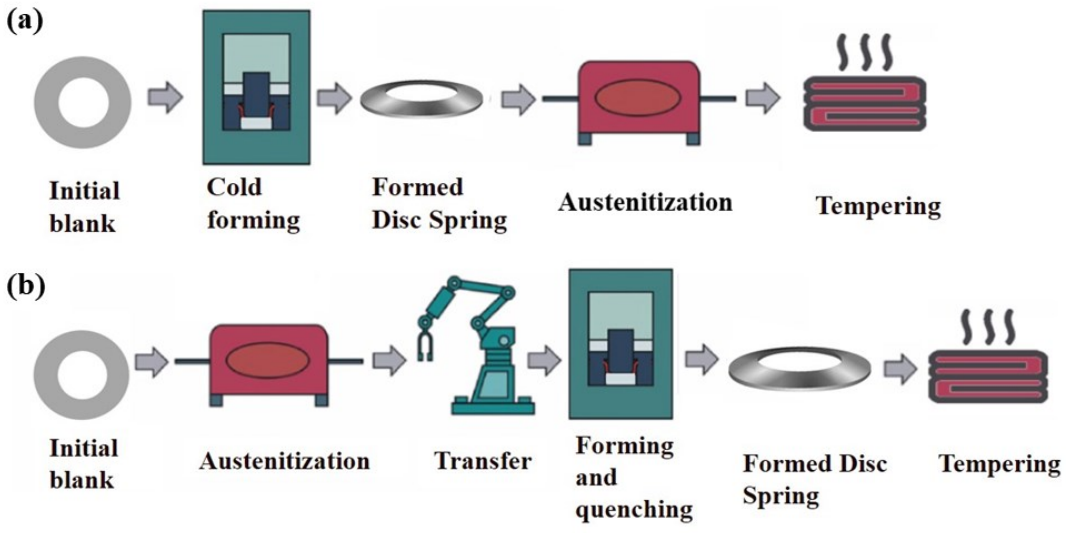

Figure 6.4 Conventional forming processes for manufacturing disc springs (a) cold forming (b) hot stamping.

6.2.2 FWS process for 60Si2Mn steel disc springs

Fast-warm stamping is a promising technology for manufacturing complex-shaped components from high strength steels. The concept of FWS process is to utilise an ultra-fast heating rate to minimize the negative microstructure changes so the as-received material mechanical properties are maintained in the formed parts. To implement the FWS technology on disc springs, the initial material needs be customised to the final part desired microstructure. Additionally, the FWS process can minimize the springback and overall manufacturing time. Therefore, the FWS technique may offer a promising alternative solution to form disc spring cost-effectively.

Figure 6.5 schematically presents the processing routes and microstructure evolutions of conventional and FWS manufacture of a disc spring from commercial spring steel 60Si2Mn. In the conventional method, as-delivered spring steel blank sheets, consisting of ferrite and perlite, are first cut from a coil and cold stamped in forming tools; the preformed parts are subsequently heated to 860°C and soaked for 5 mins for austenitization, followed by oil quenching to obtain martensitic microstructure (Ishikawa et al., 2014). As-quenched martensite normally has limited ductility and toughness, and thus, the hardened disc springs must be tempered for 30 minutes, which is the favoured process to improve toughness (Li and Hu, 2012). The desired microstructure of disc springs is a mixture of ferrite and carbide particles which has high toughness and reduced hardness for sustaining a load. The overall manufacturing cycle time for this conventional process is approximately 35 minutes.

During the FWS process, initial blanks are heated to an appropriate temperature, then formed and quenched simultaneously between cold dies. Pre-heat treatments are necessary prior to the FWS to achieve the desired microstructure and mechanical properties for the initial blank. This fast process may avoid major negative microstructural changes thus enabling desirable properties to be retained for the formed components. The total cycle time for manufacturing disc springs is reduced to within 20 seconds. The shorter cycle time results in a higher production rate, efficiency and lower energy consumption.

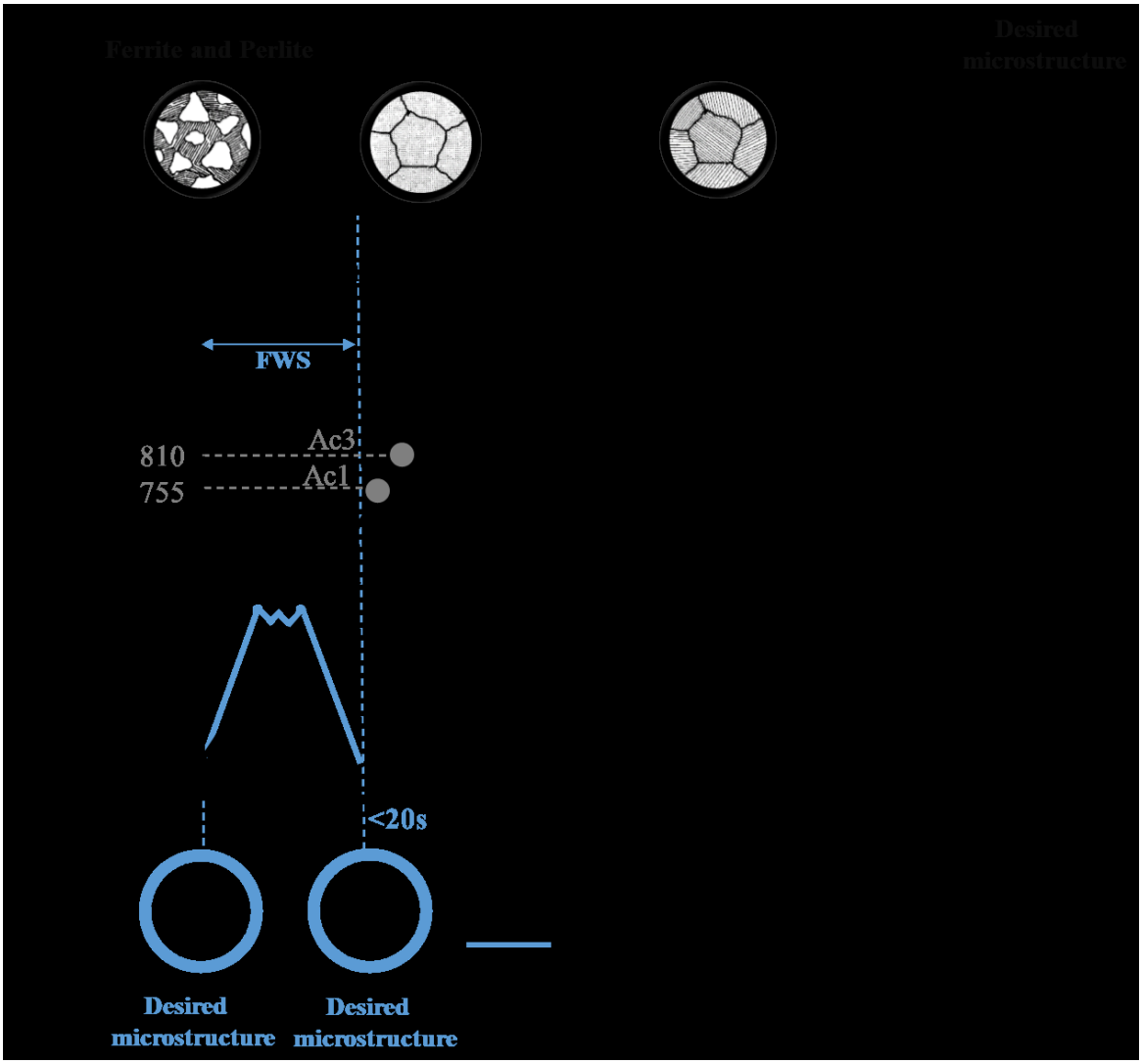

Figure 6.5 The schematic diagram of the conventional and FWS manufacturing processes for disc springs.

6.2.3 Technical specifications of a commercial disc spring

A commercial disc spring was selected as an example to be formed from spring steel 60Si2Mn by the FWS technique within the required technical specifications as shown in Figure 6.6. According to the standards of DIN 2093, 2.6mm thickness sheet material belongs to group 2 featuring a rectangular cross-section with square edges and permissible tolerances for spring geometry such as overall height, inside and outside diameter. There are certain requirements set upon the performance of disc spring. The hardness of formed disc springs must be within the range of 42-52 HRC to which has a good toughness for loading. The formed part needs to

be pressed to flat with minimum applied force of 1850N. Good surface characteristics without any defect and decarburization layer are required.

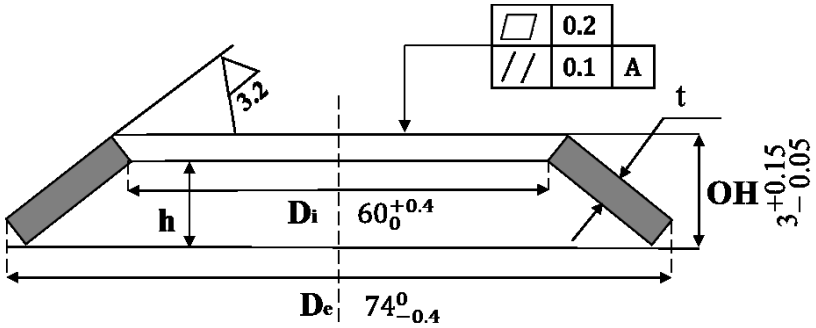

Figure 6.6 Geometrical parameters of the disc spring component (dimensions in mm).

6.3 Experimental setup and procedure

6.3.1 Material characterization of 60Si2Mn steel

6.3.1.1 Testing material

In this study, the investigated material was commercial 60Si2Mn steel of chemical composition shown in Table 6.1. The as-received material was a 2.6mm thickness steel sheet which was supplied by China Academy of Launch Vehicle Technology. The pre-heat treatment including salt bath heat treatment and tempering were conducted to transform the initial blank into the desired microstructure and post-form properties.

Table 6.1 Chemical composition of 60Si2Mn steels (wt%).

Composition	C	Si	Mn	P	S	Cr
Wt%	0.60	1.50	0.60	≤0.012	≤0.005	≤0.1

6.3.1.2 Thermo-mechanical properties under the FWS conditions

Uniaxial tensile tests at elevated temperature were conducted in a Gleeble 3800 system to characterize the thermal-mechanical properties of spring steels. The thermo-mechanical characteristics of the spring steel over the range of temperatures and strain rates were evaluated in two experimental programmes. In the first group, the specimens were heated at a rate of

50°C/s to different testing temperatures of 450, 500 and 550°C, then deformed at a constant strain rate of 0.1/s. The elongated specimens were then cooled rapidly to room temperature at a quenching rate of 40°C/s by compressed air. In the second group, the effect of strain rate (0.01, 0.1, 1/s) was examined to determine the viscoplastic deformation behaviours of 60Si2Mn steel at 500°C. The details of specimen design, experimental set up and programme for the uniaxial tensile test was given in section 3.3.1. At least three tests were performed to evaluate the flow behaviour characterization of the 60Si2Mn steel.

Rockwell hardness measurements were subsequently conducted on deformed specimens via Zwick hardness tester after each test which was used to evaluate the variation in PFH. Hardness at five random locations was measured and the average value was calculated to represent the PFH.

6.3.2 FWS forming trials for disc spring

6.3.2.1 FWS tool design

In order to validate the feasibility of the proposed fast-warm stamping process for disc springs, forming tests were performed from 60Si2Mn steel blank via the automatic production line *Uni-from*. To achieve a low cycle time whilst minimizing the cost of refining forming tools, a splitting forming die constructed from two separate parts, a cooling block and replaceable forming cap was designed and fabricated, as shown in Figure 6.7. The CAD drawings of the tools were completed by Nicholas Atherton in his final year project who was supervised by the author.

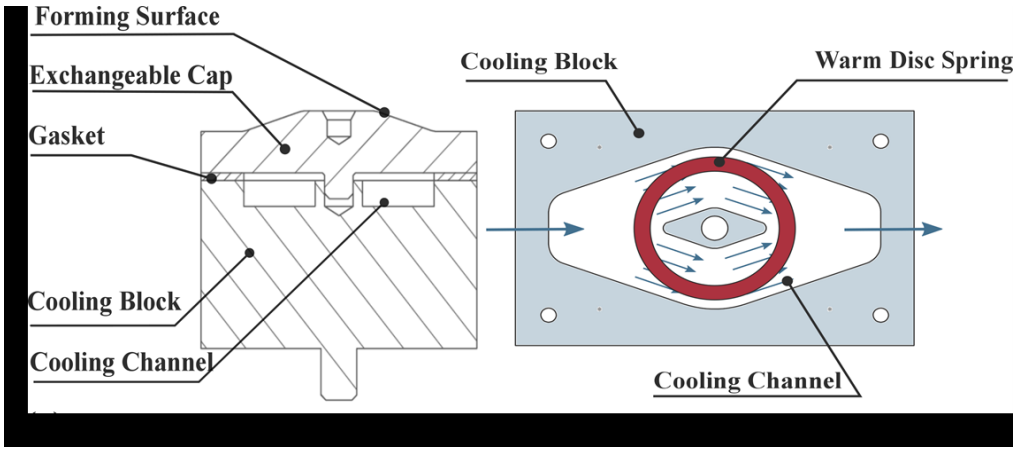

Figure 6.7 The design of form tools with water cooling channel (a) A section view of the forming tools (b) a top view of the cooling channel.

Rather than utilizing commonly used circular cooling tubes, the cooling block design makes use of square channels for the water flow, which can be milled efficiently from the top surface thus reducing manufacturing cost. The cooling block with a female replaceable cap was designed and embedded in the top frame of *Uni-from,* as shown in Figure 6.8 (a). A location pin in the centre of the female exchangeable cap ensures a good alignment between male and female die. The tools set assembly on the *Uni-form* is shown in Figure 6.8 (b).

By creating a modular forming tool, the die cap could subsequently be manufactured from alternative materials including those that are not water durable and wear resistant. Machining of the tool was also greatly reduced, allowing for the use of harder materials that could be cast with only minor post form machining required. An AISI M11 high speed tool was selected for the die caps as it had good thermal conductivity and the hardness properties required for the fast warm-stamping of spring steel. For the cooling block, a softer stainless steel, AISI 304, was used which is quicker and cheaper for machining whilst exhibiting superior water durability.

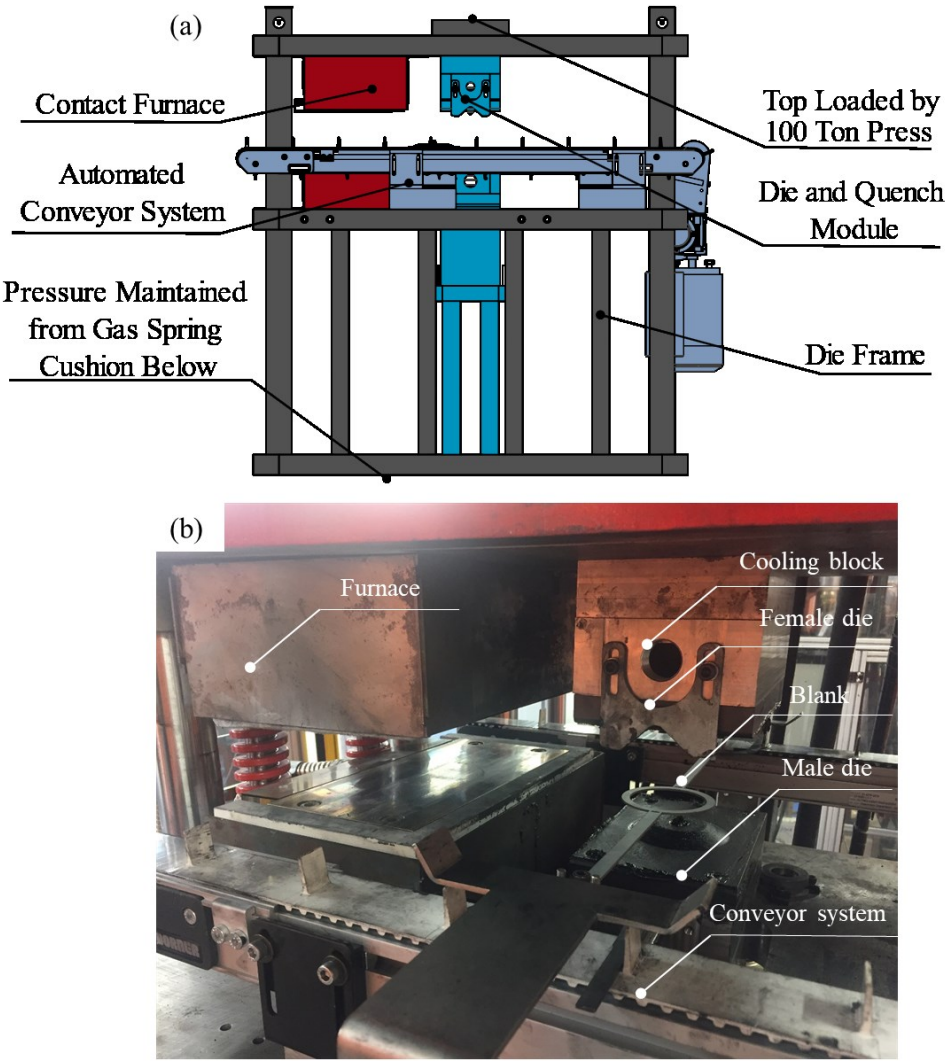

Figure 6.8 A diagram of *Uni-form* with tool set for the FWS disc springs (a) tool assembly in CAD (b) tool assembly.

6.3.2.2 Specimen design and experimental programme

Figure 6.9 shows the specimen design for the FWS tests for disc springs through the *Uni-form* system. The blank was waterjet cut from the sheet alloy and screwed at each side with two blank holders. The blank holders were accurately fixed within two cleats on the belt. In the FWS tests, the automatic conveyor system transported the blank to the furnace and heat it to the target temperature. Once heated, the warm blank was transferred from the contact heater to the forming tool immediately. The hot blank was subsequently formed at different temperatures from 450 to 550°C with a 10kN blank-holding force and simultaneously quenched within the cold die for 10s.

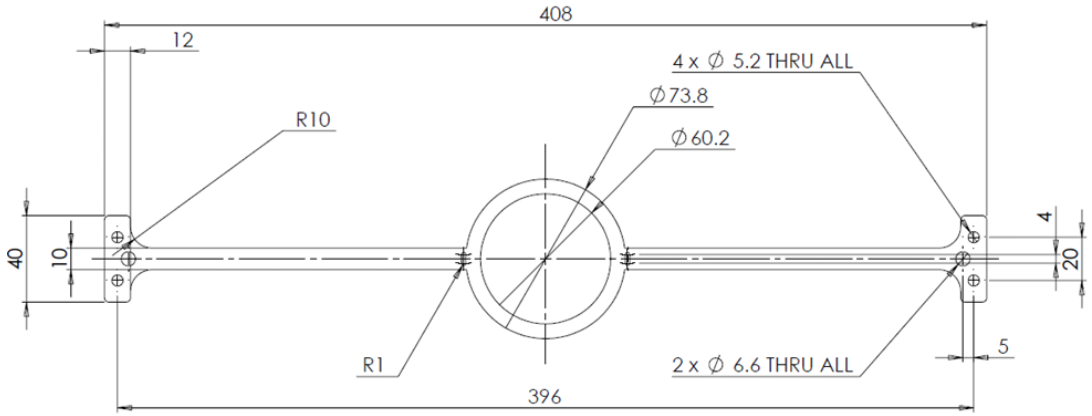

Figure 6.9 Specimen design for disc springs.

6.3.3 Post-form properties evaluation of formed components

Experiments including hardness measurement, dimensional accuracy measurement, compression test and surface roughness test were conducted on formed components to ensure that all technical requirements were successfully achieved. The Rockwell hardness measurements were performed on different locations along the cross-section of the formed parts. A digital height gauge, coordinate measuring machine and micrometre were utilized for measuring dimensional accuracy of formed disc springs. Compression tests were performed to evaluate the load capability of formed disc springs via the Instron machine. The post-form surface roughness of the disc springs was measured through a 3D white light interferometry surface profilometer.

6.3.3.1 Compression test

A universal testing machine of Instron 3369 is employed for compression tests. Figure 6.10 shows the experimental set up in evaluating disc spring load-deflection performance. A hard (55HRC) compression platen was fixed firmly to the load cell by the upper grip to avoid any minute movements. The load cell and displacement output port were connected to a computer to record the full load-displacement history. Disc springs were placed on a hardened block and compressed at a speed of 0.1mm/s. The lubricant Wisura oil was applied on the disc spring and compression platens to minimize the friction.

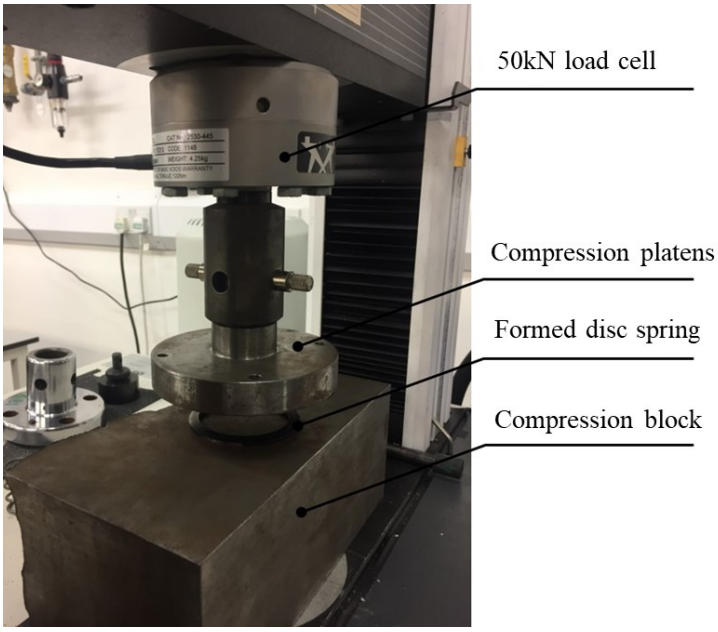

Figure 6.10 Compression test set up for evaluating the load capacity of formed disc spring.

6.3.3.2 White light interferometry test

The surface metrology of the disc springs was evaluated by a Veeco WykoNT9100 white light interferometer as shown in Figure 6.11. The specimen was placed on the stage and tilted so that the plane was perpendicular to the optical axis. The illumination was adjusted to obtain the best topographic map. Four different locations were measured to calculate at upper and lower surfaces of the formed disc spring and at least 3 measurements were conducted to calculate the average surface roughness at each position.

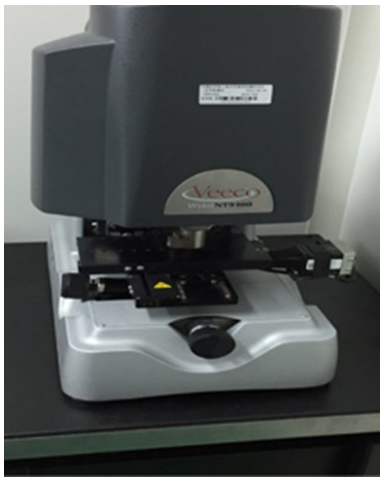

Figure 6.11 White light interferometry test testing machine (Veeco Wyko NT9100).

6.4 Thermo-mechanical properties of 60Si2Mn steel under FWS conditions

6.4.1 Flow behaviour of 60Si2Mn steel at different temperatures and strain rates

The effect of deformation temperature on the flow stress of spring steel was investigated with true stress-strain curves plotted in Figure 6.12. With the increasing temperature, an appreciable reduction on the flow stress is observed. The peak flow stress of spring steel decreases by approximately 34.89% from 1132MPa to 737MPa when deformation temperature increased from 450 to 550°C. The gradual increase of flow stress with increasing strain is mainly associated with strain hardening, which was caused by dislocation accumulation and interactions. In addition, it is noted that strain to failure increased from 450 to 550°C at a strain rate of 1/s. Compared to low ductility (less than 10% elongation) at room temperature, excellent ductility, at over 1.15 tensile strain, was achieved at the higher temperature 550°C. This was due to more activated grain boundary sliding and rotation which dominated the viscoplastic deformation. Moreover, stronger recovery and recrystallization at elevated temperatures induced an improvement in ductility.

Figure 6.12 (b) shows the effect of strain rate on the flow behaviours of the 60Si2Mn steel at 500°C. It was found that increasing strain rate resulted in a noticeable increase in flow stress of 60Si2Mn steel. The pronounced strain rate hardening effect was widely observed in the visco-plastic materials and this was caused by the tangled dislocations generated during plastic deformation. Moreover, the strain hardening was more pronounced during high strain rate testing due to the short deformation time resulting in less recovery. The differences of strain to failure were not significant. When the strain rate increased from 0.01 to 1 /s, the corresponding strain to failure slightly decreased from 1.09 to 1.03.

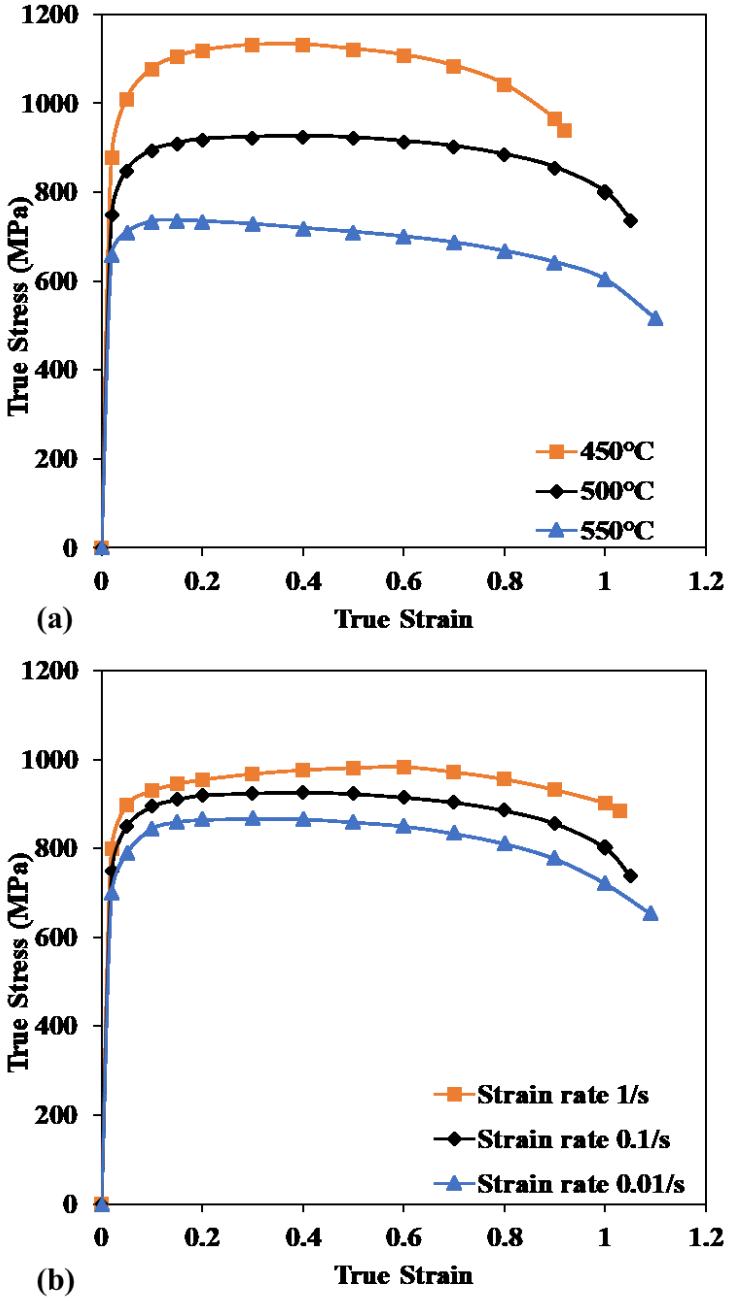

Figure 6.12 Flow stress-strain curves of the 60Si2Mn spring steel tested at (a) different temperatures, (b) strain rates.

6.4.2 Post-formed hardness of 60Si2Mn steel at various conditions

Figure 6.13 shows the post-form hardness (PFH) of 60Si2Mn steel as a function of temperatures and strain rates. As shown in Figure. 6.13 (a), the PFH of testing material decreased with increasing forming temperature, where PFH is expressed as a percentage of the

hardness of 60Si2Mn steel prior to forming. For reference, the hardness value of the prepared initial material was approximately 49HRC. It was found that the PFH of the specimen decreased with increased heating temperature. When the FWS process was performed at 450°C, the PFH of 60Si2Mn steel only reduced by approximately 2% to 48HRC. The nearly full strength was achieved in the sample at 450°C demonstrating the lower forming temperature would not cause a substantial change to the microstructure. When the temperature increased to 550°C, the PFH decreased by approximately 8% to 45.9HRC. The reason is believed to be that, the contribution of solid solution strengthening of carbon reduced with increasing temperature and thus induced a lower PFH. In addition, a higher temperature resulted in more activated carbide coarsening and recovery process, which diminished the PFH. These results are consistent with those reported by in Samuels (2014).

Figure 6.13 (b) shows the PFH evolution of spring steel at 500°C as a function of strain rate. Compared to a high strain rate of 1/s, the slow strain rate of 0.01/s led to a slight reduction by 2.1% in PFH. This was because a faster deformation process significantly reduces the time that the material is exposed at unfavourable elevated temperature. Moreover, rapid forming minimised the continuous carbides coarsening and recovery, which induced a higher hardness. The requirement of post-form hardness (42–52HRC) and a significantly improved ductility were achieved at selected testing conditions, which indicated that a temperature range from 450 to 550°C and a fast forming speed was preferred in the FWS process of disc springs.

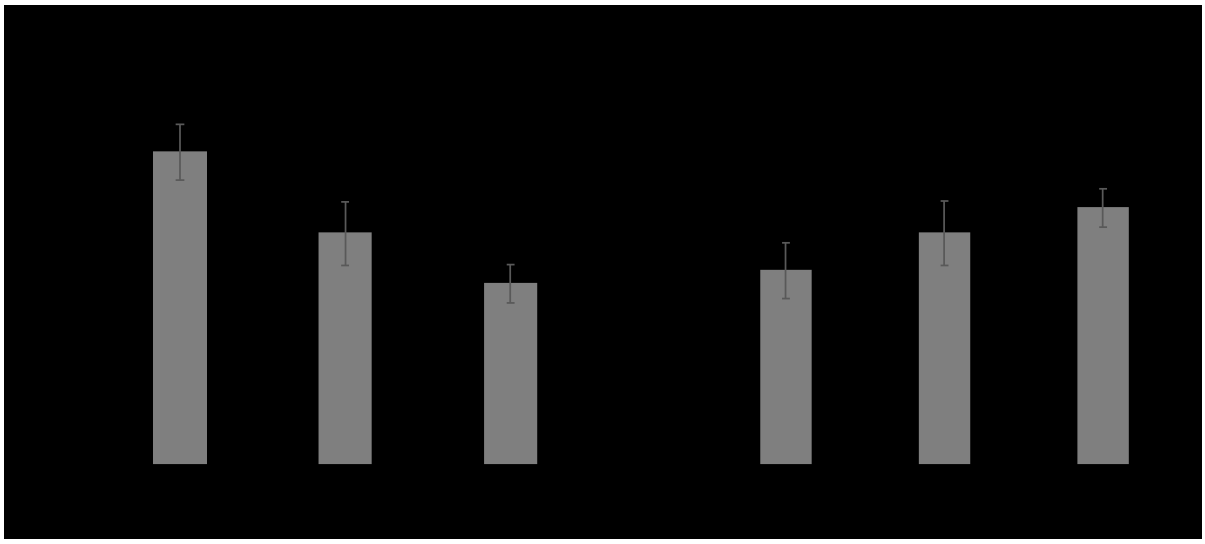

Figure 6.13 Evolution of the post-form hardness as a function of (a) heating temperature, (b) strain rate.

6.5 Post-form properties evaluation of disc springs

In this study, forming trials were successfully performed using *Uni-form* at forming temperatures ranging from 450 to 550°C and a forming speed of 250mm/s. A disc spring with good surface quality formed at 550°C as shown in Figure 6.14. The dimensions including inner and outer diameters and height of the formed part indicated a good geometric agreement with due to the minimised springback, as shown in Table 6.2. The average post-form hardness was approximately 46.7 HRC indicating over 95% of initial material strength, which met the requirement of the hardness at 42–52HRC. The overall manufacturing cycle time of the proposed FWS process including heating, transferring, forming and quenching significantly reduced from 30 minutes in the conventional disc spring manufacturing process to less than 20 seconds.

Figure 6.14 Formed disc spring with good surface quality.

Table 6.2 Dimensional accuracy of formed disc spring.

Test conditions/ parameters	Heating temp.(°C)	Thickness （mm）	D (mm)	d (mm)	H (mm)
Requirement	/	2.57	$74^{0}_{-0.4}$	$60^{+0.4}_{0}$	$4.46^{+0.15}_{-0.05}$
Average values	550	2.56	$73.98^{+0.08}_{-0.04}$	$59.71^{+0.12}_{-0.34}$	$4.41^{+0.2}_{-0.11}$

The deformation behaviour of formed disc springs was evaluated with a 11.2kN applied load. Figure 6.15 shows the load-deflection curves of the formed disc spring. According to the standard (DIN 2093), approximately 7000N was applied on the disc spring when the disc springs compressed by nearly 75% of the stroke, which meets the minimum requirement loading of 1850N. The height of the disc spring was measured after five repeated compression tests to ensure a consistent value.

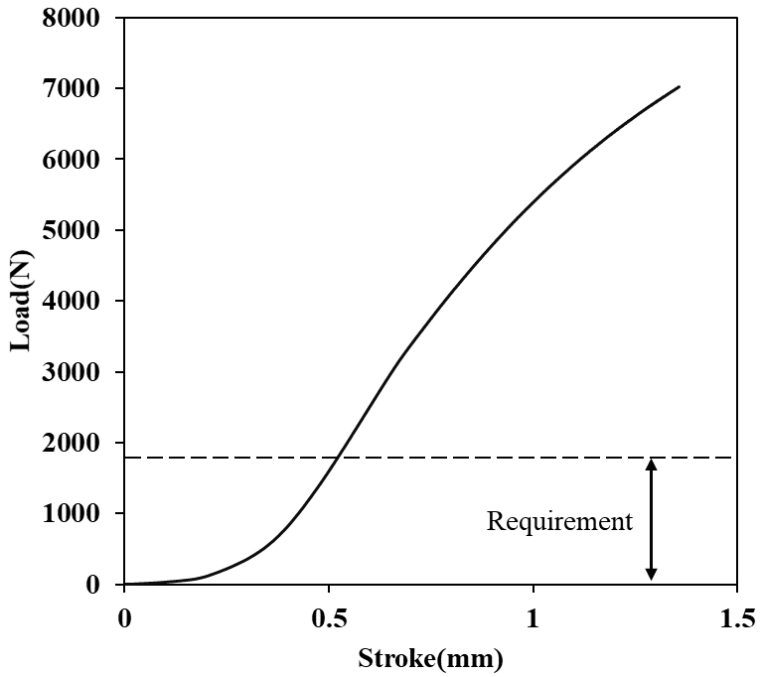

Figure 6.15 Characteristic load curves of a formed disc spring.

The arithmetic average surface roughness (Ra) of the disc spring was measured at two different positions, the upper and lower surface of the formed part. Figure 6.16 shows the surface roughness of as-received material was 782.87 and 745.15 nm at position 1 and 2, respectively. The surface roughness values increased to 1040.26nm at position 1 and 989.07nm at position 2, which are significantly lower than the required value (3.2μm). The slightly increased surface roughness is the result of the blank becoming softer and more susceptible to damage at elevated temperature when contacting the forming tools. The evaluations performed on formed parts indicate that the FWS is reliable and robust process for manufacturing disc springs.

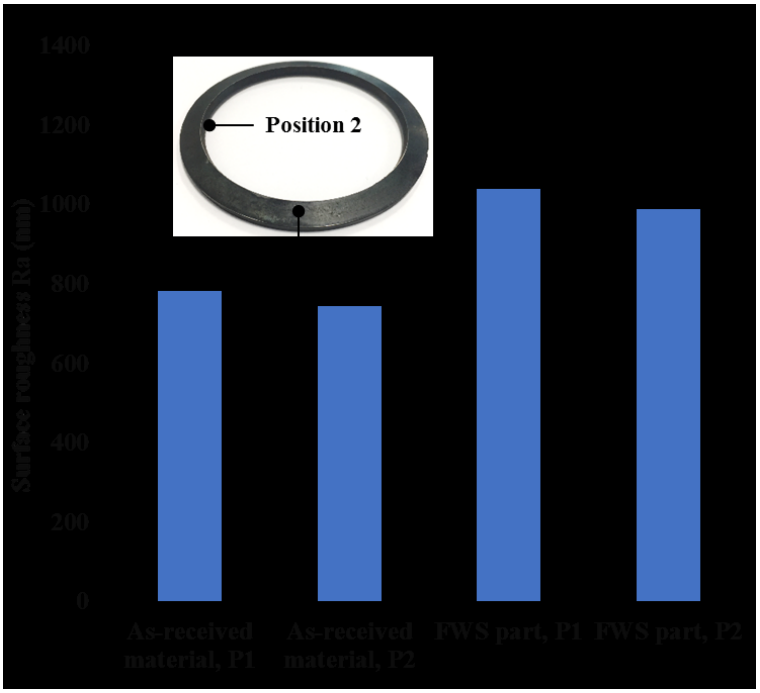

Figure 6.16 Surface roughness of as-received material and formed component at two different positions.

6.6 Summary

In this chapter, a novel processing route has been successfully implemented for manufacturing disc springs from 60Si2Mn steel. A separate forming tool set with a replaceable forming surface can reduce the manufacturing cost of tooling. A disc spring was successfully formed using the proposed forming process to the required dimensional precision, PFS and surface roughness. Formed disc springs indicated a good load and deflection capability for successful implementation. Additionally, the FWS has enabled a tremendous reduction of total cycle time from 30 minutes to less than 20 seconds and corresponding productivity improvement for a mass production setting.

Chapter 7. Conclusions and suggestions for future work

7.1 Conclusions

In this thesis, a novel forming technology, fast-warm stamping has been proposed and experimentally verified using MS1180 steel. To develop the optimised processing window of the FWS process and obtain a comprehensive understanding of the microstructural mechanisms, experimental investigations on different process variables were conducted. The validation of the FWS process was performed by forming U-shaped components through the dedicated pilot production line *Uni-form* on a lab-scale. An FE model of the FWS process of a U-shaped component was successfully generated and verified by comparing to the results of experimental forming trials. Additionally, implementation of the FWS technology was successfully performed on 60Si2Mn spring steel by manufacturing disc springs. The key findings from the project are highlighted as follow:

7.1.1 Thermo-mechanical properties and microstructures of the MS1180 steel under FWS conditions

The FWS process is expected to use ultra-fast heating of a steel blank, whilst minimising the major negative changes to the microstructure which are detrimental to the post-form strength. Using the proposed technology, the desired PFS and microstructures were obtained in the formed part while the cycle time and energy costs were reduced.

To study the thermo-mechanical properties of the MS1180 steel, uniaxial tensile tests were performed at designated deformation temperatures, strain rates and heating rates via the DIC system in the Gleeble 3800. The experimental results indicated that the total elongation of the MS1180 steel improved from 15.1% to 19.8% as the temperature increased from 350 to 450°C, whilst UTS reduced by approximately 21.2% from 1100MPa at 350°C to 887MPa at 450°C. At elevated temperatures, dislocation movement, grain-boundary sliding, diffusion and grain

rotation are further activated which improve ductility. The total elongation increased from 14.2% to 22.4% as strain rate increased from 0.01 to 5/s. Additionally, ultra-fast heating rate enhanced the ductility of the MS1180 steel at 450°C by 25.7% when the heating rate increased from 1°C/s to 150°C/s. The improved elongation of the MS1180 steel at a higher heating rate is mainly attributed to the dispersed distribution of fine carbide precipitates. A rapid heating rate suppressed the detrimental precipitate coarsening at elevated temperatures, where microvoids were preferentially formed around the carbide precipitates at grain boundaries. The coarser carbides at elevated temperatures for a slow heating rate around grain boundaries weaken the boundary cohesion and impair ductility.

Strength degradation tests combined with hardness testing and microstructural observation were conducted to study the post-form hardness of the MS1180 steel at various conditions. The PFH decreased from 370.4 HV to 331.2 HV as the temperature increased from 350 to 500°C. The gradual reduction of hardness was due to the fact that the higher heating temperatures accelerate the decomposition of martensite phase and the nucleation and coarsening of carbide precipitates. SEM observations at different temperatures indicated that martensitic structures were still distinguished as the carbides precipitated within laths at 350°C and the coarser distribution of carbides as the temperature increased to 500°C which induced the loss of strength. The experimental results revealed that the PFH at an ultra-fast heating rate of 150°C/s improves by approximately 5% compared to the specimens heated at a heating rate of 1°C/s. The slow heating rate diminished hardness due to the continuous carbide precipitation and coarsening. The SEM and TEM observations performed at various heating rates proved that the carbides are finer and dispersed at an ultra-fast heating rate. The carbide precipitates with the mean radius of approximately 48nm at a heating rate of 150°C/s were finely dispersed in the lath martensite matrix compared to 62nm at a heating rate of 1°C/s which leads to a roughly 5% increase in hardness.

The optimal processing window for fast-warm stamping of the MS1180 steel was suggested to be a forming temperature range of 400–450°C with a soaking period of 0–4s and a heating rate of at least 50°C/s, which can provide superior strength-ductility combinations.

7.1.2 FWS tests and verification of the FE simulation

The validation of the FWS technology was conducted by forming U-shaped components through the dedicated pilot production line *Uni-form*. Based on the test results, the fast-warm stamped parts at 400°C exhibited over 92% of the mechanical strength of original as-received material consisting of 1140MPa UTS and 370HV hardness, whilst the lath martensitic structure remained which was almost identical to the microstructure of the as-delivered material. The overall manufacturing cycle time in the FWS process was within 10s. Springback under FWS conditions was successfully characterized at various temperatures and forming speeds. It was found that a higher blank temperature and a fast forming speed reduced the amount of springback in the formed component. The size of the sidewall springback angle reduced by 60.7 % as the stamping temperature increased from 25 to 400°C. This was attributed to the overall reduced flow stress level in the blank with increasing forming temperature. It was concluded that the FWS technique is an alternative solution to form high strength steel components with desired mechanical properties and microstructures.

An FE model of the FWS process for a U-shaped component was successfully generated in PAM-STAMP and verified by comparing with the results from experimental forming trials. A close correlation was obtained for both the temperature and thickness distribution. A good agreement for springback predictions of formed parts at various temperatures and forming speeds were achieved with experimental values falling within the error bars.

The limitation of the proposed forming technology is also considered in the research. The FWS technology may not suitable for every steel grade used in hot/warm stamping process. The complexity of form part in the FWS constricted by the formability which may limit its wider applications. It is necessary to form a more complex geometrical part by using the MS1180 steel.

7.1.3 Implementation of the FWS technology for spring steel

Considerable deformation during heat treatment in the conventional disc spring manufacturing processes affects the final dimensional accuracy, which significantly shortens the fatigue life and increases the tool cost. The FWS technology has been successfully implemented for manufacturing disc springs from 60Si2Mn spring steel. A separate forming tool set with a

replaceable forming surface was developed which can reduce the manufacturing cost for tooling. Experimental results showed that a disc spring was successfully formed using the proposed forming process to the required dimensional precision, post-form strength and surface roughness. Additionally, formed disc springs indicated a good load and deflection capability for successful implementation. This forming technique was shown to enable a tremendous reduction of overall cycle time from 30 minutes to less than 20 seconds and corresponding productivity improvement for a mass-production setting.

7.2 Suggestions for future work

7.2.1 Formability test for the MS1180 steel at elevated temperatures

In this thesis, it was found that process variables such as deformation temperature, strain rate and heating rate significantly affected the thermo-mechanical properties and microstructures of the test material. In order to understand the formability of the MS1180 steel at elevated temperatures, it is necessary to perform formability tests to evaluate the forming limit of the MS1180 steel under FWS conditions. This is important for identifying the application scope of the FWS technology, in terms of part complexity. In the future, formability tests of the MS1180 steel can be conducted to investigate the influences of temperature, strain rate and pressure on forming limit.

7.2.2 Development of unified viscoplastic constitutive model

The microstructural evolution of the MS1180 including the precipitate formation and growth and phase transformation was investigated at different temperatures and heating rates to understand the relationship between microstructure and mechanical properties. The damage of the materials during large deformation forming processes is important as the failure of materials for these processes should be predicted to avoid defects and control damage tolerance in the formed components. Therefore, it is necessary to develop a unified constitutive modelling to correctly predict the deformation behaviour and material failure.

7.2.3 Further investigations and limitations of the FWS technology

A comprehensive study of FWS technology of the MS1180 steel including fundamental experiments, mechanism analysis and forming trials are presented in this work. However, the selected case study of the FWS technology using spring steel concentrates on the development of disc springs. Microstructural investigation of the spring steel during the FWS was not significantly investigated. A further study can be performed to identify the influence of processing parameters on the microstructural evolution of the FWS process to understand the complex material behaviour. Investigation of this can help identify the critical cooling rate for martensitic transformation, which is an important parameter in industrial production.

FWS technology is a promising solution to manufacture components with excellent mechanical properties and is not limited to high strength steels. In this thesis, the feasibility study on the FWS technology was also conducted on a lightweight material thermoplastic composite by producing a demonstrator part. The success of this technology to produce a part using composite with targeted dimensions depends on the appropriate selection of the processing parameters, such as temperature, pressure and consolidation time. For example, the optimal temperature should be determined to achieve sufficient formability while avoiding the resin melting. In the next stage, a comprehensive experimental study must be conducted to investigate the effects of processing parameters on material behaviour. A complex geometry component is suggested to be formed via the FWS technology by refining the modular forming tools.

References:

Altan, T., 2007a. Hot-stamping boron-alloyed steels for automotive parts Part II: Microstructure, material strength changes during hot stamping. Stamping Journal 19, 14-15.

Altan, T., 2007b. Hot-stamping boron-alloyed steels for automotive parts, Part I: Process methods and uses. Stamping Journal 19, 10-13.

ArcelorMittal, 2018a. MartINsite® steels. https://automotive.arcelormittal.com/products/global_offering/martensitic_steels/martinsite.

ArcelorMittal, 2018b. Steels for hot stamping - Usibor® and Ductibor®. https://automotive.arcelormittal.com/products/global_offering/PHS/usibor_ductibor.

Aspacher, J., 2008. Forming hardening concepts. First International Conference on Hot Sheet Metal Forming of High Performance Steel.

Berglund, G., 2008. The history of hardening of boron steel in northern Sweden, First International Conference on Hot Sheet Metal Forming of High Performance Steel, pp. 175-177.

Bhadeshia, H., Honeycombe, R., 2017. Chapter 9 -Tempering of martensite, In: Bhadeshia, H., Honeycombe, R. (Eds.), Steels: Microstructure and Properties (Fourth Edition). Butterworth-Heinemann, pp. 237-270.

Bhattacharya, R., Stanton, M., Dargue, I., Aylmore, R., Williams, G., 2011. Experimental evaluation of springback in aluminium alloys using optical measurement and numerical analysis. AIP Conference Proceedings 1353, 241-246.

Biradar, A., Deshpande, M.D., 2014. Finite element analysis of springback of a sheet metal in wipe bending process. International Journal of Science and Research (IJSR) Volume 3 852-858.

Bouaziz, O., Zurob, H., Huang, M., 2013. Driving force and logic of development of advanced gigh strength steels for automotive applications. steel research international 84, 937-947.

Burakova, L.N., Burakova, A.D., Burakova, O.D., Dovbysh, V.O., 2018. Increasing fuel efficiency of passenger cars with the “climate-control” system as a method of improving the ecological safety of the urban infrastructure. IOP Conference Series: Earth and Environmental Science 115, 012011.

Burchitz, I., 2005. Springback: improvement of its predictability:Literature study report.

Chang, Y., Wang, C., Zhao, K., Dong, H., Yan, J.W., 2016. An introduction to medium-Mn steel: Metallurgy, mechanical properties and warm stamping process. Materials & Design 94, 424-432.

Choi, M.K., Huh, H., 2014. Effect of punch speed on amount of springback in U-bending process of auto-body steel sheets. Procedia Engineering 81, 963-968.

Chu, T., Poudel, A., 2014. Digital image correlation techniques for aerospace applications.

Dharan, C.K.H., Bauman, J.A., 2007. Composite disc springs. Composites Part A: Applied Science and Manufacturing 38, 2511-2516.

DIN2093, 1992. Dimensions and quality of conical disc springs.

DuPont., 2017. Vehicle weight reduction for optimal performance. http://www.dupont.co.uk/industries/automotive/articles/lightweighting.html.

ESI, G., 2015. Pam-Stamp 2015.1 User's Guide.

European Commission, 2018a. Reducing CO2 emissions from passenger cars. https://ec.europa.eu/clima/policies/transport/vehicles/cars_en.

European Commission, 2018b. Safety in the automotive sector. https://ec.europa.eu/growth/sectors/automotive/safety_en.

European Commission, 2019. CO2 emissions from cars: facts and figures. http://www.europarl.europa.eu/news/en/headlines/society/20190313STO31218/co2-emissions-from-cars-facts-and-figures-infographics.

Foard, J.H.D., Rollason, D., Thite, A.N., Bell, C., 2019. Polymer composite Belleville springs for an automotive application. Composite Structures 221, 110891.

Gharbi, M.M., Palm, C., 2017. Trends and challenges in hot stamping technology, AIP Conference Proceedings, p. 050018.

Government Response, 2018. Road vehicles improving air quality and safety. https://assets.publishing.service.gov.uk/government/uploads/system/uploads/attachment_data/file/714540/road-vehicles-consultation-response.pdf.

Grigorieva, R., Drillet, P., Mataigne, J.M., Redjaïmia, A., 2011. Phase transformations in the Al-Si coating during the austenitization step. Solid State Phenomena 172-174, 784-790.

Gucker, G., 2008. From profile hardening to custom made components, Proc. 1st International Conference on Hot Sheet Metal Forming of High-Performance Steel, pp. 22-24.

Güler, H., Ertan, R., Özcan, R., 2014. Investigation of the hot ductility of a high-strength boron steel. Materials Science and Engineering: A 608, 90-94.

Gwynn, I., 2010. Handbook of sample preparation for scanning electron microscopy and X-Ray microanalysis. Microscopy and Microanalysis 16, 358-359.

Hardy, M., NiobelCon, b., 2014. Martensitic automotive steel sheet - Fundamentals and metallurgical optimization strategies. Journal of Advanced Materials Research 1063, 130-142.

Hein, P., Kefferstein, R., Dahan, Y., 2006. Hot stamping of USIBOR 1500 P: Part and process analysis based on numerical simulation, NTERNATIONAL CONFERENCE, New developments in sheet metal forming. IFU, Stuttgart, Germany, pp. 163-176.

Hu, P., Ying, L., He, B., 2017. Hot stamping technology and the main equipment, Hot Stamping Advanced Manufacturing Technology of Lightweight Car Body. Springer Singapore, Singapore, pp. 19-44.

Huang, Q., Li, C., Li, Y., Chen, M., Zhang, M., Peng, L., Zhu, Z., Song, Y., Gao, S., 2007. Progress in development of China Low Activation Martensitic steel for fusion application. Journal of Nuclear Materials 367-370, 142-146.

International industrial springs, 2019. Disc spring symbols & units. http://www.discspringsindia.com/products/discsprings/disc_spring_symbol_units_index.html.

Ishikawa, T., Mori, K., Zhang, C., Liu, X., Zhou, L., Liu, Y., 2014. Influence of pearlite interlamellar spacing on strain hardening behaviour in spring steel 60Si2MnA. Procedia Engineering 81, 1283-1287.

Jonsson, M., 2008. Press hardening, from innovation to global technology, Proceedings of the 1st international conference hot sheet metal forming of high-performance steel, Kassel, Germany, pp. 22-24.

Judge, V.K., Speer, J.G., Clarke, K.D., Findley, K.O., Clarke, A.J., 2018. Rapid thermal processing to enhance steel toughness. Scientific Reports 8, 445.

Karbasian, H., Tekkaya, A.E., 2010. A review on hot stamping. Journal of Materials Processing Technology 210, 2103-2118.

Keeler , S., Kimchi, M., Peter, J.M., 2017. Advanced high-strength steels application guidelines version 6.0.

Khoo, S.W., Karuppanan, S., Tan, C.S., 2016. A review of surface deformation and strain measurement using two-dimensional digital image correlation. 23, 461.

Kim, D., Cha, M.H., Kang, Y.S., 2017. Development of the bus frame by flexible roll forming. Procedia Engineering 183, 11-16.

Kim, H.S., Koç, M., 2008. Numerical investigations on springback characteristics of aluminum sheet metal alloys in warm forming conditions. Journal of Materials Processing Technology 204, 370-383.

Konrad, T., Feuser, P., 2015. Improvement of the ductility of press-hardened plane sheets through a modified heat treatment. Key Engineering Materials 639, 243-248.

Krauss, G., 2001. Deformation and fracture in martensitic carbon steels tempered at low temperatures. Metallurgical and Materials Transactions B 32, 205-221.

Krauss, G., 2014. 12.11 - Quench and tempered martensitic steels: Microstructures and performance, In: Hashmi, S., Batalha, G.F., Van Tyne, C.J., Yilbas, B. (Eds.), Comprehensive Materials Processing. Elsevier, Oxford, pp. 363-378.

Krauss, G., 2016. Tempering of martensite, Reference Module in Materials Science and Materials Engineering. Elsevier.

Kusumi, K., Nomura, N., Yamamoto, S., Nakata, M., Abe, M., Suehiro, M., 2014. Improvement of cylindrical deep drawability in hot stamping. Procedia Engineering 81, 1719-1724.

Kwansoo, C.T.K., Rahul, K.V., Taejoon, P., Hoon, H., Gihyun, B., 2011. PartC: Benchmark problems and results, The 8th NUMISHEET conference, Seoul National University: Seoul,Korea.

KWIPPED, 2019. FEI Tecnai F20 TEM. https://www.kwipped.com/rentals/product/fei-tecnai-f20-tem/7383.

Kyu, K.H., Seong, H.L., Choi, H., 2015. Evaluation of contact heat transfer coefficient and phase transformation during hot stamping of a hat-type part.

Landgrebe, D., Putz, M., Schieck, F., Sterzing, A., Rennau, A., 2015. Towards efficient, interconnected and flexible value chains – Examples and innovations from research on production technologies, Proceedings of 5th International Conference on Accuracy in Forming Technology, Chemnitz pp. 61–78.

Li, A.M., Hu, M.J., 2012. Modifying the microstructure and property of 30 crmnsi steel by subcritical austenite reverse transformation quenching. Engineering Review 32, 181-185.

Li, N., 2013. Fundamentals of materials modelling for hot stamping of UHSS panels with graded properties, Mechnical Engineering. Imperial college London.

Li, N., Lin, J.G., Dean, T.A., Dry, D., Balint, D.S., 2014. Concept validation for selective heating and press hardening of automotive safety components with tailored properties. Key Engineering Materials 622-623, 1124-1131.

Li, X., Chang, Y., Wang, C., Hu, P., Dong, H., 2017. Comparison of the hot-stamped boron-alloyed steel and the warm-stamped medium-Mn steel on microstructure and mechanical properties. Materials Science and Engineering: A 679, 240-248.

Li, Y., Lu, Y.-p., Wang, C., Li, S.-t., Chen, L.-b., 2011. Phase stability of residual austenite in 60si2mn steels treated by quenching and partitioning. Journal of Iron and Steel Research, International 18, 70-74.

Lin, J., 2015. Fundamentals of Materials Modelling for Metals Processing Technologies. Imperial College Press, Imperial College London.

Liu, F., Lin, X., Song, M., Yang, H., Song, K., Guo, P., Huang, W., 2016. Effect of tempering temperature on microstructure and mechanical properties of laser solid formed 300M steel. Journal of Alloys and Compounds 689, 225-232.

Liu, X., El Fakir, O., Zheng, Y., Gharbi, M.M., Wang, L., 2019. Effect of tool coatings on the interfacial heat transfer coefficient in hot stamping of aluminium alloys under variable contact pressure conditions. International Journal of Heat and Mass Transfer 137, 74-83.

Liu, X., Kopec, M., El Fakir, O., Qu, H., Wang, Y., Wang, L., Li, Z., 2020. Characterisation of the interfacial heat transfer coefficient in hot stamping of titanium alloys. International Communications in Heat and Mass Transfer 113, 104535.

Luan, X., Zhang, O., El Fakir, O., Wang, L., Gharbi, M.M., 2017. A pilot production line for hot/warm sheet metal forming integrated in a cloud based smartforming platform. Advanced High Strength Steel and Press Hardening, 492-497.

Massardier, V., 2014. Evolution of microstructure and strength during the ultra-fast tempering of Fe–Mn–C martensitic steels. Journal of materials science v. 49, pp. 7782-7796-2014 v.7749 no.7722.

Mastricola, N.P., Dreyer, J.T., Singh, R., 2017. Analytical and experimental characterization of nonlinear coned disk springs with focus on edge friction contribution to force-deflection hysteresis. Mechanical Systems and Signal Processing 91, 215-232.

Materialography, A., 2016. Grinder and polisher SAPHIR 520, pp. 319-320.

Materialography, A., 2019. Hot mounting press OPAL 410, pp. 70-72.

Matlock, D.K., Speer, J.G., 2009. Third generation of AHSS: Microstructure design concepts, In: Haldar, A., Suwas, S., Bhattacharjee, D. (Eds.), Microstructure and Texture in Steels. Springer London, London, pp. 185-205.

Megan, G., 2016. EPA reaffirms 54.5mpg target fuel economy by 2025. https://arstechnica.com/cars/2016/12/epa-reaffirms-55-4mpg-target-fuel-economy-by-2025-automakers-turn-to-trump/.

Merklein, M., Lechler, J., 2006. Investigation of the thermo-mechanical properties of hot stamping steels. Journal of Materials Processing Technology 177, 452-455.

Merklein, M., Lechler, J., 2008. Determination of material and process characteristics for hot stamping processes of quenchenable ultra high strength steels with respect to a FE-based process design. SAE International Journal of Materials and Manufacturing 1, 411-426.

Moore, P., Booth, G., 2015. 8 - Failure modes and analysis in metals, In: Moore, P., Booth, G. (Eds.), The Welding Engineer Guide to Fracture and Fatigue. Woodhead Publishing, Oxford, pp. 95-110.

Mori, K., Akita, K., Abe, Y., 2007. Springback behaviour in bending of ultra-high-strength steel sheets using CNC servo press. International Journal of Machine Tools and Manufacture 47, 321-325.

Mori, K., Bariani, P.F., Behrens, B.A., Brosius, A., Bruschi, S., Maeno, T., Merklein, M., Yanagimoto, J., 2017. Hot stamping of ultra-high strength steel parts. CIRP Annals 66, 755-777.

Mori, K., Maki, S., Tanaka, Y., 2005a. Warm and hot stamping of ultra high tensile strength steel sheets using resistance heating. CIRP Annals-Manufacturing Technology 54, 209-212.

Mori, K., Maki, S., Tanaka, Y., 2005b. Warm and hot stamping of ultra high tensile strength steel sheets using resistance heating. CIRP Annals 54, 209-212.

Mori, K.I., 2012. Smart hot stamping of ultra-high strength steel parts. Transactions of Nonferrous Metals Society of China 22, s496-s503.

Morsdorf, L., Tasan, C.C., Ponge, D., Raabe, D., 2015. 3D structural and atomic-scale analysis of lath martensite: Effect of the transformation sequence. Acta Materialia 95, 366-377.

Mostafaei, M.A., Kazeminezhad, M., 2016. Effect of starting microstructure through severe plastic deformation and ultra-rapid annealing of low-carbon steel. Steel Research International 87, 1527-1533.

MW Industries, 2019. Belleville Washers & Disc Springs.
https://www.mw-ind.com/products/belleville-disc-spring-washers/.

Naderi, M., 2007. Hot stamping of ultra-high strength steels.

Naganathan, A., Penter, L., 2012. Hot stamping. Sheet metal forming: processes and applications. ASM International, Materials park, Ohio, 135-156.

Nakagawa, Y., Mori, K.-i., Yashima, S., Kaido, T., 2018. Springback behaviour and quenchability in hot stamping of thick sheets. Procedia Manufacturing 15, 1071-1078.

Olson, G.b., W.S., O., 1991. Martensite ASM international.

Ormaetxea, A., Aramburu , A., Belategi, I., 2013. Improved productivity and energy comsumption on press hardening by means of mechanical servo press technology Proceedings of 4th International Conference on Hot Sheet Metal Forming of High-Performance Steel, 185-190.

Osakada, K., Mori, K., Altan, T., Groche, P., 2011. Mechanical servo press technology for metal forming. CIRP Annals 60, 651-672.

Pan, B., Qian, K., Xie, H., Asundi, A., 2009. Two-dimensional digital image correlation for in-plane displacement and strain measurement: a review. Measurement Science and Technology 20, 062001.

Patangtalo, W., Aimmanee, S., Chutima, S., 2016a. A unified analysis of isotropic and composite Belleville springs. Thin-Walled Structures 109, 285-295.

Patangtalo, W., Hyer, M.W., Aimmanee, S., 2016b. On the non-axisymmetric behavior of quasi-isotropic woven fiber-reinforced composite Belleville springs. Journal of Reinforced Plastics and Composites 35, 334-344.

Peters, W.H., Ranson, W.F., 1982. Digital imaging techniques in experimental stress analysis. Optical Engineering 21, 427-431, 425.

Ploshikhin, V., A., P., Kaiser, J., Bisping, R., Linder, H., Lengsdorf, C., Roll, K., 2011. New heating technology for the furnace-free press hardening process. Tools and Technologies for Processing Ultra High Strength Materials.

Posco, 2017. POSCO GIGA STEEL Increases Strength, Improves Safety in Autos. https://newsroom.posco.com/en/posco-giga-steel-increases-strength-improves-safety-autos/.

Raj, A.S.V., Veeraghavan, S., Bade, S., Srinivas, K., 2018. Performance Comparison of Belleville Washer under Compressive Load using Experimental and Simulation Methods. Materials Today: Proceedings 5, 8486-8494.

Raji, N., Oluwole, O., 2012. Effect of Soaking Time on the Mechanical Properties of Annealed Cold-Drawn Low Carbon Steel. Materials Sciences and Applications 3, 513-518.

Revilla, C., López, B., Rodriguez-Ibabe, J.M., 2014. Carbide size refinement by controlling the heating rate during induction tempering in a low alloy steel. Materials & Design (1980-2015) 62, 296-304.

Sackl, S., Zuber, M., Clemens, H., Primig, S., 2016. Induction Tempering vs Conventional Tempering of a Heat-Treatable Steel. Metallurgical and Materials Transactions A 47, 3694-3702.

Saha, D.C., Biro, E., Gerlich, A.P., Zhou, Y., 2016. Effects of tempering mode on the structural changes of martensite. Materials Science and Engineering: A 673, 467-475.

Saito, N., Fukahori, M., Minote, T., Funakawa, Y., Hisano, D., Hamasaki, H., Yoshida, F., 2018. Elasto-viscoplastic behavior of 980 MPa nano-precipitation strengthened steel sheet at elevated temperatures and springback in warm bending. International Journal of Mechanical Sciences 146-147, 571-582.

Samuels, L.E., 2014. Tempering of Martensite. Metallography, Microstructure, and Analysis 3, 70-90.

Sauveur, A., Martens, A., 1900. Martens Metallographis.

Scherdel, 2019. Spring manual: Version 7.1 Disc springs

Semiatin, S.L., 2006. Contour Roll Forming, In: Semiatin, S.L. (Ed.), Metalworking: Sheet Forming. ASM International, p. 0.

Shah, J.R., Sharma, S.K., Patel, B.C., 2011. Investigating Springback effect in U-Die Bending Process by varying different Parameters, International Conference on Engineering, Ahmedabad, India.

Shao, Z., Li, N., Lin, J., Dean, T., 2017. Strain measurement and error analysis in thermo-mechanical tensile tests of sheet metals for hot stamping applications. Journal of Mechanical Engineering Science 232, 1994-2008.

Singh, M., 2016. Application of Steel in Automotive Industry. 9001.

SMMT, 2017. New Car CO2 report.

Steve, H., 2001. Heat treatment of steels - The processes. https://www.azom.com/article.aspx?ArticleID=543.

Struers, 2015. LaboPol-21-Instruction Manual Spare Parts and Diagrams, pp. 1-11.

Suehiro, M., Maki, J., Kusumi, K., Ohgami, M., Miyakoshi, T., 2003. Properties of Aluminized Steels for Hot-Forming. SAE International.

Tamarelli, C.M., 2011. AHSS 101:The Evolving Use of Advanced High-Strength Steels for Automotive Applications.

Taylor, T., 2016. Novel cold-rolled martensitic ultra-high-strength steels for roll forming technologies. Materials Science and Technology 32, 1730-1741.

Tekkaya, A., Karbasian, H., Homberg, W., Kleiner, M., 2007. Thermomechanical coupled simulation of hot stamping components for process design. Production Engineering 1, 85-89.

Thyssenkrupp, 2016. Steel MS-W Product information for martensitic-phase steels, pp. 1-8.

Tokita, Y., Nakagaito, T., Tamai, Y., Urabe, T., 2017. Stretch formability of high strength steel sheets in warm forming. Journal of Materials Processing Technology 246, 77-84.

Traub, T., Chen, X., Groche, P., 2017. Experimental and numerical investigation of the bending zone in roll forming. International Journal of Mechanical Sciences 131-132, 956-970.

Vasundhara, S., Dharankar, C., Tirupathi, R., 2016. High Strength Steel for Automotive Applications. International Research Journal of Engineering and Technology (IRJET) 03, 966-968.

Venezuela, J., Liu, Q., Zhang, M., Zhou, Q., Atrens, A., 2015. The influence of hydrogen on the mechanical and fracture properties of some martensitic advanced high strength steels studied using the linearly increasing stress test. Corrosion Science 99, 98-117.

Verhulp, E., Rietbergen, B.v., Huiskes, R., 2004. A three-dimensional digital image correlation technique for strain measurements in microstructures. Journal of Biomechanics 37, 1313-1320.

Volvo, 2016. Advanced high strength steel technologies in the 2016 Volvo XC90. https://www.autosteel.org/-/media/files/autosteel/great-designs-in-steel/gdis-2016/track-2---volvo-xc90.ashx.

Wang, A., Zhong, K., El Fakir, O., Liu, J., Sun, C., Wang, L., Lin, J., Dean, T.A., 2017a. Springback analysis of AA5754 after hot stamping: experiments and FE modelling. The International Journal of Advanced Manufacturing Technology 89, 1339-1352.

Wang, C., Li, X., Han, S., Zhang, L., Chang, Y., Cao, W., Dong, H., 2017b. Warm Stamping Technology of the Medium Manganese Steel.

Wang, Z., Hu, Q., Yan, J., Chen, J., 2017c. Springback prediction and compensation for the third generation of UHSS stamping based on a new kinematic hardening model and inertia relief approach. The International Journal of Advanced Manufacturing Technology 90, 875-885.

William Chandler Roberts-Austen, 1914. Charles Griffin & Co.

Xie, Z., Fang, Y., Cui, Y., Wang, X., Shang, C., Misra, R.D.K., 2016. Effect of reheating rate on microstructure and properties of high-strength-toughness steel. Materials Science and Technology 32, 691-696.

Yanagimoto, J., Oyamada, K., Nakagawa, T., 2005. Springback of High-Strength Steel after Hot and Warm Sheet Formings. CIRP Annals 54, 213-216.

Yang, L., Smith, L., Gothekar, A., Chen, X., 2010. Measure Strain Distribution Using Digital Image Correlation (DIC) for Tensile Tests The Advanced High Strength Steel Stamping Team of the Auto/Steel Partnership.

Yoshida, T., Isogai, E., Sato, K., Hashimoto, K., 2013. Springback Problems in Forming of High-Strength Steel Sheets and Countermeasures, Nippon steel technical report, pp. 4-10.

Zeiss, 2019. ZEISS Sigma 300 with RISE.
https://www.instrument.com.cn/netshow/C234210.htm.

Zhao, K., Chang, Y., Hu, P., Wu, Y., 2016. Influence of rapid cooling pretreatment on microstructure and mechanical property of hot stamped AHSS part. Journal of Materials Processing Technology 228, 68-75.

Zhao, Y., Ren, X., Hu, Z., Xiong, Z., Zeng, J., Hou, B., 2018. Effect of tempering on microstructure and mechanical properties of 3Mn-Si-Ni martensitic steel. Materials Science and Engineering: A 711, 397-404.

Zheng, E., Jia, F., Zhou, X., 2014. Energy-based method for nonlinear characteristics analysis of Belleville springs. Thin-Walled Structures 79, 52-61.

Zwick/Roell, 2019. Universal Hardness Tester.
http://www.directindustry.com/prod/zwickroell-gmbh-co-kg/product-15660-1100165.html.

Appendix-A Fast-warm stamping on thermoplastic composites

Carbon fibre reinforced thermoplastic composites have long-held huge potential for mass-producing lightweight structural components in the aerospace, aircraft and automotive industries. High Pressure Resin Transfer Moulding (HP-RTM) is already being used to produce automotive components from reinforced thermoplastic composites. However, lengthy cycle times due to the long duration of the injection and curing processes remain an obstacle to the adoption of this technology for mass production. Press forming of reinforced thermoplastic composite sheets using convection or infrared ovens is also time and energy-intensive. Great efforts have been therefore made to achieve a less-than-one-minute cycle time manufacturing process for higher performance thermoplastic composites. Therefore, the development of new forming technology may be an alternative solution to form thermoplastic composites into complex shapes whilst reducing the cycle time.

The FWS technology is proposed which enables mass production of complex-shaped components from reinforced thermoplastic composites. The thermoplastic composite used in this process is a material that preferably contains a matrix and reinforcement. For high-volume applications in the automotive industry, the proposed technology provides a cost-effective process that reduces the total cycle time to within 15s. The feasibility of rapid thermoforming technology has been verified experimentally (lab-scale).

The process is a non-isothermal method in which a reinforced thermoplastic composite sheet is formed into a desired geometric configuration. A powerful contact heating system, which can provide a rapid heating rate, is first used to heat the thermoplastic composite sheet to an appropriate temperature, sufficiently slightly below the melting temperature of the polymer. A rapid heating rate of up to 60°C/s is achieved by using a contact heating method that can significantly decrease the heating time. The heated workpiece is then transferred to the forming tools within a desirable time in which the hot workpiece is still soft. The material is then formed

by applying a specific pressure between the two cold dies, immediately forming and quenching the formed part to room temperature.

The post-form strength of parts formed in accordance with the developed process has even been found to provide similar strength properties to those of the sheet before it was heated and formed. Compared to other technologies, the rapid heating rate and shorter or even zero soaking period of the FWS process not only increases the production rate but also improves energy efficiency. The total cycle time can be reduced to within 15s including heating, soaking, transferring, forming and quenching.

Figure A.1 shows the proposed forming process for carbon fibre reinforced thermoplastic that comprises of the following steps:

1. The first step is heating the reinforced thermoplastic composite sheet: the blank is heated to the target temperature, slightly below the melting temperatures at a critical heating rate, e.g. 20-60°C/s. Specific pressure is applied to the hot blank during this step. The heating rate and forming temperature utilized vary depending on the desired geometric configuration.
2. The second step is blank soaking: An extremely short to zero soaking period is applied to the hot blank at a specific pressure once the target temperature is reached.
3. The third step is blank transferring: transferring the hot blank into a cold die set within a determined period while maintaining a sufficient forming temperature in which the blank is still soft.
4. The fourth step is forming and quenching: the blank is formed into the desired configuration at the appropriate temperature within the cold die set and cooled down at a critical quenching rate, under a critical forming force.

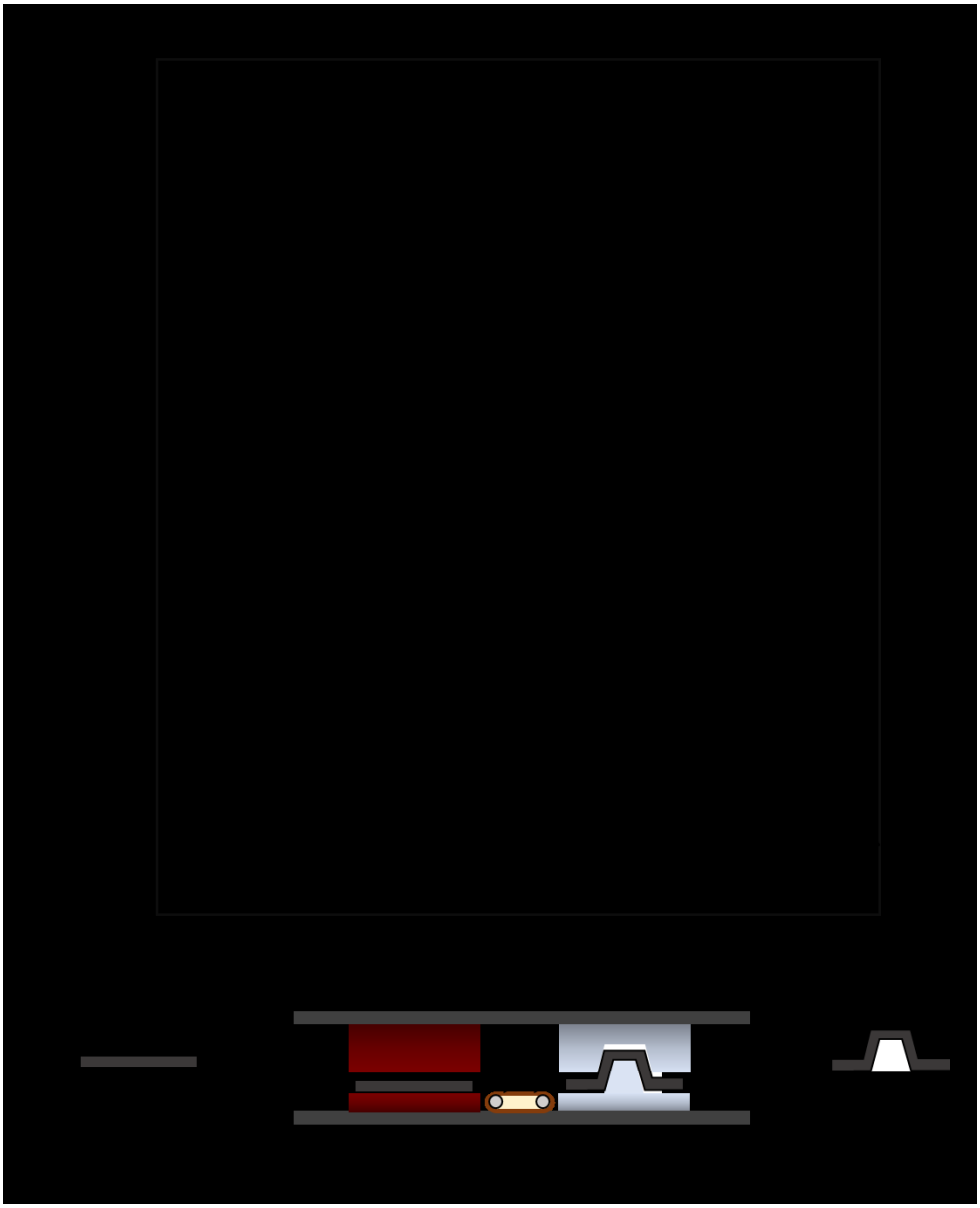

Figure A.1 Thermal profile and schematic diagram of the fast-warm stamping technology for carbon reinforced thermoplastic composites.

Thermoset polymers have been used more commonly than thermoplastic polymers in fibre reinforced composites because they are cheaper and easier to produce due to the ease of working with liquid resin. Composites made with thermosets have high strength and fatigue resistance although are unable to be fully recycled as the polymer cannot be re-moulded.

A feasibility study on the proposed forming technology was conducted on a commercial thermoplastic composite called CF-PEEK boards. The material has exceptional chemical

resistance, high abrasion resistance, low water absorption, a low coefficient of friction and no volatile components. This is in addition to the usual carbon fibre composite properties of high strength and stiffness. Material properties of CF-PEEK boards are presented in Table A.1. The initial thickness of the CF-PEEK boards was 2.6mm. The as-received composite sheet used for this study exhibited 600MPa tensile strength and 1% elongation to failure at room temperature. Haufler produces CF-PEEK boards by pressing and pre-consolidation and hence a curing/consolidation stage during thermostamping is not required, allowing rapid manufacture of components.

Table A.1 Material characteristics of CF-PEEK boards.

Mechanical properties	Value
density [g/cm³]	1.5
tensile strength [MPa]	550
elastic modulus [GPa]	55
compressive strength [MPa]	500
Elongation to failure (%)	1
Fibre orientation	0/90º
Service temperature (Cº)	260

A warm stamping tool set was designed to be set on the *Uni-form* system for forming a U-shaped demonstrator part. The U-shape tool was manufactured to evaluate the ability of the FWS process to form complex shapes. The schematic diagram of the stamping tool set for U-shape forming tests is shown in Figure A.2. The width of the punch is machined to 69.4mm. The gas spring was charged to 20 bar to ensure sufficient pressure for heating and forming.

The composite blank was waterjet cut to the designed geometry. Prior to each test, the composite blank was firstly placed between stamping die and punch. The automatic conveyor system transported the cold blank to the furnace and heated to the pre-set temperature. The ultra-fast heating rate of nearly 50°C/s was performed to heat the cold blank using a contact heater. The blank was heated to 353.45°C and then transferred from the furnace to the U-shaped cold die immediately via a conveyor system in 4s to avoid excessive heat loss. The blank was subsequently formed at a temperature of 330.28°C with a 10kN blank-holding force and

simultaneously quenched within the cold die for 5s. A schematic illustration of the temperature evolutions during the FWS technology is given in Figure A.3.

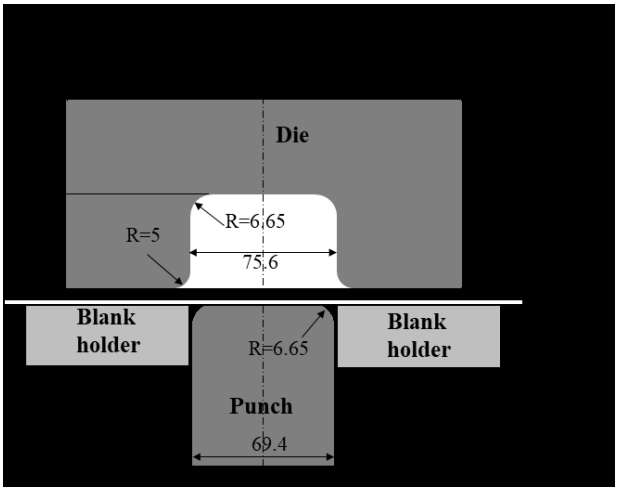

Figure A.2 Schematic diagram of U-shaped components stamping tool set.

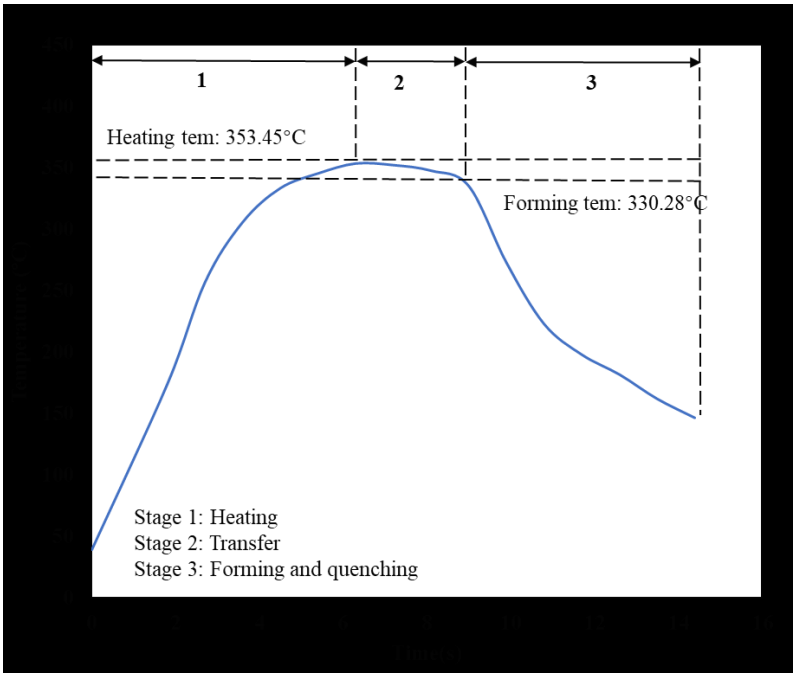

Figure A.3 Schematic illustration of the temperature evolutions during the FWS of the CF-PEEK.

Figure A.4 shows the formed U-shaped part via the FWS technology which has a good surface quality at the corners. The shorter cycle time leads to a higher production rate and lower energy consumption. The total manufacturing time was reduced to within 15 seconds. Uniaxial tensile

tests were conducted at room temperature through the DIC system to evaluate the PFS on formed U-shaped components. The experimental procedure and tensile specimen design were given in Chapter 3.3.3. Figure A.5 shows the flow stress-strain behaviour of as-received material and formed part. It was found that the post-form strength of formed components was approximately 458.6 MPa, which is nearly 90% of the as-delivered material strength.

In summary, the FWS technique enables a reduction of total cycle time from 2-5 minutes to less than 15s and corresponding productivity improvement for a mass-production setting. A demonstrator component was successfully formed using the proposed forming process with 90% post-form strength of as-delivered material. These benefits enable this forming technique to be an alternative solution to form a complex shape part with thermoplastic composites.

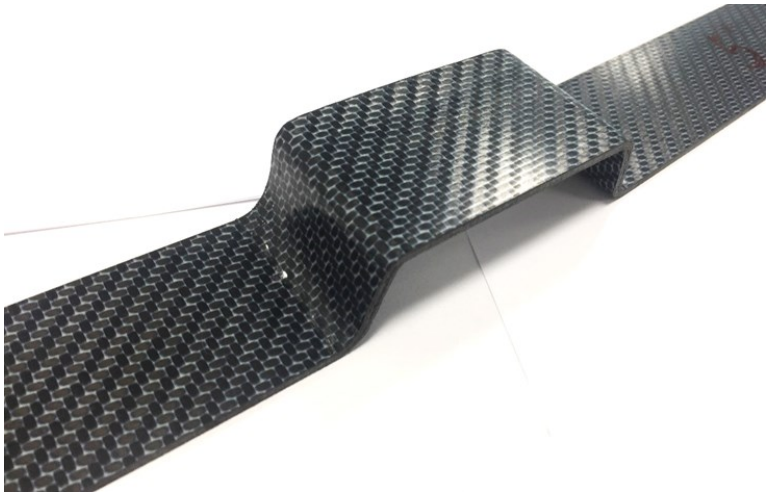

Figure A.4 A U-shaped formed component from carbon fibre reinforced polyetheretherketone composite (CF/PEEK) with good surface characteristics.

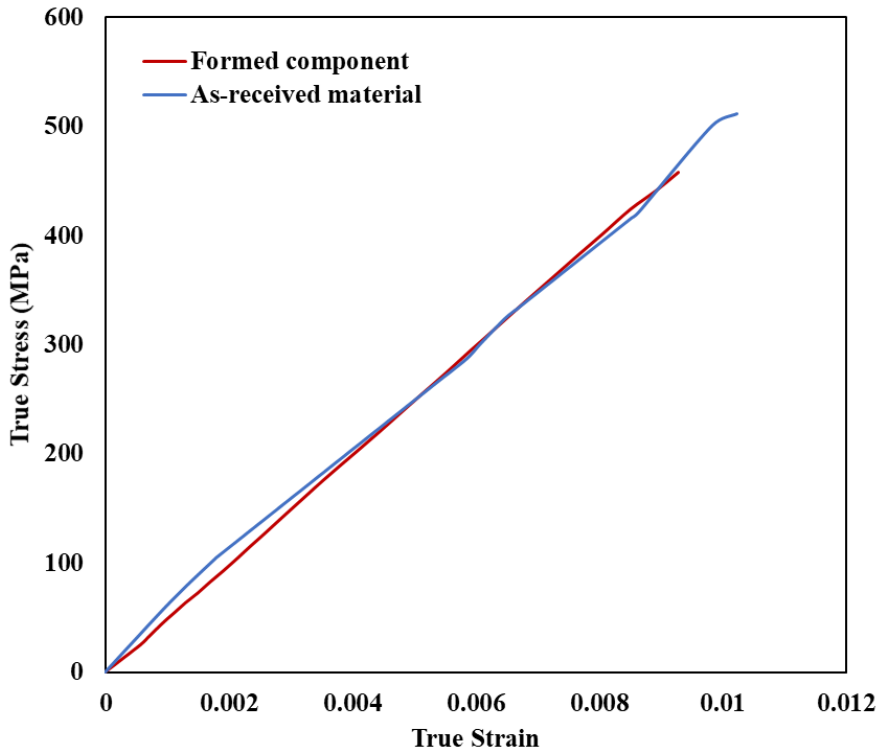

Figure A.5 Flow stress-strain curves of as-received material and formed part.

Appendix-B Strength degradation test facility

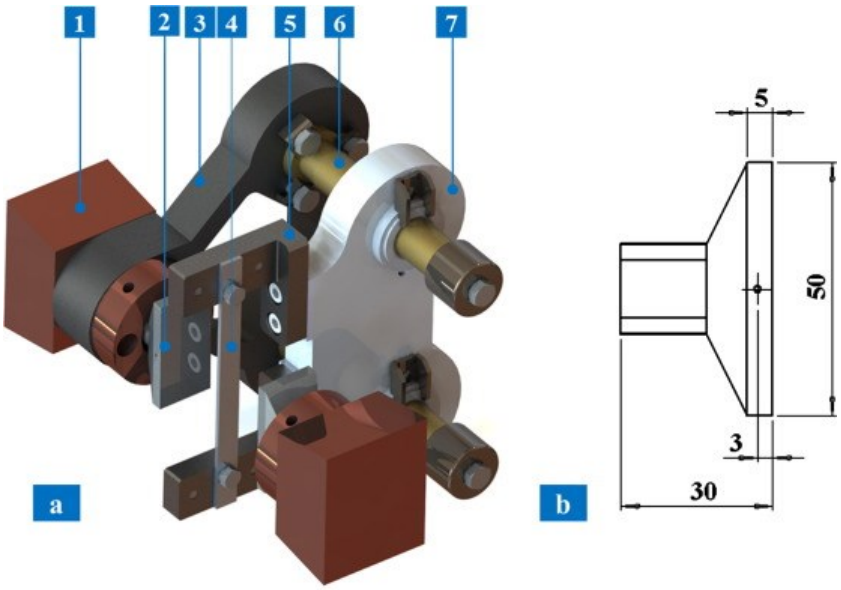

Figure B.1. Design of the IHTC test facility (b) geometry of the punch/die (Liu et al., 2019).

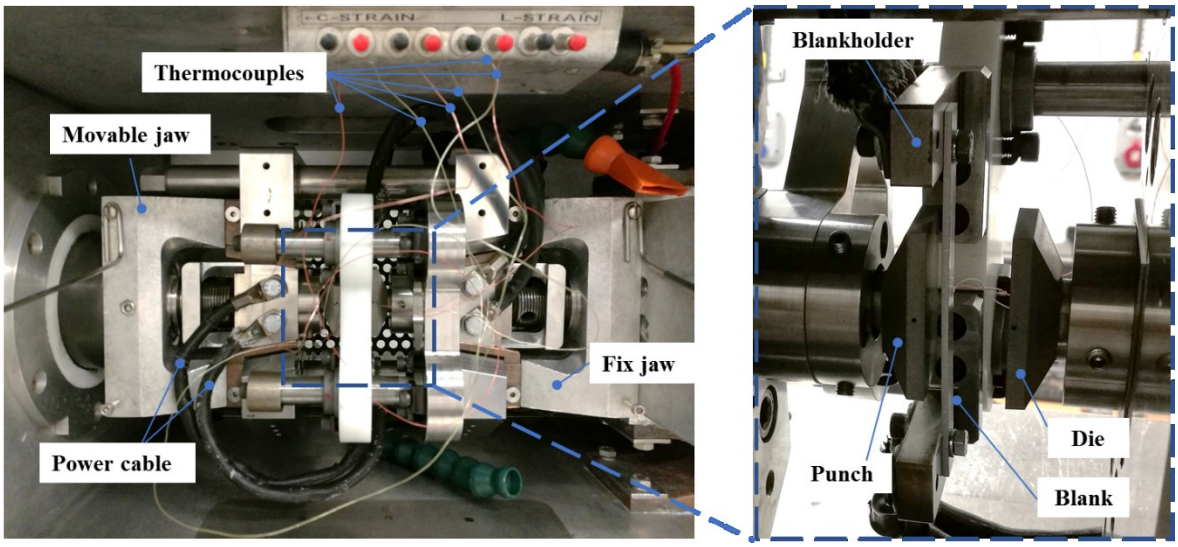

Figure B.2 IHTC experimental setup in Gleeble 3800.

Appendix-C Hardness measurement of the MS1180 steel at various conditions

Table C.1 Hardness measurements of the MS1180 steel at different temperatures.

Temperature (°C)	1 (HV)	2 (HV)	3 (HV)	4 (HV)	5 (HV)	Average (HV)	Standard deviation (HV)
350	370.7	371.9	375.1	367.2	372.2	371.4	2.3
400	370.1	361.0	353.0	355.0	351.2	358.1	6.3
450	346.4	361.4	338.2	348.2	349.8	348.8	6.8
500	326.4	334.7	331.9	329.4	333.8	331.2	2.8

Table C.2 Hardness measurements of the MS1180 steel at different strain rates.

Strain rate (/s)	1 (HV)	2 (HV)	3 (HV)	4 (HV)	5 (HV)	Average (HV)	Standard deviation (HV)
0.01	329.8	334.3	331.2	327.2	329.4	330.4	2.1
0.1	339.5	334.2	341.2	341.1	338.0	338.8	2.4
1	346.4	361.4	338.2	348.2	349.8	348.8	6.8
5	368.4	361.6	352.8	354.0	373.2	362.0	7.2

Table C.3 Hardness measurements of the MS1180 steel at different heating rates.

Strain rate (°C/s)	1 (HV)	2 (HV)	3 (HV)	4 (HV)	5 (HV)	Average (HV)	Standard deviation (HV)
1	342.1	337.0	334.2	339.4	333.6	337.3	2.9
10	345.7	330.5	343.7	340.0	343.9	340.8	5.0
25	351.2	344.2	341.3	339.2	342.4	343.7	3.7
50	346.4	361.4	338.2	348.2	349.8	348.8	6.8
90	345.9	359.2	347.9	348.8	361.7	352.7	5.9
150	357.5	351.8	353.6	363.1	357.8	356.8	3.6

Table C.4 Hardness measurements of the MS1180 steel at different soaking time.

Soaking time (s)	1 (HV)	2 (HV)	3 (HV)	4 (HV)	5 (HV)	Average (HV)	Standard deviation (HV)
0	374.6	377.6	389.0	389.2	382.6	382.6	5.4
2	381.4	386.2	376.2	384.0	384.5	382.5	3.2
4	384.8	381.8	382.4	368.7	375.9	378.7	5.3
6	371.3	363.9	381.7	380.1	381.2	375.6	6.4
8	366.3	375.1	367.3	370.8	373.9	370.7	3.2

Appendix-D The frame motion in the FWS process

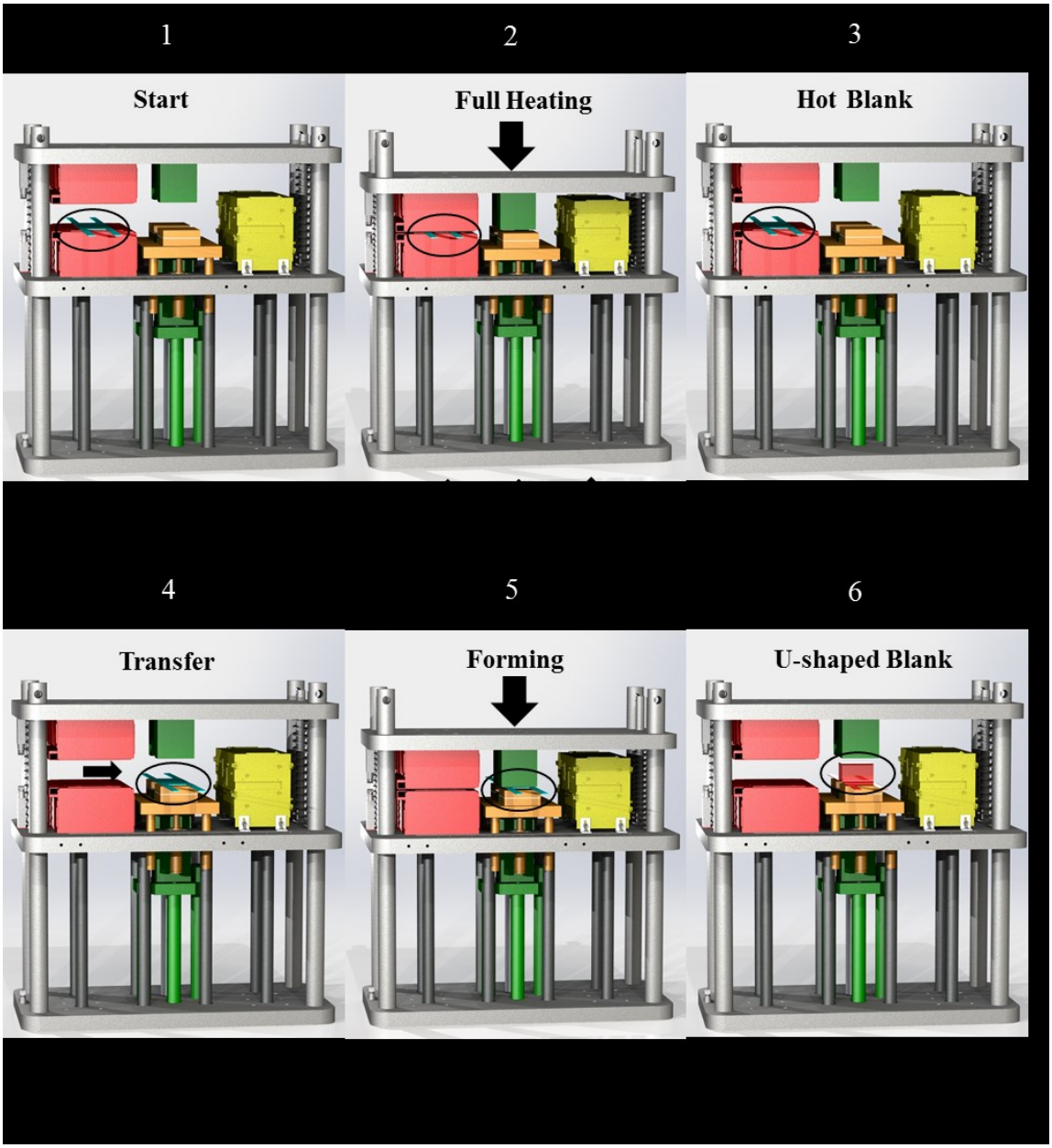

Figure D.1 The frame motion in the FWS process.